DOE/GO/10017-17

THE $2000 ELECTRIC POWERTRAIN OPTION-1 PROGRAM

Final Technical Report
January, 1996 – February, 1999

Northrop Grumman Corporation
Electronic Sensors and Systems Sector
Baltimore, Maryland 21203

Date Published: June, 1999

PREPARED FOR THE UNITED STATES
DEPARTMENT OF ENERGY

Under Agreement No. DE-FC36-94-GO10017

DISCLAIMER

DISCLAIMER

Portions of this document may be illegible in electronic image products. Images are produced from the best available original document.

Table of Contents

Table of Contents (Continued)

List of Figures

List of Figures (Continued)

List of Tables

1 INTRODUCTION

This report describes the tasks accomplished as part of Northrop Grumman's TRP "$2000 Electric Powertrain Option-1" program. Northrop Grumman has strived to achieve technology advances and development considered as high priority to the success of future electric vehicles. Northrop Grumman has achieved the intent of the program by taking several steps toward reducing the cost of the electric vehicle powertrain, demonstrating technologies in the form of hardware and introducing enhancements into production that are consistent with the needs of the market.

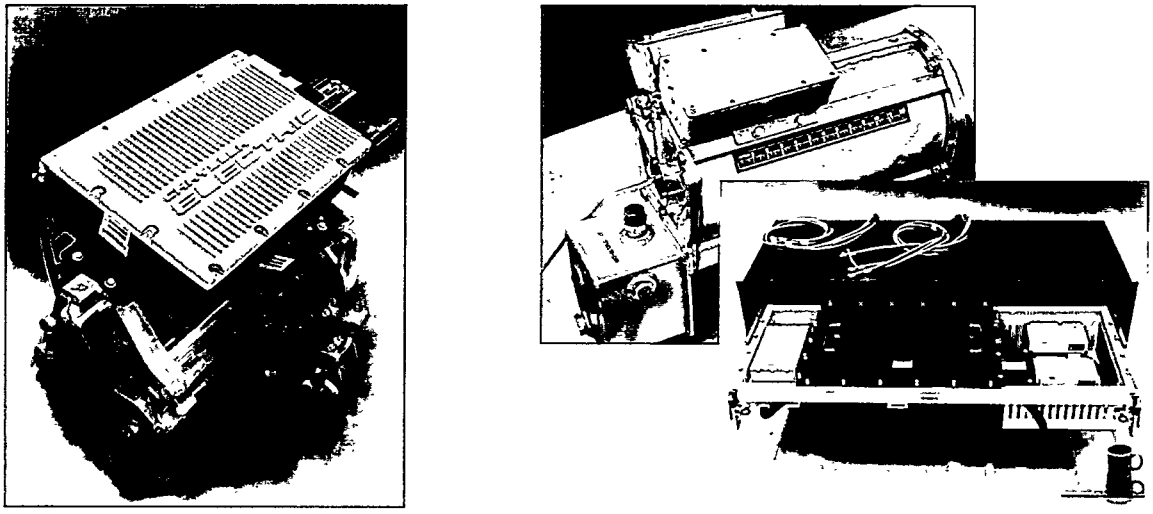

Figure 1.1-1 Production Powertrain Systems (100hp on left, 230hp on right)

1.1 PROJECT OVERVIEW

The $2000 Electric Powertrain Option-1 program encompasses three major categories of effort; technology demonstrations, powertrain enhancements, and expanded powertrain application. Each of these three categories equates to approximately one-third of the total efforts expended on the program and each is described in this report in individual sections.

The Technology Demonstration section describes technologies that were investigated because of their potential for significantly reducing the cost of the electric powertrain. The technologies investigated were considered to be potential enhancements for powertrain production in the near future (3 to 5 years). The technology demonstrations include an integrated power block costing roughly half of the present production design. Also included is an experiment in methods for resolverless motor control, which could eliminate a costly motor position sensor.

The Powertrain Enhancements section describes manufacturing and support cost reductions that have been implemented into the production powertrains. The powertrain enhancements include software/algorithm improvements in order to increase efficiency and to improve performance. The powertrain enhancement effort also includes powertrain upgrades as a result of validation testing and manufacturing acceptance testing which provide for higher

reliability and lower support cost. In addition, enhancements in producibility are described in this section and include modular test equipment that supports every level of powertrain assembly, and manufacturing process enhancements for producing the powertrain product, increasing its production rate, and reducing hands-on labor time.

The Expanded Powertrain Application section describes enhancements to the powertrain or its major subsystems to adapt it for use in applications other than the pure electric vehicle market. These other markets are targeted because of their need for a similar product and would have a major impact on manufacturing quantity. One of the powertrain enhancements described in this section is the adaptation of the electric powertrain to hybrid-electric vehicle platforms. Also described are changes to the powertrain's motor controller software to adapt it for use in industrial power generation applications.

1.2 SUMMARY OF EFFORTS

A summary of each of the major efforts undertaken as part of this TRP project is included below. The efforts are presented in the order that each topic is described in the later sections of this report.

Integrated Power Block

The focus of this activity was to cut the cost of the IGBT inverter assembly, the most expensive electronic element within the powertrain, in half. Cost reductions were realized by combining the cooling structure, the power distribution buses, and the electronic devices into a single integrated assembly and selecting the most cost effective materials and manufacturing processes for the assembly. In addition, the electrical characteristics were improved by focusing on a low inductance implementation of the power electronics and snubbing capacitors. Even though the integrated power block will require further development, the estimate of manufacturing cost indicates that the cost reduction goal can be achieved.

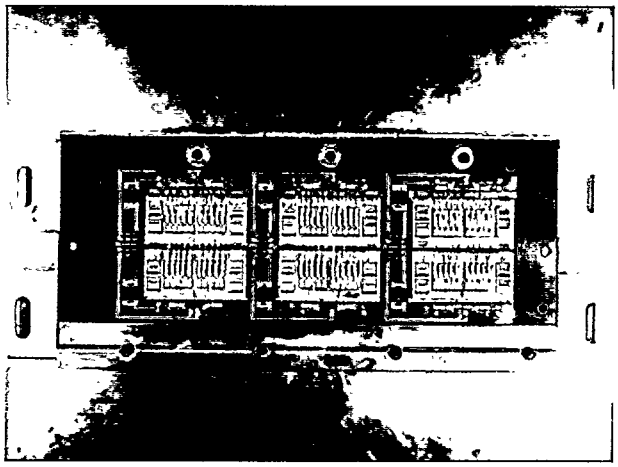

Figure 1.2-1 Integrated Power Block

Resolverless Motor Control

A costly and complex function, required by the motor control algorithm, is the determination of the speed and position of the electric motor rotor. A sensor commonly referred to as a resolver is used in the production powertrain to provide the rotor information. Powertrain simplifications and cost reductions would result from a development of a resolverless control system. A production powertrain was modified to support the development of this motor control concept. The modified powertrain was tested using a dynamometer test cell in the development laboratory.

DSP Enhancements

The purpose of this task was to enhance the performance of the Digital Signal Processing (DSP) software by reducing the processing timeline and incorporating new capability into the system for supporting a broader range of applications. The DSP code, the heart of the powertrain controls, computes and outputs voltage control signals that drive the IGBTs, generating three-phase A/C currents and thereby applying the requested torque to the motor shaft. This lowest level of motor control was optimized for processing timeline, maintainability, and improved flexibility.

Production Validation and Acceptance Test

The production validation test program was developed to determine the stress mechanisms within the powertrains and to implement enhancements to increase design margins of the systems. The environment and stress mechanisms were defined and tests were determined. Test procedures were written and the powertrains were subjected to the defined tests. Test results were compiled and as powertrain enhancements were implemented, the enhancements were subjected to an applicable subset of the validation tests.

Manufacturing Acceptance Test
and Test Equipment

The objective of developing the manufacturing acceptance tests was to implement an efficient and cost effective method of testing each powertrain during the manufacturing process and of supporting increasing production volumes. Each powertrain requirement was examined to determine the lowest level of assembly at which the requirement could be tested and to specify the test equipment to be used. Test procedures to verify each requirement were developed and implemented on the production assembly line.

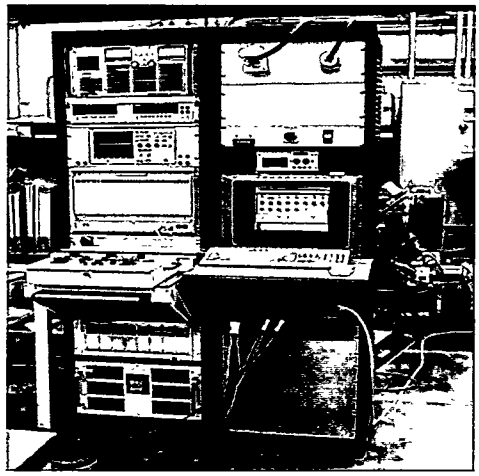

Figure 1.2-2 Manufacturing Test-Set

Manufacturing Process Development

The manufacturing process used for the assembly of the powertrain was reviewed and optimized for product assembly flow including tooling and workmanship inspection. Each assembly procedure was included in a process failure mode and effects analysis (PFMEA) which helped to determine the critical aspects of the manufacturing process.

Industrial Turbo-Generator Software Development and Test

The 3-phase inverter of the electric powertrain was modified to support the needs of the new micro-turbine industrial power sources. The powertrain software was modified, based on the existing powertrain code, to convert the turbine's output to a regulated, 3-phase, 480v power source for industrial use. Units were tested in the lab as well as in electric utility test sites. The near-term, high volume market is expected to reduce the cost of the power electronics as well as put in place the infrastructure for training and supporting power electronic equipment similar to the powertrain electronics.

Hybrid-Electric Powertrain

To increase the potential market for the electric powertrain, the pure electric powertrain system was modified to operate in hybrid-electric vehicle systems. Enhanced power flow control was implemented and power management techniques were analyzed. The modified powertrains were integrated into vehicles and tested in the lab and in transit bus fleet application.

Electric Vehicle Auxiliary Subsystems

As the production drive systems were being tested and evaluated by customers, the customers identified electric vehicle issues that were outside the extent of the electric powertrain. Vehicle level system investigations of these issues have been initiated and potential solutions have been explored. The emphasis of this task has been to aid the end-user in addressing the broad range of issues that arise when new technology is introduced into the market place.

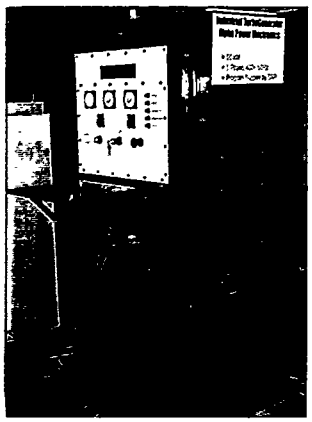

Figure 1.2-3 Industrial Turbine-Generator Power Electronics Unit

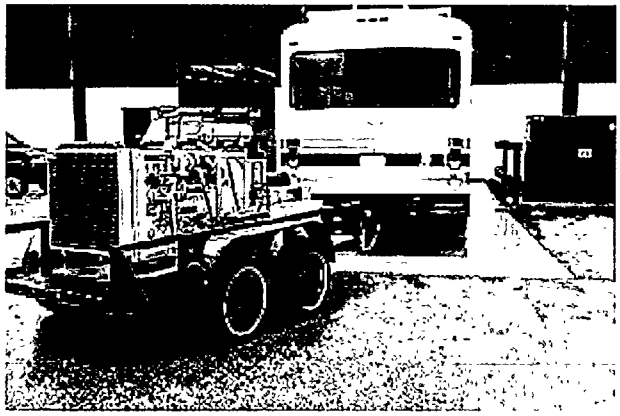

Figure 1.2-4 Initial Hybrid-Electric Powertrain Evaluation Platform

Northrop Grumman's $2000 Electric Powertrain Option-1 activities have been successful in reducing the cost of the electric powertrain and enhancing system performance. The Integrated Power Block that was investigated for technology insertion into future electric vehicle powertrains is estimated to reduce the power electronics cost by one-half. The field demonstrations of both the hybrid-electric powertrain and the industrial power generation systems can lead to increased production volume, thereby reducing product cost and assuring infrastructure development to support the product. Additional benefits of Northrop Grumman's efforts are described in subsequent sections of this report.

2 TECHNOLOGY DEVELOPMENT

The technology development section describes technologies that were investigated because of their potential of significantly reducing the cost of the electric powertrain. The technologies investigated were considered to be potential enhancements for near future (3 to 5 years) production powertrains. The technology demonstrations include an integrated power block costing roughly half of the present production design. Also included is an experiment in methods for resolverless motor control, which could eliminate a costly motor position sensor.

2.1 INTEGRATED POWER BLOCK DEVELOPMENT

2.1.1 Introduction

The purpose of this task was to develop an integrated power block module (integrated three-phase bridge) suitable for the control of electric motor traction drives in commercial and military applications. An integrated, liquid-cooled, three-phase bridge was designed, built, and tested with the 230 HP electric bus motor developed on the electric vehicle program. The 230 HP drive and the smaller 100 HP electric motor controllers were originally developed with commercially available IGBT modules to form three-phase power bridges mounted on custom designed liquid-cooled heat sinks. The 100 HP controller has one bridge for the single winding in the 100 HP motor and the 230 HP controller has two bridges for each of two separate windings in the 230 HP motor. The purpose of the integrated design was to improve the thermal performance by lowering the thermal resistance between the silicon and the cooling fluid. The lower thermal resistance reduces the amount, and therefore, the cost of the silicon for a given power requirement. In this comparison, one integrated bridge would replace two of the discreet component bridges. The goal/result of the IPB development effort is reflected in Figure 2.1-1.

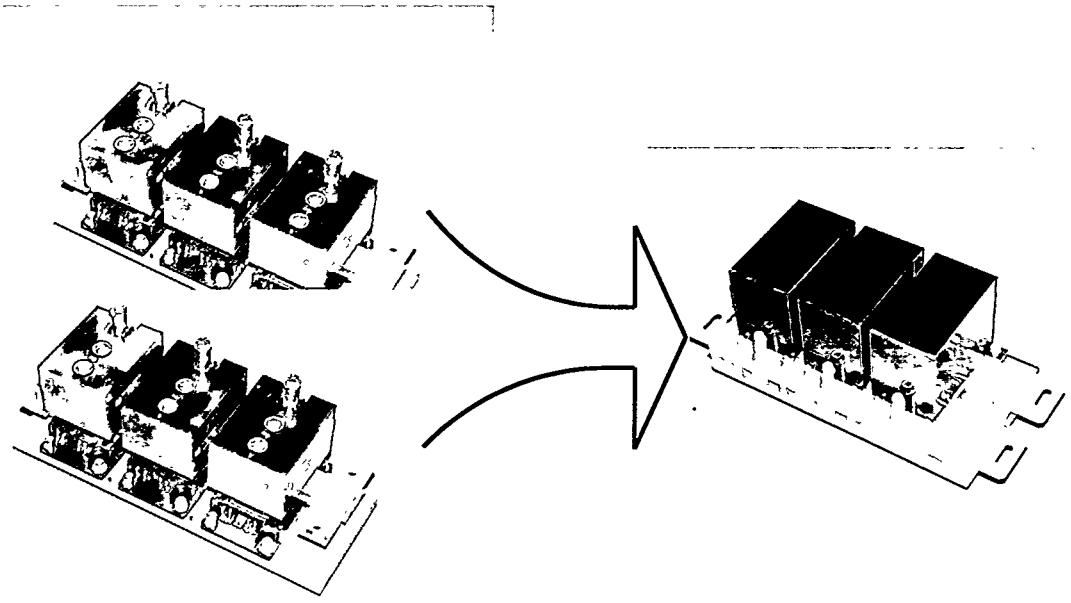

Figure 2.1-1 Integrated Power Block Reduces Cost and Size 2:1

The integrated power block was tested in two ways. One way was with liquid coolant flowing through copper porous metal heat exchangers located directly below each die. In this configuration, the integrated power block could dissipate 2.08 times as much heat as the standard discreet bridge for the same silicon and coolant temperatures. The other test configuration was to allow the liquid coolant to flow over the top surface of the chips and wire bonds as well as through the porous heat sink. In this configuration, the power block could dissipate 2.97 times as much heat as the standard discreet module with the same silicon and coolant temperatures. One solid state switch survived a DC current of 1000 Amps while dissipating over 5,000 Watts per square inch in this configuration. The normalized thermal resistances of the discreet bridge and the two configurations of the integrated power block are: 0.115, 0.055, and 0.038 (degrees C * square inch)/Watt, where the square inch figure refers to the silicon chip area under the chip but not including the area of the top side.

2.1.2 Module Construction

The integrated bridge has three main parts, a laminated structure, a base manifold, and a cover/snubber. The laminated structure with the coolant manifold below it and with the cover/snubber assembly above it is shown in Figure 2.1-2.

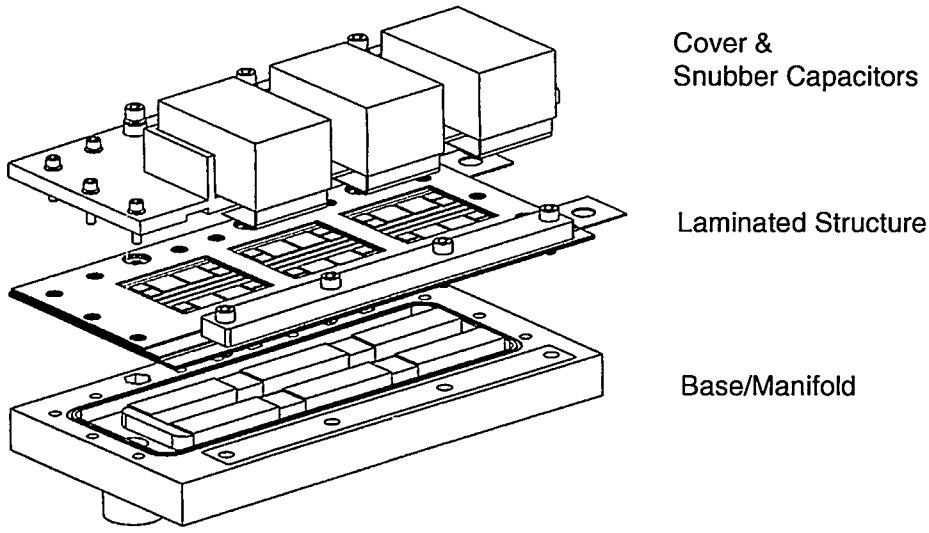

Figure 2.1-2 Major Parts of the Integrated Power Block

The laminated structure (shown exploded in Figure 2.1-3) contains several layers including positive and negative copper DC planes, three common collector-emitter terminations for the three phase outputs, a gate drive distribution conductor layer, and a base layer to provide a seal for the liquid coolant.

The four layers were laminated together with .005 inch thick DuPont "Pyralux" acrylic b-stage impregnated glass fabric commonly used to attach heat sinks to P.C. boards. The dielectric strength is 2000 volts/mil. This material was chosen because it has a higher operating temperature and higher strength than other b-stage materials.

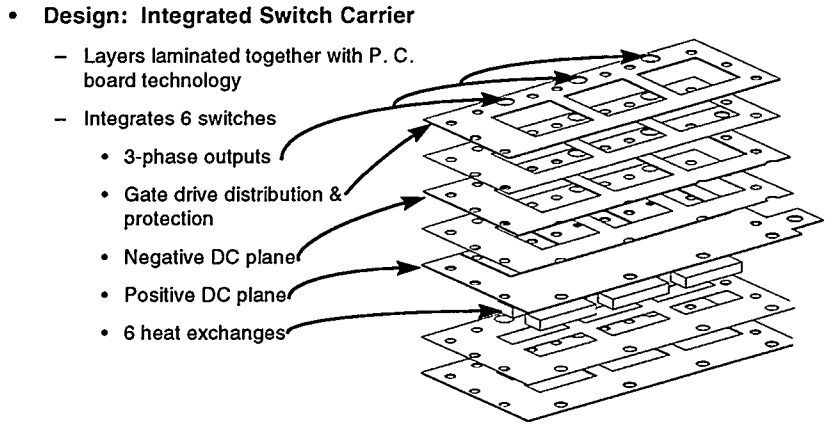

Figure 2.1-3 IPB Laminated Structure

A unique feature of this laminated structure is that it has six porous metal heat sink structures brazed to the underside of the copper layer which will form the positive DC bus (common collector) and the three separate collector-emitter segments for the three phase leads. These porous heat sinks are the main defining feature of the module and are responsible for the low thermal resistance between the IGBT chips and the cooling fluid, which flows through the porous metal. These six porous metal structures are formed simultaneously in a furnace brazing operation where copper particles are brazed to each other and to the underside of the copper sheet at the same time. Therefore, all six are nearly identical on any one module in terms of thermal conductivity and flow restriction.

Figure 2.1-4 is a picture of the bottom side of the copper sheet with six porous copper heat-sink structures simultaneously formed and brazed in place. Three of these are on a common plane, which is the common collector of the bridge. The other three are temporarily connected together but will be separated by trimming off the copper strip holding them together so each can become a common collector-emitter connection for each phase.

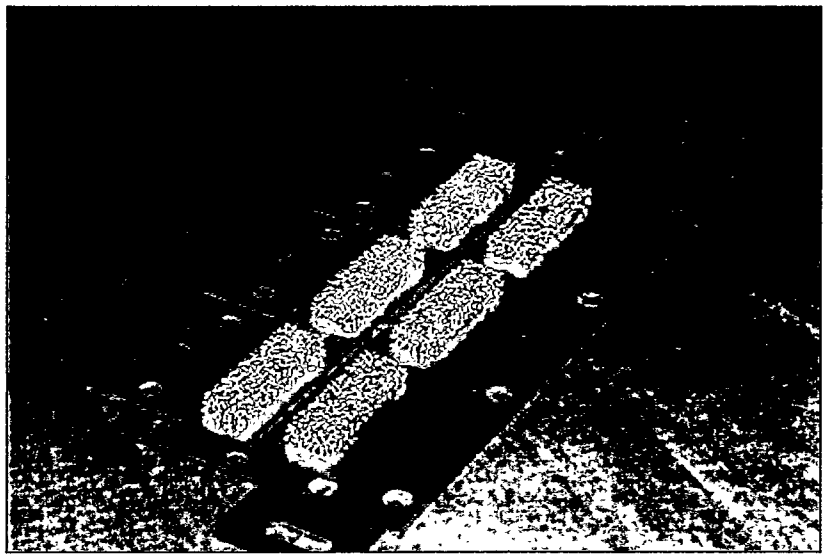

Figure 2.1-4 Copper Sheet with Porous Copper Heat-sinks

Figure 2.1-5 shows the laminated structure with the plastic coolant manifold below it and with the plastic cover/snubber assembly above it. The plastic coolant manifold directs coolant through the six heat-sinks in parallel so that all six receive the same flow rate of oil at the same inlet temperature. The plastic cover/snubber assembly protects the electronics and hold the three low inductance snubber capacitors. For this phase of the project, the manifold and cover were machined from plexiglas to make the interior visible for examination during testing. In production, the manifold and cover would be injection molded plastic parts to lower the cost. The three large blocks on top of the cover are snubber capacitors connected between the positive and negative DC planes of the module.

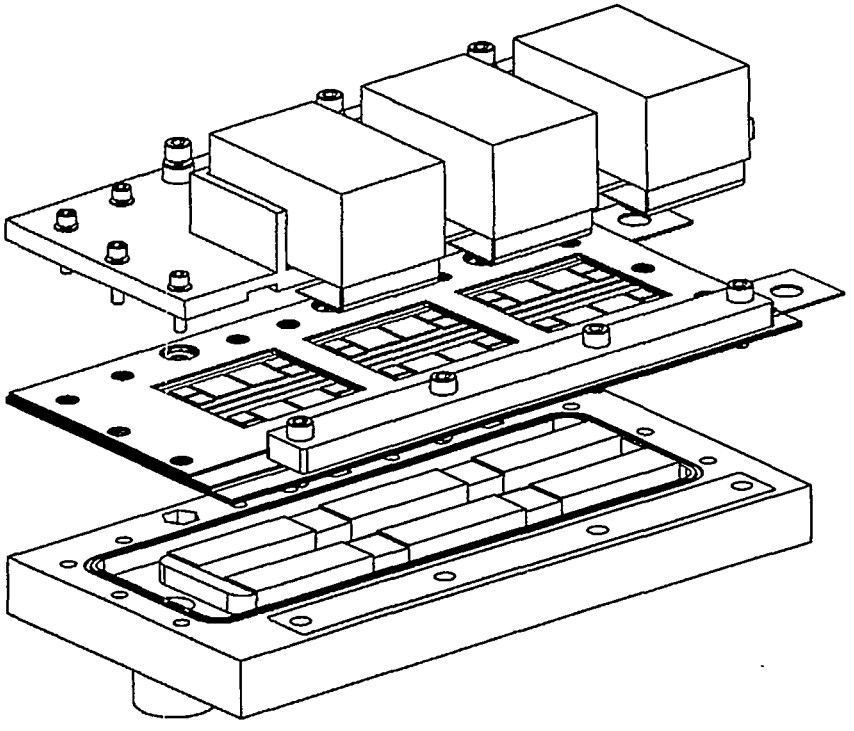

Figure 2.1-5 Exploded View of the Integrated Power Block

2.1.2.1 Thermal Path

The thermal path can be seen in Figure 2.1-6, which shows two switches in series forming one of the three poles. Each switch us made up of a metal carrier (Cu/W, Cu/Mo/Cu, Cu/graphite, etc.) with two IGBT die and four diode die mounted on the top side. After this chip mounting operation the chip carriers are screened before they are soldered to the copper layer of the laminated board containing the integral porous metal heat sinks. The thermal path is through the silicon, through the metal layers, which are either soldered or brazed together, to the porous copper heat sinks, and into the coolant pumped through them.

- **Design: Thermal Path**

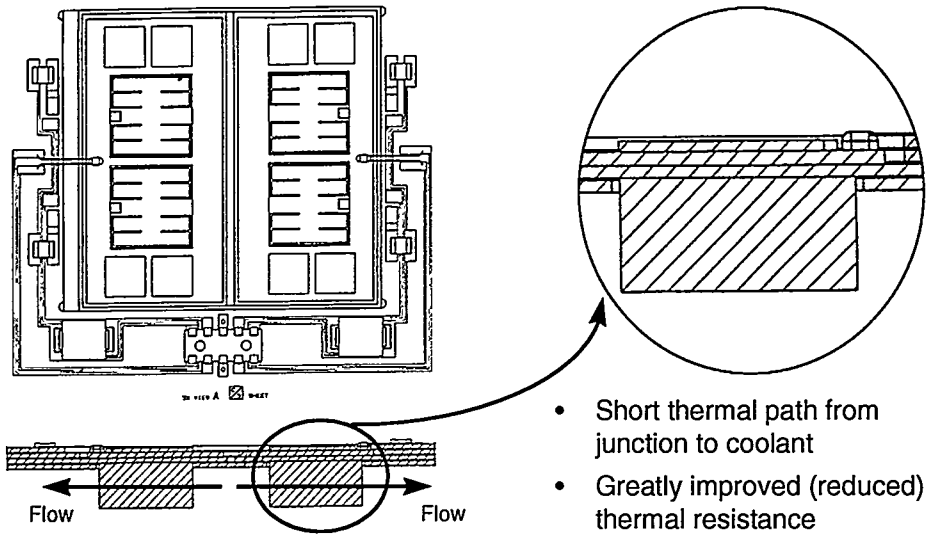

Figure 2.1-6 Top View & Profile of a Single Pole

2.1.3 Microelectronic Assembly

The microelectronics assembly effort of this task was to develop the manufacturing processes that are required to assemble modules for test and evaluation. The development results were implemented into the production of the integrated power block. The key goals were the following:

1) Remove heat, up to 1-kilowatt, from the 0.27 in ^{2} (0.523"x0.523") silicon area of each of two IGBT chips in each switch. (1.4 kW per chip was demonstrated)
2) Avoid high current regions on the semiconductor chips.
3) Provide a high current carrying capability with aluminum stitch-bonded wires
4) Avoid the domino effect failure due to uneven current sharing between connections and devices.
5) Providing voltage isolation of 500 VDC minimum.

2.1.3.1 Void-Free Solder Attachment

The assembly requires mounting 2 IGBT chips (size .523 x .523) and 4 diode chips (size .258 x .258) on metal carriers and then soldering 6 of these carrier sub-assemblies to the liquid cooled bus bars of the IPB. The process called for a hierarchy of solders; 80Au/20Sn with melting point 280°C for chip mounting on carriers done under vacuum & inert gas. For processes requiring soldering subsequent to the mounting of the chips on the carrier, a 63Sn/37Pb solder was used with a melting point of 183°C.

Vacuum soldering equipment manufactured by DAP was used. The initial vacuum soldering run used the normal 80/20 solder reflow profile. Initially, the IGBT chip soldering had considerable voids. In view of this, several fixture and solder reflow profile modifications were

tested to achieve void free soldering. The following vacuum soldering process enhancements were implemented for a successful solder reflow:

- Soldering fixture using graphite material, shown in Figure 2.1-7.
- Increase inert gas pressure in chamber.
- Add access hole to the fixture to direct gas to the chips.
- Use additional weight on each IGBT chip.
- Use ultrasonic and plasma cleaning procedures.
- Add soak time preceding the solder reflow.

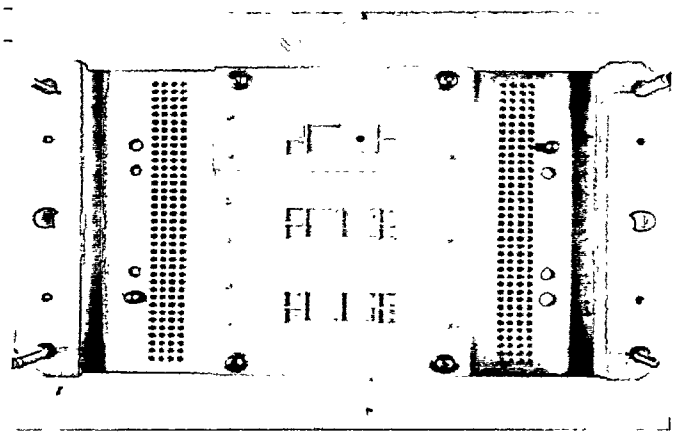

Figure 2.1-7 Graphite Chip Mounting Soldering Fixture

Figure 2.1-8 is an optical photograph of the chips mounted to a metal carrier. Figure 2.1-9 is an X-ray of the carrier assembly showing voids in the gold-tin solder using a standard solder reflow process. Figure 2.1-10 is an X-ray which shows the greatly reduced voids after optimizing the solder reflow process.

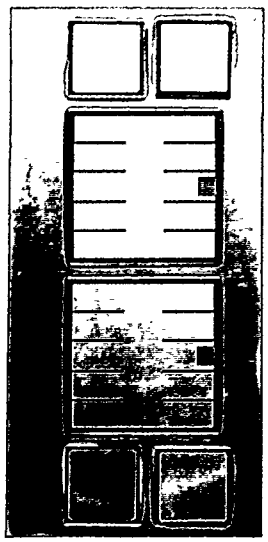

Figure 2.1-8 Carrier with Chips Mounted

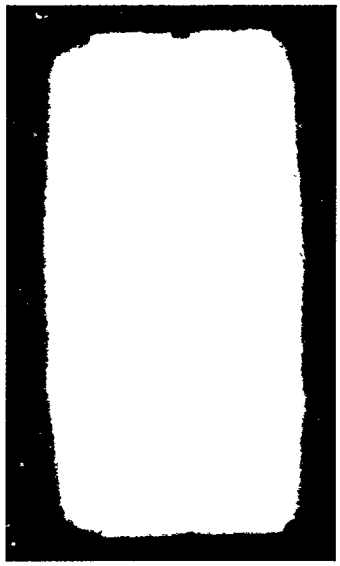

Figure 2.1-9 X-Ray of Carrier Showing Voids Under Chips

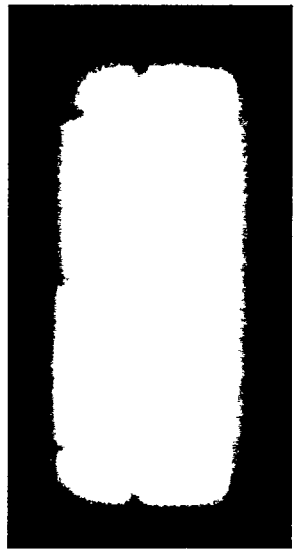

Figure 2.1-10 X-Ray of Carrier Showing Improved Process

2.1.3.2 Solder Attachment of Chip Carriers to Bus Bars

The eutectic 63 /37 tin/lead solder alloy was used for attaching the chip carriers to the copper bus bars. An experiment was performed in a glove box to determine the solder temperature profile required for use in the Watkins-Johnson's belt furnace. Two critical requirements of this process were to obtain high voltage isolation (500 VDC) and to produce void-free solder joints between the carrier and heat sink to maintain low thermal resistance. The spacing between the carriers and the edges of the DC planes had to be maintained at 25 mils minimum to meet the high voltage isolation and a minimum of 80% solder coverage had to be obtained for each carrier mounted to the bus bars of the IPB.

2.1.3.3 Wire Bonding Development

It was observed that the 20-mil diameter aluminum wire would fuse or melt at a DC current of about 40 amps when tested in still air. The proximity of the parallel wires bonding the IGBT and diode chips has less cooling than a single wire in still air. The fusing current of these parallel wire bonds has been observed to be 35 amps per 20-mil wire. As seen in Figure 2.1-11, the lower switch has eighteen 20-mil wires bonded to the two IGBT chips. The upper switch, not shown, has 20. The lower switch is defined as the one with its emitter connected to the negative DC plane. The position of the gate bond wire in the lower switch makes it necessary to eliminate one of the 20-mil bond wires. The current limit of the lower IGBT switch, based on the fusing of bond wires, is 630 amps in air. This low current was identified as a potential limitation to the performance of the IPB. An alternative cooling concept of flowing cooling oil directly over the chips and wire bonds was explored for raising the 630 amp limitation. A single, 20-mil aluminum wire tested in still cooling oil fused at a DC current between 100 and 115 amps. The current limit of the lower IGBT switch, based on the fusing of bond wires, is 1800 amps with oil cooling flowing past the wires on the top side of the switch in addition to the oil flowing through the porous copper heat sinks. Tests were conducted using both the non-flooded and flooded cooling approaches.

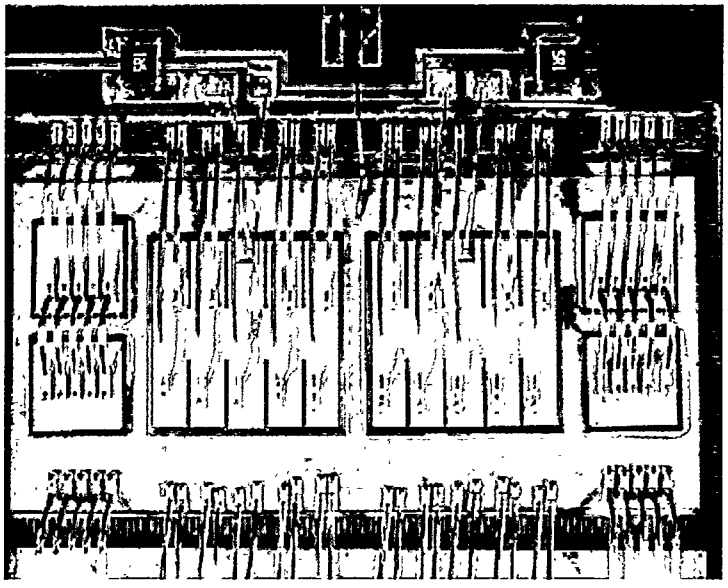

Figure 2.1-11 Chip Carrier with 20 mil Wire Bonds

The 0.020 inch diameter aluminum wire bond process for the IGBT and diode chips had to be developed. The development was done using both a K&S manual ultrasonic bonder and an Orthodyne 360 automatic heavy ultrasonic bonder. A critical aspect of bonding the 20-mil aluminum wire was the selection of bonding parameters. They must allow each wire to be bonded on a thin IGBT chip without electrically or mechanically damaging the device. It was uncovered that 0.020" aluminum wire was not used in industry and user guidelines of the wire bond process had not been established. During the first development phase, 20% of the IGBT devices failed electrical test largely due to damage incurred during the wire bonding process. A Design of Experiment statistical process control step, was incorporated to establish the optimum bonding parameters

Design Of Experiment (DOE) was used to improve yield or optimize a manufacturing process. The experiment used the Orthodyne Model 360C, an automatic large wire bonder. A central composite design of experiment was chosen with 3 different factors on two types of wire, SPM .9999 Al and SPM .99999 Al. The parameters tested were the following:

1) force - gram force exerted by the tool onto the work surface.
2) time - duration of ultrasonic energy output to the transducer.
3) power - level of ultrasonic energy output to the transducer.

The bonding process was applied on experiment coupons, which were identical to IGBT chips attached to metal carriers used for the IPB. Prior to wire bonding, the IGBT die were examined for damage, such as cracks and scratches, and then tested electrically. After wire bounding, sample coupons that passed the visual and electrical test were subjected to high current tests. Each IGBT chip was subjected to a high current DC test, and high current AC test.

After all testing was completed, sample coupons that passed the visual and electrical test were destructively tested. Some were subjected to tensile pull tested before and after the heat-age test at 300°C for 1 hour. Others were subjected to higher and higher current levels until failure occurred.

2.1.3.4 Microelectronics Final Assembly Process

The final assembly process was used to build prototype integrated inverters. This process is summarized in Table 2.1-1. Figure 2.1-12 is a photograph of a completed IPB's laminated structure.

Table 2.1-1 Chip Bounding Process

Step No.	Process Description
1	Wire bond IGBT chip subassemblies, such that one end of each wire is connected to the IGBT chip, the other end of this wire is left unconnected (pig tail).
2	The subassembly is then subjected to the electrical test.
3	Solder mount six IGBT subassemblies (prepared per steps #1 & #2) on the bus bar assembly using 63Sn/37Pb solder preforms, hydrogen belt furnace, and the fixture fabricated for this soldering process.
4	Tack the loose ends of wires in step #1 to the bus bars of the inverter.
5	Hand solder surface mount devices, such as connectors, resistors, zeners, and thermistors using 63Sn/37Pb solder.

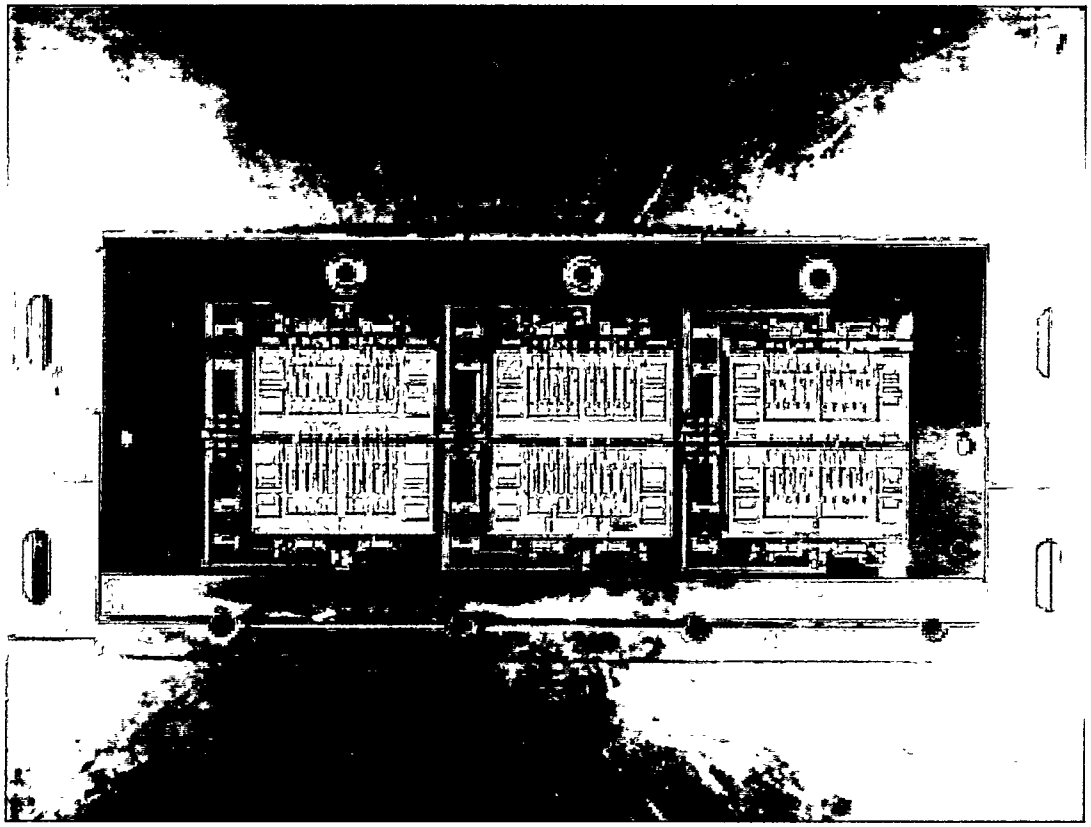

Figure 2.1-12 Integrated Bridge Showing Soldering and Wire Bonding

2.1.4 Integrated Power Block Testing

2.1.4.1 Switch Test

Each switch of the fully assembled inverter was subjected to an electrical test at the maximum current and voltage rating of the IPB. This required high current and voltage measurement equipment, an IGBT custom designed driver circuit, and an inductive load. The electrical test power level was initially 450-ampere DC at 350 VDC. As electrical testing continued, the test current eventually increased to a final (one-time) test of 1000 amps (DC conduction loss at low voltage). To support the original design intent, the goal of the manufacturing process development was to obtain a minimum power density 1,300 watt / in^2, which is about double the existing state-of-the-art value (750 watt / in^2). The 1000 amp test mentioned above, was over 5,000 Watts per square inch.

2.1.4.2 DC Voltage Overshoot Test

A test was run to determine the effectiveness of the low inductance snubber capacitors in terms of controlling the DC voltage overshoot when the IGBT switches turn off. Figure 2.1-13shows the results of two switching tests superimposed on the same graph. One test was run on the standard bridge which is made up of Powerex 400 amp IGBT modules and the other one is of the integrated bridge. In each case the switch under test is turned off and the voltage vs. time history of the DC link is measured and recorded.

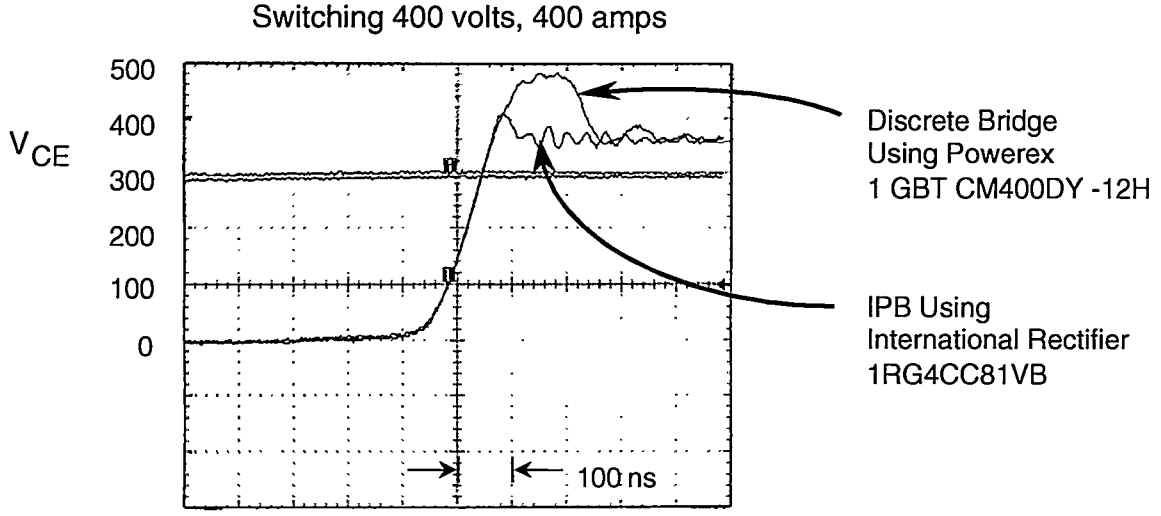

Figure 2.1-13 Low Inductance IPB Reduces Over-Shoot By 67%

In both cases, the DC link voltage was 360 volts. In the case of the standard bridge, the DC voltage came up to about 480 volts before settling back to 360 volts. The integrated bridge switch came up to about 400 volts before settling back to 360 volts. The overshoot for the standard bridge was about 120 volts and for the integrated bridge, about 40 volts. The inductance of the improved capacitor was measured at about 5 nano-Henrys compared to about 50 nano-Henrys for the standard capacitor.

2.1.4.3 DC Thermal Dissipation Tests

DC tests were run on the switches where the DC current and voltage drop across the IGBT die (collector to emitter) were data-logged in order to measure DC power dissipation. Each of the six chip carriers had a 10 K Ohm miniature thermistor mounted near the two IGBT die. The oil inlet temperature and thermistor temperature were also data-logged and plotted (see Figure 2.1-14). During this test, the gate voltage was toggled on and off by hand at approximately five-second periods in order to observe temperature response. The thermal resistance from the chip carrier to the coolant inlet temperature was almost exactly 0.10 degrees C/Watt (per switch) in this test. The porous copper heat sinks were cooled but the coolant was not flowing past the top surface of the die. The graph shows a dissipation of one kW and a carrier-to-oil temperature difference of 100 degrees C measured from the top of the chip carrier to the cooling oil inlet (Mil L-23699 synthetic oil). The one KW dissipation recordings were at a current of about 468 amps (DC) and a collector to emitter voltage drop of about 2.13 volts.

In another thermal dissipation test, a switch was tested first with coolant provided only to the porous metal heat sink and then again with coolant flowing both through the porous metal heat sink and over the tops of the IGBTs. The coolant was PAO, polyalphaolefin dielectric coolant fluid, Mil-C-87252B. The coolant was allowed to enter the three chambers above the three poles by drilling two small holes between the upper and lower switches of each pole. The holes were drilled through the polyimide-glass board which is laminated to the under side of the bus bar structure. These holes are right above the inlet channel of the lower coolant manifold so they allow coolant to flow to the topside of the structure. The cover of the module was designed with flow channels, which allow the coolant to escape through the cover and flow to the lower main manifold where it can exit the module.

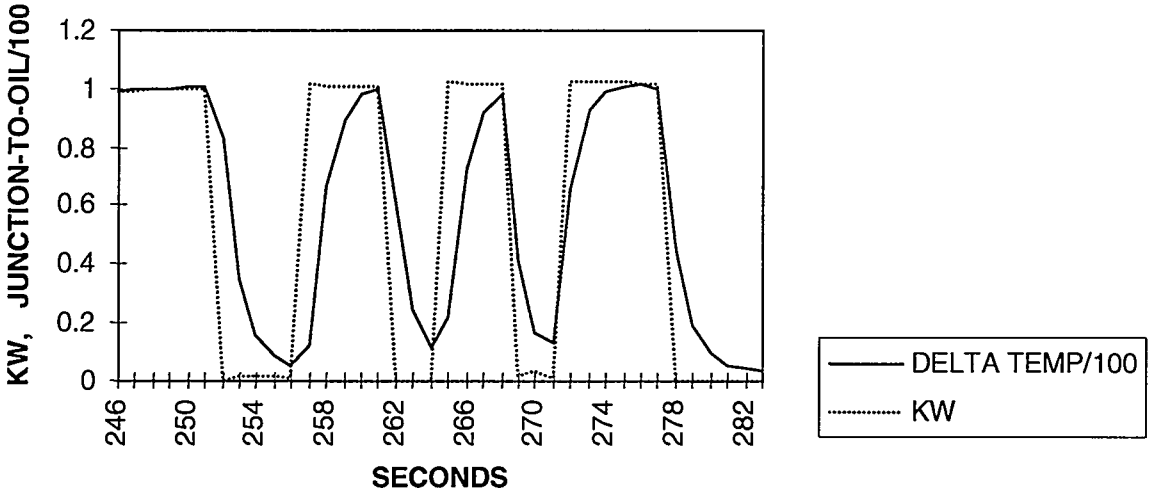

Figure 2.1-14 Junction Temperature and Output Power Data

Figure 2.1-15 shows the results of the test with and without coolant flowing over the chips and wire bonds. During the first 125 seconds of the x-axis, the current was slowly increased to 600 Amps. The voltage drop across the IGBTs increased to about 2.15 volts and the power dissipation increased to about 1.3 kW. The heavy green line is the thermal resistance calculated at each data entry point, that is, once per second. It is found by subtracting the switch temperature from the coolant inlet temperature and dividing by the calculated power. When the switch thermistor temperature stops changing, the calculated number is the thermal resistance measured from the thermistor to the coolant, about .08 degrees C/Watt for this switch.

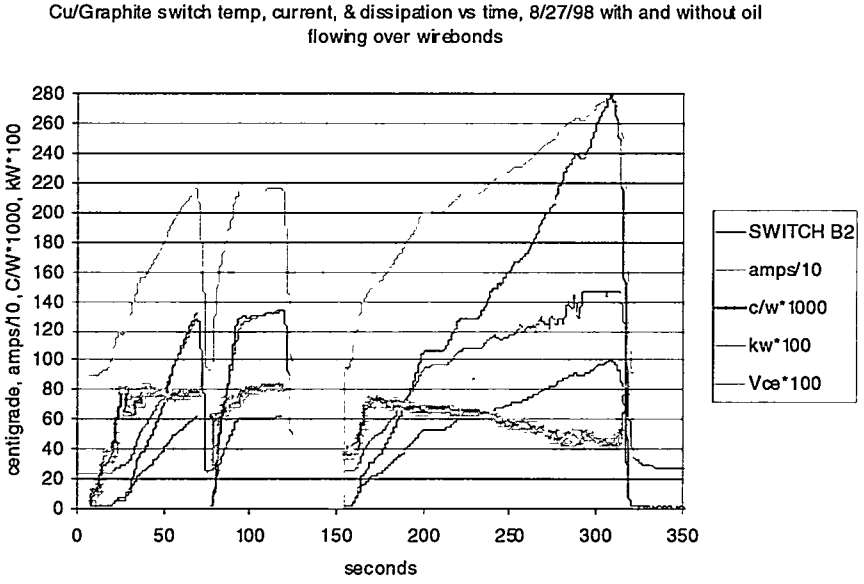

Figure 2.1-15 High Power DC Test Comparing Non-Flooded and Flooded Cooling

The rest of the graph shows the same switch with coolant flowing over the topside of the IGBTs

as well as through the porous heat sinks. In this case the current was slowly increased to 1000 amps, the voltage drop increased to 2.8 volts, the dissipation increased to 2.8 kW. The heavy green line representing the thermal resistance decreases from about .07 degrees C/Watt to about .05 degrees C/Watt at full power. The reason for this noticeable decrease is probably due to the decreased viscosity of the coolant oil. The film coefficient, and therefore the heat transfer, is higher with lower viscosity. The power dissipation in this DC test was over 5000 Watts per square inch of silicon (787-watts/square cm). The temperature was too high for silicon (160 C) but not too high for silicon carbide.

This data is plotted in another way in Figure 2.1-16. In this graph, the switch thermal resistance is plotted against the switch dissipation with and without cooling oil flowing over the wire-bonds. For comparison, the thermal resistance of the standard bridge is shown.

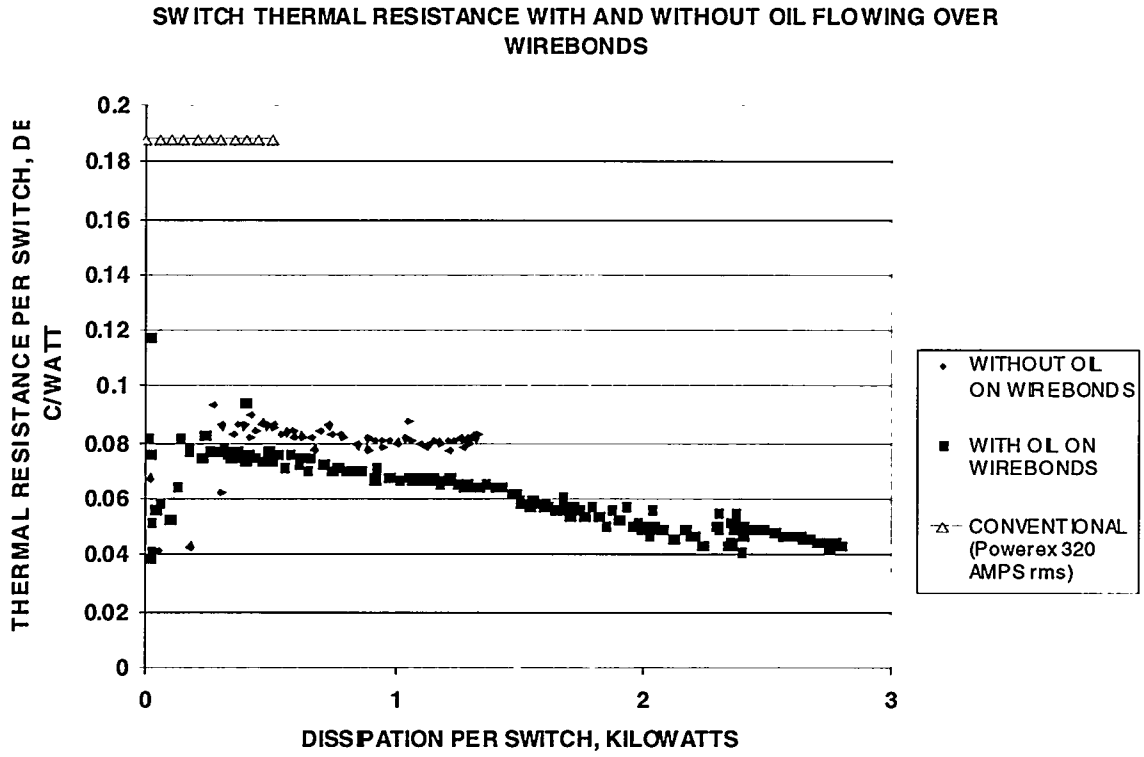

Figure 2.1-16 Thermal Resistance With & Without Oil Flowing Over Wire Bonds

2.1.4.4 AC Dynamometer Tests

The integrated bridges were designed so they would fit into the motor controller that was developed for the electric bus motor drive. This motor controller was designed with two of the standard bridges made up of discrete 400 amp Powerex IGBT modules. Each of the two bridges drives a separate 3-phase winding in the bus motor. When the bus motor was used to test the integrated bridge, both windings of the motor were connected to the integrated bridge in parallel.

While the bus motor was driving a dynamometer load, the six thermistors on the integrated

bridge switches were recorded with a data logger, once per second throughout the test. In one test, done on 10/1/98, the bridge was cooled by the porous metal heat sinks only (without oil cooling on the topside of the chips). The shaft horsepower was indicated with a Lebow rotary torque sensor and RPM counter. The motor speed was held at 7,000 RPM and the controller current and dynamometer load were increased to produce a reading of 25 shaft HP. This was held for one minute and then increased to 50 HP for one minute, then 75 HP, 100 HP, 125 HP, 150 HP, and 175 HP each for one minute. At this level, the highest switch thermistor temperature was about 95 C (and the lowest about 75 C). We had seen switch temperatures much higher than that in the DC tests, but increasing the power higher caused catastrophic failure of the bridge.

Another bridge was prepared for test with the same motor and dynamometer. This bridge had holes drilled through the laminated structure to allow cooling oil to flow directly on the chips. The test was done in a similar manner by holding the power at 25, 50, 75, 100, 125, 150 and 175 HP for one minute. When the power was increased beyond 175 HP the IPB, once again, failed catastrophically.

Figure 2.1-17 shows the switch thermistor temperatures recorded over time for the "dry" test first, up to the 550 second mark an the x axis, and the "wet" test shown on the rest of the graph. Figure 2.1-18 shows the average of the 6-switch temperature recorded during the two-dynamometer tests. The lower line is the average temperature of the switches when cooled with oil flowing on top of the switch as well as through the porous metal heat exchangers.

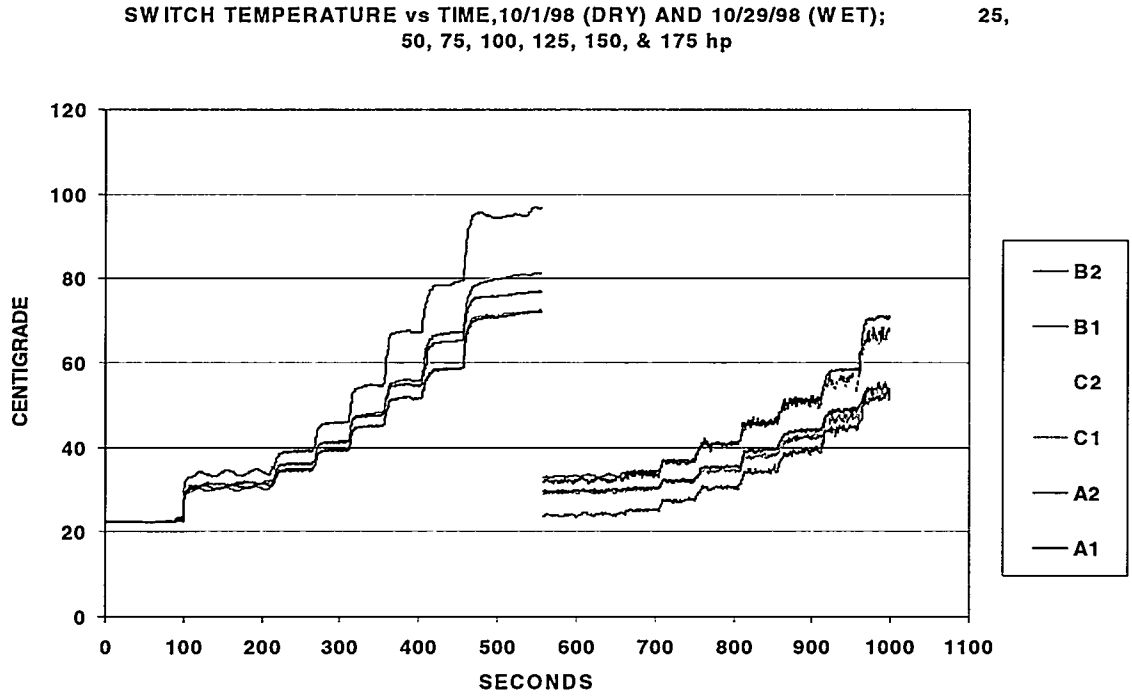

Figure 2.1-17 Switch Temperatures at Various Power Levels

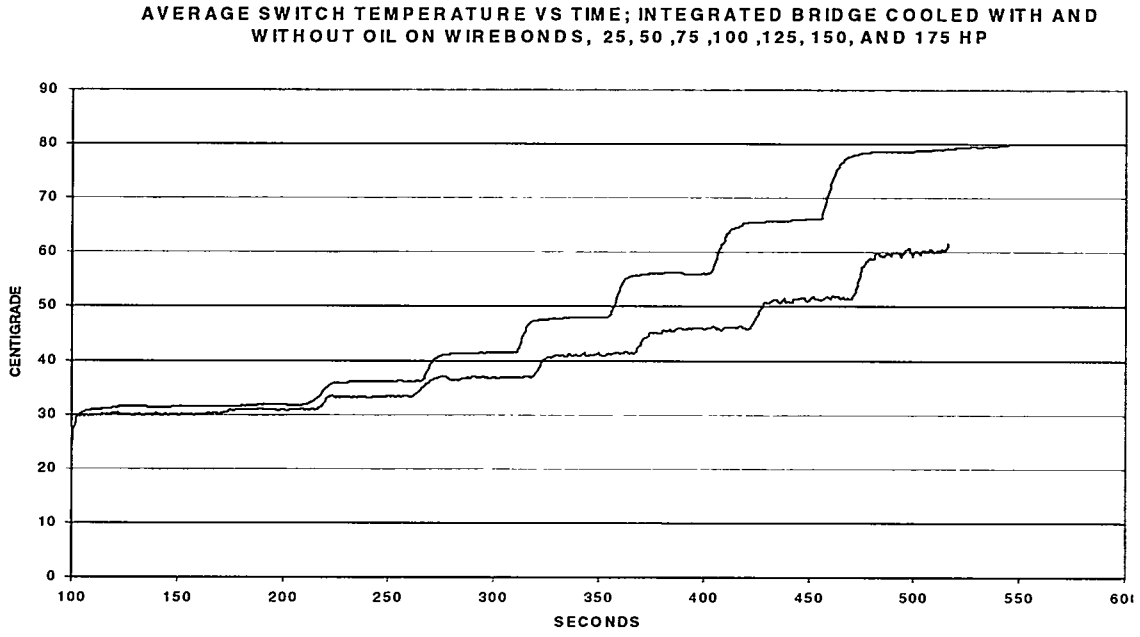

Figure 2.1-18 Temperature Comparison With and Without Oil on Chips

Due to the catastrophic failures of the IPBs at thermistor temperatures well within the silicon's operating range, an investigation was initiated to determine the cause(s) of the failures. Tests conducted on an IPB driving an electric motor at a continuous power level of 175 HP, indicated a maximum thermistor temperature of only 95°C, 65°C above ambient. Based on this data the IPB should have been able to drive the motor to 250 HP without exceeding 125°C on the thermistor. The 125°C represented a very conservative junction temperature, however the IPB failed violently has soon as the power was increased above 175 HP. Other IPB modules failed in a similar fashion. The IPB driving a 175 HP load continuously met the expectations of the IPB, however the weakest link known to exist in the design was for wire bond fusing (melting) at a power level of over 200 HP.

Several areas were selected for investigation. The conductivity of the oil flowing over the wire bonds, the gate drives, the difference in temperature between the thermistor and the IGBT chips and the sharing of losses between paralleled chips.

Conductivity of the Cooling Oil

Before the IPBs were tested at high power, they were all subjected to high potting tests. 550 VDC was applied across the supply rails and from the rails to chassis to check for leakage and voltage break down. Some clearance problems and assembly defects were found and corrected via these tests. As an extra precaution high potting to 500 VDC of each individual arm of the bridge was initiated during this investigation. Units that passed high pot tests without cooling oil on the wire bonds were then subjected to the same high pot tests with oil flowing over the wire bonds.

When the IPB voltage break down test was performed with cooling oil flowing over the chips numerous voltage break downs were detected. It was known that the cooling oil (Exxon 2389) fresh out of the drum had a very high resistivity, therefore, water and/or particle contamination was suspected. The two oils that are normally used for cooling the electric vehicle powertrian

systems (Exxon 2389 and Braco 881) were found to be hydroscopic (will absorb moisture directly from air). To avoid the possibility of water and eventually acid contamination of the oil a fresh supply of Royco 602 was obtained for use in further testing. This oil is >98% PAO (polyalphaolefin) and is not hydroscopic. High pot tests were now run with a much higher success rate. Only IPBs that passed the oil immersed high pots tests were used for further testing in oil.

Gate Drive Investigation

The paralleled IGBT chip arrangement used in each pole of the IPB was also used in a commercial IGBT module. The data sheets for this module provide dynamic characteristics using a +/-15 VDC gate drive with 15 Ohms for a turn on resistance and 0 Ohms for a turn off resistance. The gate drive used during high power motor drive tests also has +/-15 VDC supplies but has 12.5 Ohms for both turn-on and turn-off. This raised a concern that the IGBT gates were neither being turned off nor held off hard enough.

When an "off" IGBT is subjected to the reverse recovery of its freewheeling diode, the collector voltage rises quickly from a level close to zero to a level close to full link voltage. This high dv/dt causes current to flow through the collector/gate capacitance and raises the gate/emitter voltage. If the gate is not biased off through a sufficiently low impedance this rise in gate/emitter voltage can turn "on" the supposedly "off" IGBT. This can lead to a shoot-through condition destroying the pole. The switching waveforms of the IPB were examined for any sign of this problem.

Figure 2.1-19 shows the voltage waveforms across both IGBTs in a pole that is switching 400 Amperes through an inductive load in parallel with an off top IGBT as the bottom IGBT is turned on. Figure 2.1-20 shows the current in the top IGBT as its diode goes through reverse recovery. The turn-on voltage waveform of the bottom IGBT shows a slight discontinuity but the current waveform is clean giving no indication of a shoot through. This pole was tested for several 50% duty cycle pulses at an 8 kHz rate to an average of 900 Amperes as shown in

Figure 2.1-21. No abnormal conditions were detected. The output resistance of the standard gate drive was cut in half to see if driving the gate harder had any advantages. The resulting gate drive waveforms showed higher than desirable oscillations and it was decided not use the stiffer gate drive for any further testing. No problems were found with the gate drive and gate drive faults were ruled out as a cause of IPB failures.

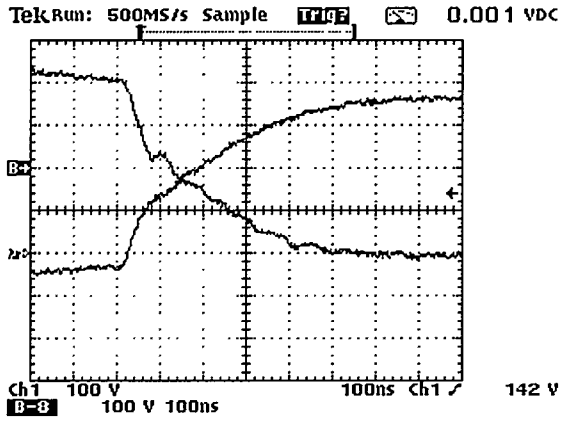

Figure 2.1-19 IGBT Voltage Waveform

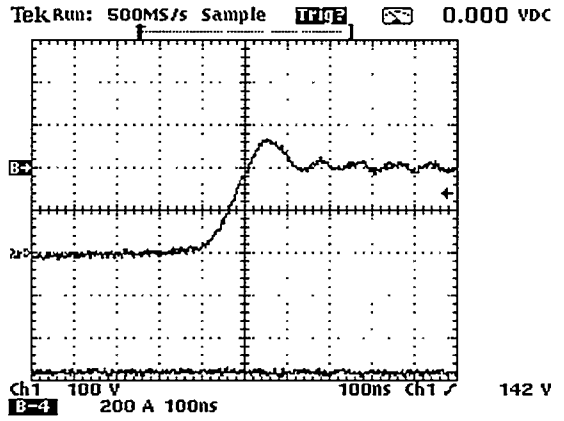

Figure 2.1-20 IGBT Current Waveform

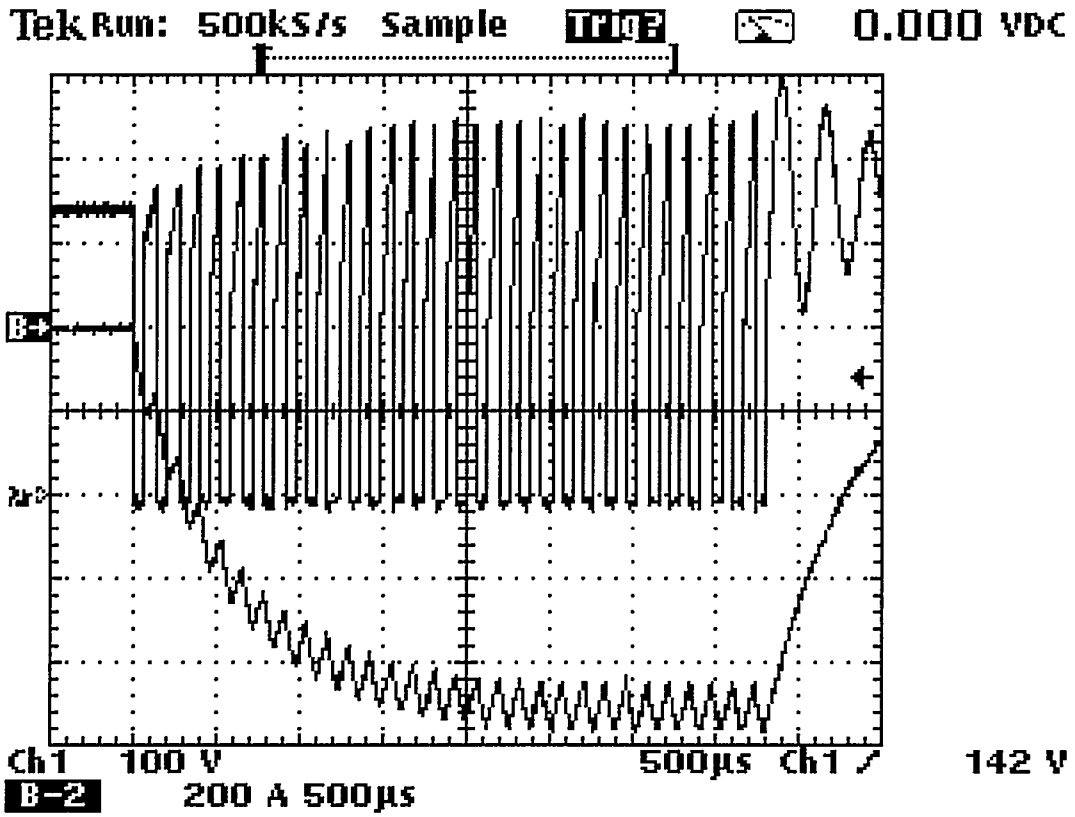

Figure 2.1-21 8kHz Single Pole Output

High Temperature Investigation

Tests were conducted on individual switches in an IPB to determine the maximum temperature of each chip under varying load and switching frequency conditions. The maximum surface temperature of each chip was measured using an IR camera. Because the IR camera can not "see" well through oil or the IPB cover, these tests were conducted without cooling oil flowing over the chips and with the cover removed. The temperatures measured by this method should be very close to the maximum junction temperature. For the following discussions it is assumed that the maximum temperatures measured by the IR camera are accurate representations of the hottest spots in the chip junctions.

The IR thermal imaging proved to be an excellent method for monitoring the surface temperatures of the chips. When initially investigating the potential use of an IR thermal imaging system, it was uncovered that a process for using the IR camera on exposed chips of a power circuit had not been established by industry and that such a process would have to be developed. The process developed in support of this investigation is detailed in a later section of this report. Also, when working with IGBTs it is understood that a local hot spot will cause the IGBT to go into thermal runaway when that spot gets to a high enough temperature. The maximum allowable hot spot temperature seems to vary from chip to chip and from manufacturer to manufacturer but generally in the range of 150°C-175°C.

Three switches were tested with load currents of 110 and 220 Amperes at DC and at three AC switching frequencies (4, 8 and 12 kHz, each with a 50% duty cycle). During the DC tests, saturation voltages across the IGBTs were measured to provide an accurate power loss in each switch. The DC input voltage during these tests was 340 Volts. The data collected is shown in Table 2.1-2.

Since the power lost in each chip was not known, an effective thermal resistance had to be calculated. The effective thermal resistance can be calculated by taking the greatest temperature rise between the cooling oil and surface of the chip and dividing it by the average power lost in that switch. The three switches tested had effective thermal resistances between 0.163 and 0.248 °C/Watt. The cause of the large variation was not determined but it may be due to differences in mounting, differences in chips and how well the two parallel IGBT chips shared the losses.

In previous calculations of thermal resistance, it was assumed that the temperature of the thermistors provided a good estimate of the chip temperatures. This was shown not to be the case indicated in the data of Table 2.1-2. The chip temperatures were much higher than the thermistor temperatures, by as much as 46°C for the lower switch in pole-C running at 220 Amperes and 12 kHz. When the data logger temperatures are corrected for the proper thermistor curve this maximum difference increases to about 51°C, almost half of the rise from cooling oil to chip. This indicates that the thermistors on the chip carriers should not be used to monitor junction temperatures of the chips.

In general the temperatures of the two IGBT chips in each switch are fairly close ($\Delta T < 4°C$) during the DC tests. This indicates that the two chips are sharing conductive losses fairly well. When switching losses are introduced the differences become much greater. In the case of the lower switch in pole-C, the ΔT actually changes sign. At DC, I1 appears to have slightly more conduction losses than I2 but when switching, I2 has much higher temperatures than I1. This indicates that I2 is taking more of the switching losses than I1. Matching IGBTs to share conduction losses is standard practice but forcing them to share switching losses is much more difficult. This inability to share losses must be accounted for in the maximum power rating of paralleled IGBTs. The lower switch in pole-C has the worst ΔT between IGBT chips and a thermal resistance of 0.185 °C/W. If the worst ΔT and the highest thermal resistance occurred on the same switch, the chip temperatures would be even higher and the power rating would be further reduced. The switching losses from the lower switch in pole-C and the effective thermal resistance of the upper switch in pole-C (highest thermal resistance) will be used to estimate a worst case temperature rise of an IPB chip while driving a motor.

By using the thermal resistances calculated from DC data and the temperature rise of the chips during switching, the switching losses in the IGBT chips can be estimated. For the lower switch in pole-C, the total losses at 8 kHz and 220 Amperes are estimated to be (113 °C – 27.2 °C)/(0.185 °C/W) = 464 Watts. The conduction losses are estimated to be half the DC losses at 220 Amperes or 161 Watts. The switching losses are the difference or 303 Watts. The actual switching frequency for the 8 kHz tests was 7827 Hz, which is the motor drive PWM frequency. The energy lost per cycle at 220 Amperes is therefore 303/7827 or 0.039 Joules. The IGBT collector/emitter saturation voltage measured during testing was 1.5 Volts at 220 Amperes and 1.9 Volts at 440 Amperes. This agrees very well with the manufacturer's typical switching loss and saturation voltage data.

Table 2.1-2 IGBT Temperature Data

Switch	Amps	Data Item	DC Power (W) Total (I1+I2)	Temp (° C) DC	Temp (° C) at Frequency (50% Duty Cycle) in kH: 4	8	12
Upper Switch, Pole C (diodes on lower switch)	110	I1	139 5	60 5	51.6	58 0	67 7
		I2		58 3	49.3	53 3	61 4
		D1		n/a	43 8	42 2	44 4
		D2		n/a	43 9	41 6	44 3
		D3		n/a	43.5	42 7	44 4
		D4		n/a	43 1	42 5	43 4
		Upper Switch Thermistor, IR Camera Reading		48 9	44 1	47 6	53 6
		Lower Switch Thermistor, IR Camera Reading		26 7	32 7	31 0	32 0
		Upper Switch Thermistor, Datalogger Reading		48 4	45 6	47 5	57 7
		Lower Switch Thermistor, Datalogger Reading		25.7	31.9	30 0	32 1
		Estimated Oil Temperature (avg. of other thermistors)		25.9	26.6	25 0	26 6
		Thumbnail Code		B08	B06	A01	B04
		Appoximate Time of Video Recording		12:21 PM	11 55 AM	11 00 AM	11 30 AM
		Date of Video Recording		2/23/99	2/23/99	2/18/99	2/23/99
	220	I1	315 4	97 8	85 2	108 0	125 0
		I2		93 9	78.1	98 1	109 0
		D1		n/a	65 5	65 3	70 0
		D2		n/a	67 1	65 4	71 3
		D3		n/a	64 5	65 3	68 0
		D4		n/a	65 3	65 5	69 5
		Upper Switch Thermistor, IR Camera Reading		70 9	66 0	73 9	83 6
		Lower Switch Thermistor, IR Camera Reading		29 8	40.6	39 9	43 6
		Upper Switch Thermistor, Datalogger Reading		72 2	67 8	73 4	94 7
		Lower Switch Thermistor, Datalogger Reading		27 1	39.5	37 9	41 6
		Estimated Oil Temperature (avg. of other thermistors)		27 0	28.1	27 7	30 3
		Thumbnail Code		B09	B07	A02	B05
		Appoximate Time of Video Recording		12.21 AM	11.55 AM	11 00 AM	11 30 AM
		Date of Video Recording		2/23/99	2/23/99	2/18/99	2/23/99
Lower Switch, Pole C (diodes on upper switch)	110	I1	140 7	54.9	47.5	58.7	69 5
		I2		53 3	48.7	64 4	79 1
		D1		n/a	41.3	46 7	49 4
		D2		n/a	42.4	47 1	49 8
		D3		n/a	40.5	45 7	48 0
		D4		n/a	42.6	46 8	49 1
		Upper Switch Thermistor, IR Camera Reading		25 5	30.6	31 6	34 6
		Lower Switch Thermistor, IR Camera Reading		41 9	42 4	45 4	58 7
		Upper Switch Thermistor, Datalogger Reading		24 8	30 7	29 8	31 9
		Lower Switch Thermistor, Datalogger Reading		45 6	42 8	46 1	55 1
		Estimated Oil Temperature (avg. of other thermistors)		25 6	26 1	25 3	26 4
		Thumbnail Code		A09	A11	A03	B02
		Appoximate Time of Video Recording		5 06 PM	12.13 PM	11 00 AM	11 10 AM
		Date of Video Recording		2/18/99	2/19/99	2/18/99	2/23/99
	220	I1	321.4	90.0	79.1	101 0	122 0
		I2		86 1	81 6	113 0	141 0
		D1		n/a	63.2	72 1	78 8
		D2		n/a	67 6	75 0	81 0
		D3		n/a	60 7	69 7	77 4
		D4		n/a	65.7	73.0	80.8
		Upper Switch Thermistor, IR Camera Reading		27 1	38.3	40 3	43 6
		Lower Switch Thermistor, IR Camera Reading		67 9	63.2	74 4	83 6
		Upper Switch Thermistor, Datalogger Reading		25 7	39.0	36 6	41 6
		Lower Switch Thermistor, Datalogger Reading		69 0	65.4	71 5	94 7
		Estimated Oil Temperature (avg. of other thermistors)		26 8	29 0	27 2	28 7
		Thumbnail Code		A10	A12	A04	B03
		Appoximate Time of Video Recording		5.06 PM	12.13 PM	11 00 AM	11 10 AM
		Date of Video Recording		2/18/99	2/19/99	2/18/99	2/23/99
Lower Switch, Pole A (diodes on upper switch)	110	I1	143 3	49 3	44.9	52 2	57 5
		I2		50 0	46.6	55 4	64 0
		D1		n/a	40.2	41 5	42 0
		D2		n/a	42.0	43 3	44 6
		D3		n/a	39.9	41 0	42 0
		D4		n/a	41.3	43 2	44 2
		Upper Switch Thermistor, IR Camera Reading		25 7	29.8	30 6	30 9
		Lower Switch Thermistor, IR Camera Reading		41.3	40.5	45 5	44.1
		Upper Switch Thermistor, Datalogger Reading		25 1	28.9	29 7	29 9
		Lower Switch Thermistor, Datalogger Reading		40 9	38 3	43 3	48 1
		Estimated Oil Temperature (avg. of other thermistors)		24 9	24 5	24 8	24 9
		Thumbnail Code		A07	B10	B12	B14
		Appoximate Time of Video Recording		4 35 PM	3.25 PM	3 57 PM	4 16 PM
		Date of Video Recording		2/18/19	4/9/99	4/9/99	4/9/99
	220	I1	323 9	78 6	70.8	84 6	101 0
		I2		80.6	74.3	91.3	114 0
		D1		n/a	59.2	61 2	62 2
		D2		n/a	64.3	67 5	69 1
		D3		n/a	58.2	60 8	62 8
		D4		n/a	63.2	66 6	68 4
		Upper Switch Thermistor, IR Camera Reading		26 8	36.1	36.7	37 0
		Lower Switch Thermistor, IR Camera Reading		60 9	57.6	62 1	76 5
		Upper Switch Thermistor, Datalogger Reading		26 1	35.4	35 3	35 6
		Lower Switch Thermistor, Datalogger Reading		59 6	56.5	64 5	71 9
		Estimated Oil Temperature (avg. of other thermistors)		25 9	25.4	25 7	25 9
		Thumbnail Code		A10	B11	B13	B15
		Appoximate Time of Video Recording		4 35 PM	3.35 PM	4.05 PM	4 20 PM
		Date of Video Recording		2/18/99	4/9/99	4/9/99	4/9/99

Formulas for calculating the losses per switch in a three-phase PWM drive can be found in the POWEREX® Applications and Technical Data Book. Using these formulas and the measured/calculated values above, the switch with highest losses would dissipate 600 Watts in the IGBT chips when driving a motor at 175 HP. Using the highest effective thermal resistance (without oil flowing on top of the IPB) of 0.248 °C/W, the worst case temperature rise of the chips could be as much as 149 °C. If maximum values (from the chip manufacturer's data sheets) are used for the collector/emitter saturation voltages, this temperature could be has high as 180 °C. Higher still if worst case switching losses are used.

With oil flowing over the chips the thermal resistance and temperature rise would be reduced. How much should be the object of further study. Even if we assume the effective thermal resistance is reduced to 75% of the above values, the temperature rise would still be at least 112 °C. This would produce junction temperatures too close to the maximum rating of 150 °C.

Conclusions of the Investigation

Although the investigation was not absolutely conclusive as to the cause of the IPB failures at high power levels, many of the suspect causes were eliminated. If the IR camera thermal data is accurate then thermal stress within the IGBTs is evident. It is likely that the inability of the IGBTs to share switching losses equally and the worst case effective thermal resistance of the IPB would lead to a thermally over-stressed IGBT when trying to drive a motor above 175 HP. It should also be noted that in discussions with various IGBT manufacturers during the course of this investigation, the manufacturers all considered their processes of balancing switching losses between parallel IGBT chips as proprietary.

2.1.4.5 IPB Silicon Chip Temperature Measurement

The basic IPB was designed with thermistors placed in predefined locations to provide temperature information during test and operation of the IPB. This method of measuring temperature is limited by the fact that only the local temperature in the area surrounding the thermistor is measured. We utilized these thermistors in most of the IPB testing, however, as we pushed the IPB towards the limits of its capability it was decided that a more robust method of measuring IPB temperature was needed. The goal was to find a method of determining temperatures of the chips themselves and the temperatures of the wire-bond connections. This will allow us to accurately set a maximum operating power that has a reasonable margin of safety. It can also be used to verify thermal models.

It is difficult to measure the actual temperature of the junction(s) in a silicon chip. Additional thermistors can be glued to the top surface, but they measure the temperature of those points only. It cannot provide a temperature map of the whole surface. Thus, it is possible that the thermistor is not located on the hottest spot. The thermistor also occupies some surface area that might be used for wire-bonds. The thermistor wires must also be routed to a data logger, adding addition wiring operations. A small temperature probe is not useful here either. Direct probing of the IPB may lead to shorting the chip or damaging the chip or its wire-bonds during probing. Getting a temperature map of the silicon surface would be very time consuming and prone to operator error. In addition, the IPB operates at hazardous voltage levels.

Infrared (IR) thermal imaging offers a promising method of measuring silicon surface temperatures. An IR camera allows you to determine a temperature profile for all surfaces in the camera's field of view. In theory, we should be able to aim the camera at the IPB and get temperature readings for all the chips. A successful method of using IR was investigated and it is detailed below.

2.1.4.5.1 Thermal Recording Process

The IR camera selected to aide the detailed thermal investigation was Inframetrics' SC-1000 and is shown in Figure 2.1-22. It is light and portable and is available with remote control and analysis software.

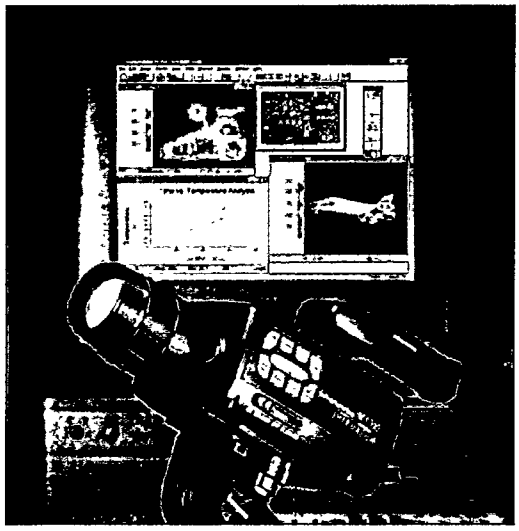

Figure 2.1-22 Inframetrics' SC1000

Prior to using the thermal imaging system, the environment for testing had to be defined. For an IR camera to provide "true" thermal data, the object being imaged must have a high emissivity (>0.8). Unfortunately the top surface of silicon chips is highly reflective and has a low emissivity (<0.1). This will cause the camera to give false temperature readings because the chip's IR emissions would be "hidden" by the IR reflections of nearby objects (i.e. lights, hot water pipes, other electrical equipment). To get accurate temperature readings of the IPB's chips, they must be coated with a low reflectivity, high emissivity substance.

The requirements for the coating were; 1) easy to apply, 2) wouldn't short out the chip, 3) have a high emissivity, 4) must be thin so that the temperature gradient through the coating doesn't significantly skew the temperature readings. Black paint was first considered because of it's high emissivity (> 0.87), however all of the paints we looked at had dielectric properties that were considered insufficient. Three other candidates were tested; 1) Dr. Scholl's Odor Destroyers Deodorant Spray, 2) molybdenum disulfide spray, and 3) aluminum oxide powder. All these ingredients have one thing in common, the main substance is a good dielectric material (the foot powder contains zinc oxide). Each was tested on a pole of an actual IPB. The first part of the coating test procedure was as follows:

1. Put IPB sans manifold, capacitors, and cover on hotplate
2. Apply heat by adjusting dial on hotplate. The amount of heat isn't important as long as it brings the IPB to a temperature above room temperature.
3. Apply the coating under test to the top surface of the IPB
4. Adjust the camera emissivity setting until camera temperature readings agree with that of a surface temperature probe.
5. Adjust dial on hotplate to change temperature of IPB. Make sure that emissivity and temperature correlates at a few different temperatures.

With the above procedure the emissivity of each coating can be determined. The molybdenum disulfide spray and the aluminum oxide powder had emissivities in excess of 0.75, which is sufficient for our needs. Since it was in a spray can, the molybdenum disulfide was easy to apply. The aluminum oxide powder had to be sprinkled on the IPB (using a powdered sugar shaker). With practice, it was possible to get consistent emissivity readings on the camera. The foot powder proved difficult to apply. Unless sprayed on thick, it always left much of the surface visible. When sprayed on thick, it was lumpy and uneven. It was difficult to get consistent emissivities for the spray. The foot powder was removed from the candidate list.

The remaining two candidate coatings were then tested for voltage breakdown. Each was sprayed on a single pole of the IPB and high voltage was applied. The pole coated with molybdenum disulfide immediately shorted and failed. It was suspected that the spray propellant was a poor dielectric and thus caused the voltage breakdown. The aluminum oxide powder passed the high voltage test. The emissivity of the Aluminum Oxide was measured to be 0.75 using the procedure listed above.

2.1.4.5.2 IPB Testing

The IPB module was mounted into our dynamometer fixture, the electrical connections were made and cooling lines were attached. As indicated in Figure 2.1-23, the IPB cover was removed and the snubber capacitors were moved to the side to allow the camera to have a clear view of all of the IPB's chips. Aluminum oxide powder was sprinkled on the surface of the pole(s) to be tested and the IR camera was mounted above the IPB at a focal distance that allowed each pole to be imaged individually.

Each switch was tested at 110 Amps and 220 Amps. For each current level, tests were run at switching frequencies of 4 kHz, 8 kHz, and 12 kHz and DC. During each test level, the silicon was allowed to reach steady state. Using the IR camera, the hotspots in each silicon chip were noted and an IR image of the pole under test was recorded. It should be noted that the IR camera actually measured the temperature of the aluminum oxide powder coating not the silicon. It is assumed that the temperature gradients from the top of the chip to the top of the powder layer were minimal.

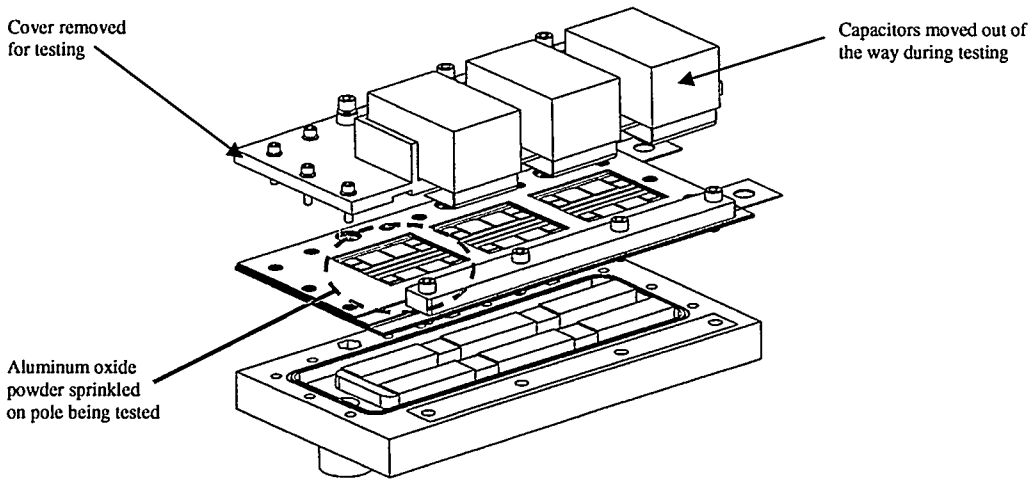

Figure 2.1-23 IPB Showing IR Image Area

2.1.4.5.3 Results

The IR camera has functionality that allows the user to queue the temperature of a specific spot on the image or determine local and overall hotspots. Using this functionality, hot spots on the IGBT and diodes were logged during individual switch testing. Figure 2.1-24 indicates the positioning of the IPB chips and thermistors during the temperature testing. The temperature of the activated switch's thermistor was checked against the IR camera temperature reading for that thermistor to continuously verify that the measurement technique remained calibrated. Figure 2.1-25 shows an example image captured by the IR camera. Note that when testing an individual switch, the IGBTs on that switch are activated while the diodes on the other switch in the same pole are activated. Also note that I1 is hotter than I2. This thermal asymmetry occurred in all the tests. In some switches, I1 was hotter than I2 and in others I2 was hotter than I1. The hottest IGBT on an entire IPB would be the limiting factor in power rating of the IPB. The IR camera proved to be the only convenient way to measure the level of thermal asymmetry in IPB electronics.

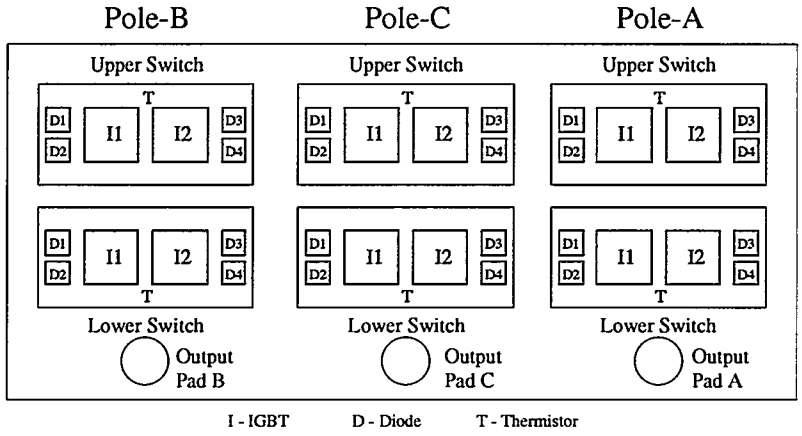

Figure 2.1-24 Layout of Devices Within The IBP

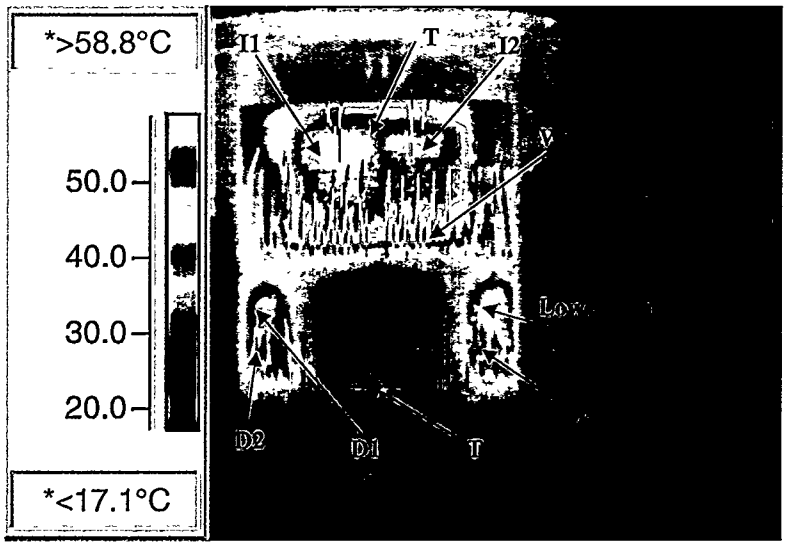

Figure 2.1-25 Thermal Image of Switch Under Test

The logged frequency dependent IGBT temperature data is plotted in Figure 2.1-26 through Figure 2.1-28. The temperatures were expected to be linear with frequency and, for the most part, are linear. Due to the timing of this thermal investigation, IPB resources were limited and only three individual switches on of an IPB were tested.

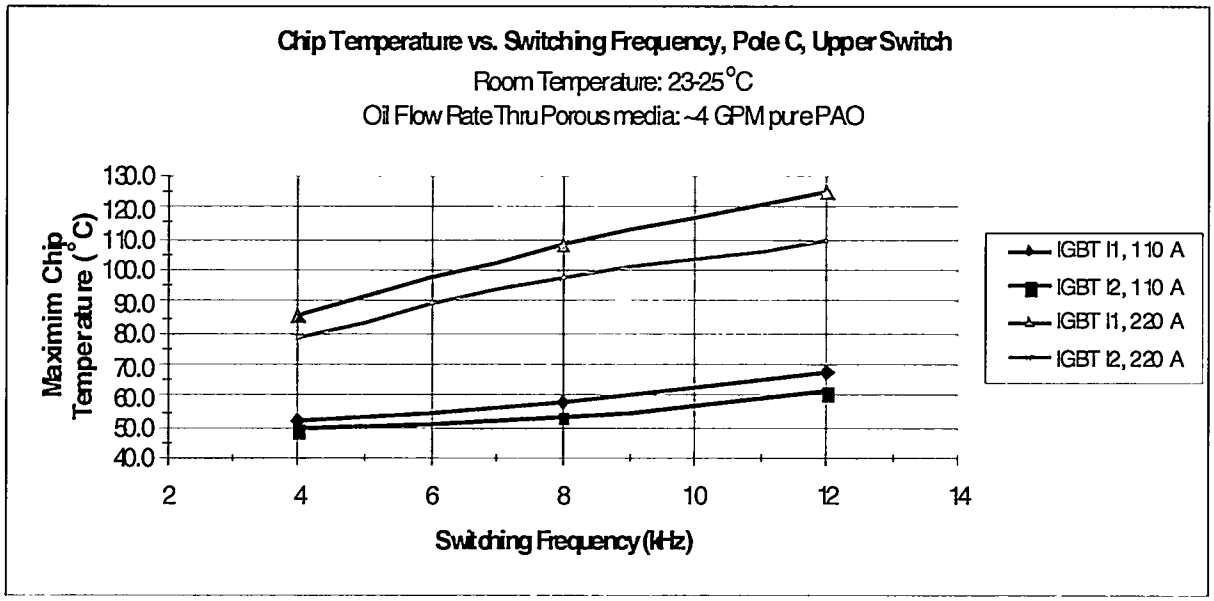

Figure 2.1-26 IGBT Temperatures, Pole C, Upper Switch

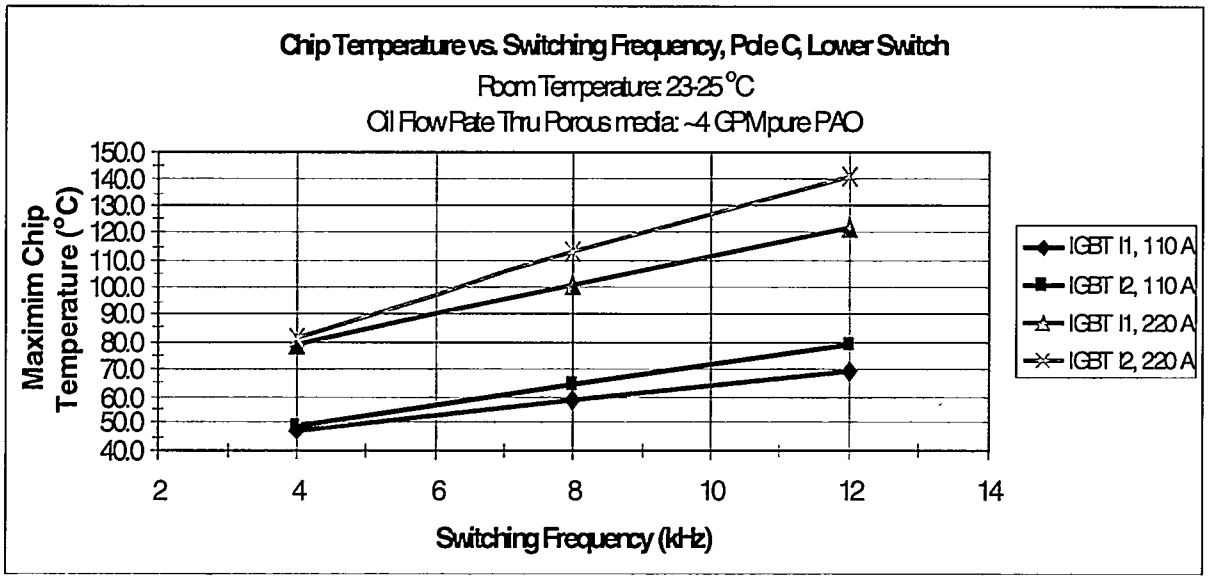

Figure 2.1-27 IGBT Temperatures, Pole C, Lower Switch

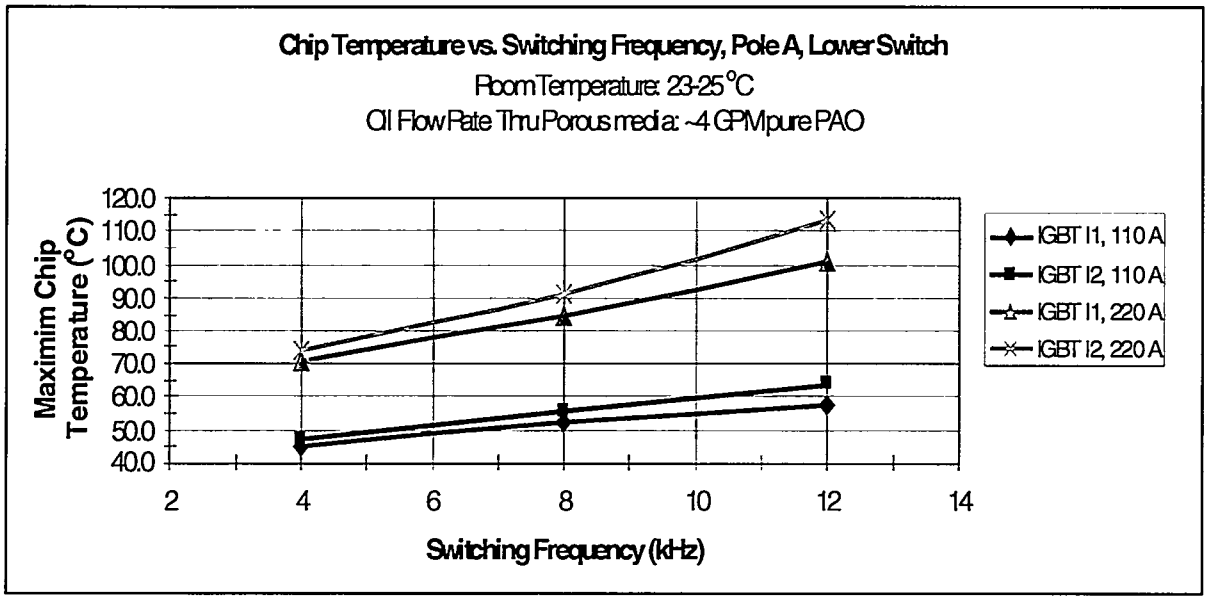

Figure 2.1-28 IGBT Temperatures, Pole A, Lower Switch

2.1.5 Conclusions

The Integrated Power Block effort was a great success. The final IPB design exceeded almost every expectation. The IPB reduced the parts count by more than 50% over the bridge design that is used in the production system. Its low inductance improves the voltage overshoot by 3:1. And the IPB manufacturing cost is projected to be 40% of the cost of the production bridge. A summary of the achievements that resulted from this effort are listed below.

1) 60% reduction in the cost of the powertrain bridge.
   - Used ½ of the silicon used in the production powertrain bridge
   - Reduced the heat sink cost by over 20:1
2) Improved the thermal resistance by more than 2:1 (3:1 when flowing cooling oil directly over chips).
3) Reduced power bridge volume by almost 3:1 and weight by 4:1
4) Superior electrical performance
   - Reduced overshoot by 67%
   - Smaller snubber capacitors
   - Better Inductance characteristics
5) Advanced assembly process for an integrated power block
   - Void-free solder attachment of large size semiconductor chips to metal carriers.
   - Solder attachment of the sub-assemblies (semiconductor devices and metal carrier) on the liquid cooled bus bars of the inverter assembly.
   - Wire bonding of large size (0.020" & 0.025" diameter) aluminum wire
   - The final assembly processes, for attachment of discrete gate drive components and thermistors.
   - Switch screening, and final electrical test
6) IR imaging of silicon power devices

The proof of principal demonstration of the IPB concept has shown great promise. The accomplishments obtained in this phase have given rise to suggestions for further experiments as listed below.

1. Measure the improvement to the thermal resistance of a flooded IPB vs. the non-flooded IPB. The investigation during this project defined an approach that proved to be successful for flowing cooling fluid directly over the high voltage power electronic devices. Although the process was successful, the increased thermal performance is not known. It would be worth while to know if this cooling process could be applied to electric vehicles.
2. Determine chip temperatures while operating all three phases of the IPB under a load (i.e. 230 HP motor). The goal here would be to show that one IPB could do the work of at least two bridges in our existing powertrain systems.
3. Compare paralleled IGBTs feeding a single motor winding to series IGBTs feeding paralleled motor windings. The goal would be to define an electric motor drive that would eliminate the highly proprietary process of matching IGBTs chips.
4. Continue to search for high emissivity, high dielectric coatings that are easier to apply than aluminum oxide powder. If one can find a coating that can be easily used during assembly, it would be possible to use IR imaging as an inspection process during testing preformed in manufacture.
5. Use available macro lens to determine quality of wire bonds. If all wire bonds are sharing current equally, they should all be roughly the same temperature.

2.2 RESOLVERLESS CONTROL

2.2.1 Goal

The objective of this effort was to reduce the system cost by eliminating the motor speed and position sensor from the motor assembly and the corresponding interfacing circuitry in the motor controller.

2.2.2 Introduction

The resolver is used to provide motor rotor position and speed inputs for the vector control algorithm. It is one of the highest cost items in the Northrop Grumman Electric Powertrain. Not only is the resolver procurement cost high, the interface wiring and circuitry is also expensive. In addition, it must be carefully aligned and mounted to function properly. Because of these issues, Northrop Grumman has investigated methods of controlling an AC induction motor without a resolver.

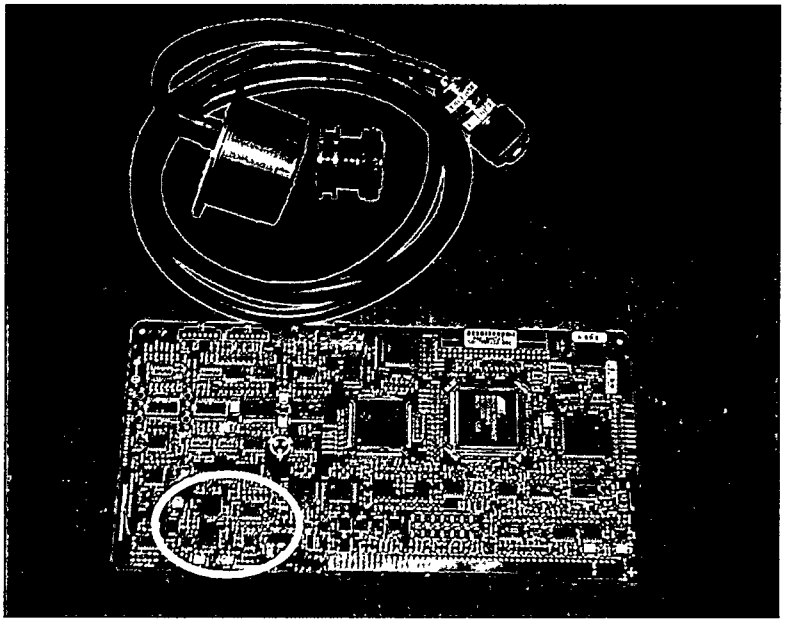

Hardware Description

Resolver Rotor

Resolver Stator

Multi-Shield Cable

Cable Connector

Mating Connector (not shown)

Interfacing Circuit

Figure 2.2-1 Production Resolver and Interface Hardware

2.2.3 Evaluation of Different Approaches

We evaluated a number of resolverless control methods from which two approaches were selected for further investigation. The first approach, Unbalanced Third Harmonic Ripple, was tested and proved to be unpractical for our application. The motors tested exhibited insignificant amounts of third harmonic ripple except at high excitation levels. The second approach was a voltage feedback method similar to that used on a previously developed commercial general-purpose motor drive. The voltage feedback method was tested in the lab using a modified controller and motor and it exhibited fairly good results.

2.2.4 Resolverless Control Design

To minimize the changes to the existing system the Voltage Feedback Algorithm shown in Figure 2.2-2 was implemented in the vector control DSP software.

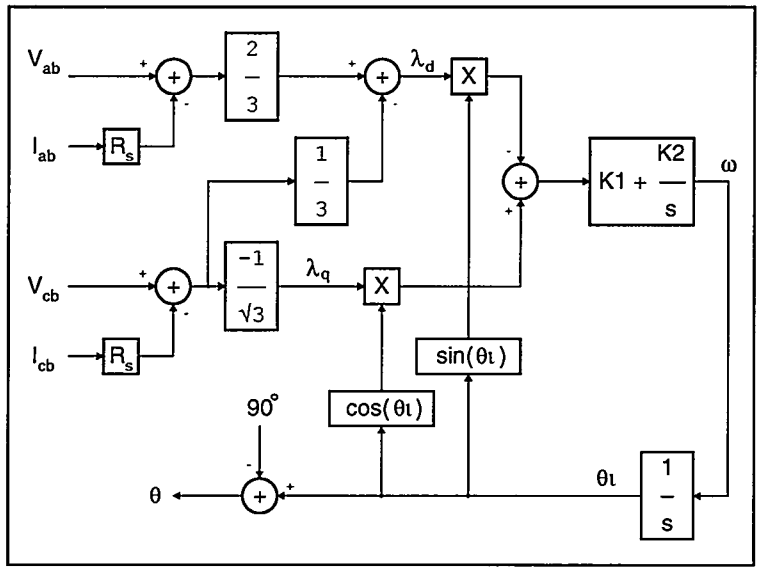

Figure 2.2-2 Voltage Feedback Algorithm

The motor shaft position (θ) is estimated from the feedback of two line-to-line voltages (V_{ab}, V_{cb}) and two line-to-line currents (I_{ab}, I_{cb}). A voltage sense circuit was designed using low offset operational amplifiers for reading the two line-to-line voltages. A/D circuitry on the Chassis Vector Control Board was added and used by the software to access the two line-to-line voltages.

2.2.5 No-Load Powertrain Testing

A standalone powertrain test setup was used for initial testing. In this setup, there is no load connected to the motor. Before attempting to run without the resolver, the software was modified to output software variables (for monitoring via an oscilloscope) representing the algorithm's estimated motor position and the resolver's motor position.

One of the first investigations was to compare the resolver's output to the algorithms calculation. This comparison showed that the estimated motor position would shift relative to the true motor position as the speed of the motor changed. It was determined that this shift was being caused by the phase response of some filters in the voltage feedback path. The low pass filters at the inputs of the current sensors A/D converters were removed and the low pass filters on the voltage sense circuit were modified for a higher cutoff frequency. Once these filters were changed, the estimated motor position was in sync with the true motor position.

Further testing uncovered a difficulty in obtaining measurable feedback from the line-to-line voltages at low speeds. Adding in a current compensation (line-to-line current times stator resistance) didn't seem to help the problem. The solution to the low speed problem was to run the controller open-loop until the motor speed reached 400 RPM, at which point the control was transitioned to closed-loop. When running open-loop, the software is ignoring the actual motor

speed and using a set speed of 400 RPM. To operate in the open-loop region, the flux as a function of torque command had to be increased.

2.2.6 Powertrain Testing with Back-to-Back Dynamometer Fixture

The resolverless control test system was setup on one of our back-to-back test fixtures. The back-to-back test fixture uses a production EV powertrain to provide a programmable load for the powertrain being tested.

When tested under load, the estimated motor position would shift relative to the true motor position (similar to the phenomenon addressed during no-load testing). The amount of shift in the estimated motor position seemed to be a function of the amount of load or current draw. A torque command factor was included in the position estimator code to account for this shift. For moderate loads (less than half of maximum torque), the control scheme worked well. For larger loads (greater than ¾ of maximum torque), the estimated motor position would shift enough to cause an over current condition that could potentially damage the system.

Two major issues arose from testing. The first issue is the limited amount of torque available while operating in the open-loop region. Under heavily loaded conditions, the amount of time required to reach 400 rpm was unacceptable. The other issue is the lack of smooth torque control during the transition from open-loop to closed-loop control. Once the transition was made to closed-loop control, the motor speed would increase at a much faster rate for the same torque command.

2.2.7 Conclusion

Due to the lack of smooth torque control during the transition from open-loop to closed-loop control, this method of resolverless control is not applicable for electric vehicles. However, this control method may be appropriate for other applications such as flywheels, generators, fans, or pumps.

3 POWERTRAIN PRODUCT ENHANCEMENTS

The powertrain enhancement tasks focused on supporting more efficient powertrain manufacturing and software. The software effort targeted a reduced processing timeline and improved software supportability. Production validation testing was performed to validate the product under the environmental extremes of automotive use. Production acceptance testing was performed to validate the product assembly processes. The following discussion highlights the accomplishments achieved as a result of these powertrain enhancement efforts.

3.1 DSP ENHANCEMENTS

This task was to enhance the performance of the system software. One of the goals of this effort was to reduce the processing timeline by analyzing algorithm implementation and by increasing the software efficiency. The second goal of this effort was to incorporate new capability into the system for supporting a broader range of applications such as hybrid electric vehicles.

3.1.1 Introduction

The Vector Control Software (VCS) is a digital implementation of the analog design developed for our first electric vehicle application using a Vector Controlled A/C Induction Motor Controller. The VCS was developed to reduce the cost of the EV powertrains that were being developed for commercial applications. Northrop Grumman has established two basic EV powertrain products, the 100 HP powertrain for light to medium-weight vehicles and the 230 HP powertrain for heavier vehicles.

The VCS operates in the Texas Instrument (TI) TMS320C50 Digital Signal Processor (DSP) onboard the Chassis-Vector Control (CVC) Board. The VCS software receives control inputs (torque requests) from the Chassis Control Processor. The Chassis Control Processor interfaces with the driver via pedals, key, etc., and with other vehicle subsystems such as the battery management system and charging system.

The VCS computes and outputs voltage control signals that drive the IGBTs, generating 3 phase A/C currents and thereby applying the requested torque to the motor shaft. The VCS also inputs the rotor position from a resolver for feedback to the vector control algorithm. The VCS computes and reports the shaft speed back to the Chassis Control Processor to close the control loop.

For supportability, much of the VCS source code is written in the "C" programming language. The remainder of the code is in the TI assembly language and maximizes processor throughput for select procedures and to meet the critical processing timeline.

The original VCS was developed to implement the functionality of the original analog system and the efficiency of the code itself was not emphasized. The VCS implementation had been applied to several engineering and prototypical systems and each implementation had success with only changes to VCS control parameters to "tune" to the application. As more applications placed additional operational requirements, such as operating in series hybrid vehicles and as turbo-generator converters, the VCS routines have been modified to broaden the control coverage.

Due to the need for increased application of the VCS and with the knowledge that the code was not optimized for execution speed, there was a task launched to review optimization methodologies and to test such optimization in the VCS. In addition it was expected that other software benefits would be realized such as maintainability, and improved flexibility.

3.1.2 Results

The DSP is supported with a "C" compiler, an assembler and documentation that provides guidelines on optimization for speed and size of code. These tools and guidelines were analyzed and a methodology was undertaken to create sample algorithms based on the VCS code to evaluate potential code optimization. This process produced a collection of significant VCS arithmetic operations in old and optimized formats for direct comparison in processor clock cycles and exactness of results.

One example of the guidelines, suggested by the manufacturer of this DSP, was to evaluate the arithmetic precision needed in calculations since 16 bit calculations generally use fewer clock cycles than 32 bit calculations. This guideline was frequently used in the optimized VCS code. As an example, a VCS algorithm required the computation of the square root of the sum of squares and it was implemented with a good approximation as shown below for both the original 32 bit algorithm, Figure 3.1-1, and the optimized 16 bit algorithm, Figure 3.1-2.

The optimized code saves 94 clock cycles with no loss of accuracy. Since the same approximation process is used later in the code to compute the square root of the difference of squares, there is an overall saving of 188 clock cycles in the processing loop. This translates to 12% of the 1500 clock cycles in the processing control loop. The key clock cycle savings comes in 16 bit handling but additional savings is achieved from using the variable of interest as the integrator to make fewer memory accesses (VectMag is put into a hardware register and most of the operations take place on the processor chip).

This version's worse case path takes 164 clocks ... 32 Bits

```
SumOfSquares = (long)Vd*Vd + (long)Vq*Vq;
if(SumOfSquares < 200000000)          /* if it's a small # make it big */
 {
        flag = 1;
        SumOfSquares = SumOfSquares << 2;
        VMIntegrator = VMIntegrator << 1;
 }

/* 2 integrations */
VMInt = VMIntegrator>>16;
VMIntegrator+=(SumOfSquares - (long)(VMInt*VMInt));
VMInt = VMIntegrator>>16;
VMIntegrator+=(SumOfSquares - (long)(VMInt*VMInt));

if(flag == 1)                         /* if I made it big, make small */
 {
        VMIntegrator = VMIntegrator >> 1;
 }

VectMag = (unsigned int)(VMIntegrator>>16);
```

Figure 3.1-1 Code for Computing Sum-Of-Squares

```
This version's worse case path takes 70 Clocks ...16 Bits

        uitemp = (Vd*Vd + Vq*Vq) >> 16;

        /*   Read as ... if the squared # is too small, make it big ... */
        sitemp=0;  if (uitemp < 7171)
                                { sitemp++;  uitemp <<= 2;  VectMag <<= 1; }
        /* 2 integrations */
        VectMag += uitemp - ((long)(VectMag*VectMag)>>16);
        VectMag += uitemp - ((long)(VectMag*VectMag)>>16);

        /* -- Reset... if made big, make small. */
        if (sitemp) VectMag >>= 1;
```

Figure 3.1-2 Optimized Code for Computing Sum-Of-Squares

Also during the review process, several instances were found where calculations were repeated (timeline efficiency). Figure 3.1-3 is an example of source code for a dc to ac transform to compute the three phase voltages prior to the code efficiency review.

```
        * compute    Va  = Vd * Cos(θ)  -  Vq * Sin(θ)     */
        CosTheta = (Theta+Pi_over2);
        accumulator =(long)(SineTable[CosTheta>>7] * Vd);
        accumulator =((long)(accumulator - (SineTable[Theta>>7] * Vq)));
        accumulator += accumulator;
        Va = (accumulator)>>16;
        VbLong = -accumulator;

        /* compute    Vc = Vq * Sin(θ – π/3)   -  Vd * Cos(θ – π/3)     */
        CosTheta = (CosTheta – Pi_over3);
        Thetatemp = (Theta – Pi_over3);
        accumulator = (long)(-SineTable[CosTheta>>7] * Vd);
        accumulator = ((long)(accumulator + (SineTable[Thetatemp>>7] * Vq)));
        accumulator += accumulator;
        Vc = (accumulator)>>16;
        VbLong -= accumulator;

        /* compute    Vb = -(Va + Vc)   */
        Vb = VbLong>>16;
```

Figure 3.1-3 Code for DC to AC Transform

The evaluation of the integrity of the above source requires a great amount of effort to verify this text book formula. In this non-optimized VCS code, the four trigonometric values (Sin(θ), Cos(θ), Sin(θ – π/3), and Cos(θ – π/3)) are computed during the ac to dc transform and then again during this dc to ac transform. As a result of the efficiency review the above VCS code was optimized as sown in Figure 3.1-4.

```
Va = (Vd * CosO      - Vq * SinO) >> 16;
Vc = (Vq * SinO_Pi3 - Vd * CosO_Pi3) >> 16;
Vb = -(Va + Vc);
```

Figure 3.1-4 Optimized Code for DC to AC Transform

These calculations are more readily comparable to the textbook equations (improved code maintenance) and now the trigonometric functions are calculated only once per processing cycle. In addition, the optimized version removed a factor of 2x (specifically, accumulator += accumulator) from this computation and placed it in the code associated with the algorithm requiring the 2x data. Although both styles get exactly the same output and are computing the correct formulae, there are substantial savings in human analysis and processor clock cycles in the optimized version. Also during the review process, there were instances found in the implementation where parameters were set to prevent arithmetic overflow from occurring. If overflow conditions were allowed and properly processed then the system performance could be enhanced. Overall, the changes to these arithmetic processes would allow the controls to exceed the preexisting (original) software design limits.

The VCS reads the input of the rotor position from a resolver to digital converter and provides the Theta measurement for computing the electrical vector rotation components and estimating the mechanical speed of the motor. The speed calculation was optimized for clock cycles and improved resolution and the earlier dependence on the application's speed scale was removed. Now the resolution is 1 RPM and the full 16 bits are passed back to the Chassis Controller for improved feedback control. Arithmetic overflow will not be an issue since the maximum motor speed is <15,000 RPM, so overflow processing is also removed to save clock cycles. Figure 3.1-5 shows how the earlier VCS consumed valuable clock cycles performing three 16 bit multiply and storing 32 bit results and Figure 3.1-6 shows the optimized version reduces the complexity to 1 16 bit multiply:

```
/* The following code computes the speed of the rotor and scales      */
/* it so that 32767 is representative of Max Application RPM          */

SpeedLong = (long)(((int)Theta - (int)OldTheta)*SpeedScale);

if (labs(SpeedLong) > 32767)  /* Protect against overflow             */
   {
   if(SpeedLong < 0) SpeedLong = -32767;
   else SpeedLong = 32767;
   }

SpeedIntegrator += (long)(SpeedConst*(int)SpeedLong) - (long)(SpeedConst*Speed);

Speed = ((long)SpeedIntegrator>>16);
```

Figure 3.1-5 Code for Computing Rotor Speed

```
/* Compute Motor Speed in RPM                                          */
/*  Baseline Resolution:          dTheta = 1q/dT = 1q / 63.875usec     */
/*                                dTheta ~= 14.33311 RPM               */
/*  Integrated Resolution: Integrate for 256 cycles ~= 16 msec         */
/*            dThetaInt * (14.33311*2^8)  = dThetaInt * 3669           */
/*            dTheta ~= 1.0 RPM                                        */

dTheta = (int)(dThetaInt >> 8);
sitemp = (int)(Theta - OldTheta) - dTheta;

if (sitemp) dThetaInt += sitemp;
else if (!dTheta)    /* else if not moving, discharge the integrator.  */
   { if      (dThetaInt > 0) dThetaInt--;
     else if (dThetaInt < 0) dThetaInt++;
   }

Speed = (int)((dThetaInt * 3669) >> 16);
```

Figure 3.1-6 Optimized Code for Computing Rotor Speed

The optimization enhancements were made to an experimental version of the VCS code and it was extensively tested. This experimental code was designated Exp-1B. A sample of the performance of the Exp-1B code tested in our dynamometer test cell is shown in Figure 3.1-7. During the B04 System Characterization, data was collected and system demonstrated a peak of 245 HP at 336 Volts and an approximate efficiency of 90%.

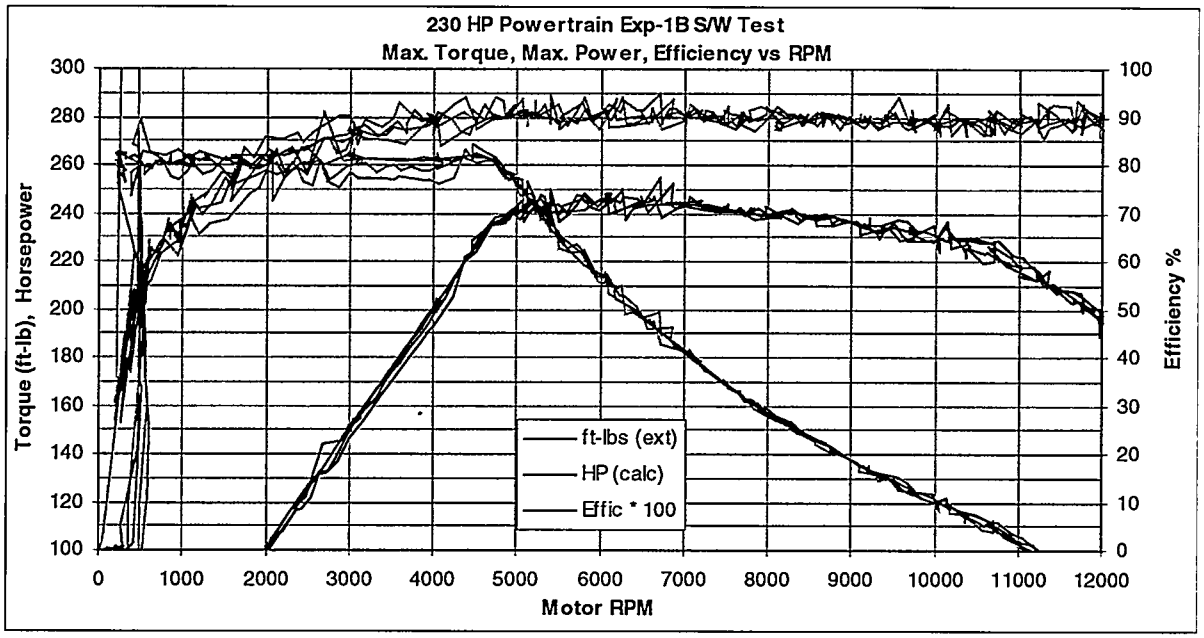

Figure 3.1-7 Exp-1B Code Reaches 245 HP When Tested In 230 HP System

The key features to be noted in Figure 3.1-7are:

0 to 4750 RPM, Flat Torque Response of >250 ft-lb.
4750 to 10000 RPM, Nearly Flat Response of >230 HP
4000 to 13390 RPM, Flat Efficiency Response of ~90%.
Peak Power of ~ 245 HP

In addition to the enhanced system performance shown in the Exp-1B testing, the code optimization task was so successful in improving the processing timeline a fundamental design change to system could be made. The system design established a timing cycle of 1500 clocks for the VCS. The original VCS code could not perform all the processing in the allotted time so indexed stages was implemented for the processing loop. The primary loop, those calculations required in every cycle, consumed approximately ½ the processing timeline. All the remaining processes were divided into 4 nearly equal processing stages such that each individual secondary stage would not completely consume the last ½ of the timeline. Each secondary stage was indexed into the processing schedule, such that each of these secondary processes repeated after four cycles of the primary loop. With the optimized code, all the VCS processing is performed within the1500 clock cycle timeline. This eliminates the need to have the indexed processing and therefore improving the bandwidth of the previously indexed processing 4:1.

This code, designated as Version-3, was also tested in our dynamometer test cell and the results are shown in Figure 3.1-8. The VCS Version-3 has reduced the overall number of lines of source code, has reduced the complexity of the code for readability and maintainability, has enhanced the arithmetic to operate beyond previous design limits, and has also changed subroutines to inline code to remove the calling overhead. The integrity of the implementation of algorithms has been verified and validated. And now, this optimized VCS Version-3 performs all the processing within the 1500 clock cycle timeline.

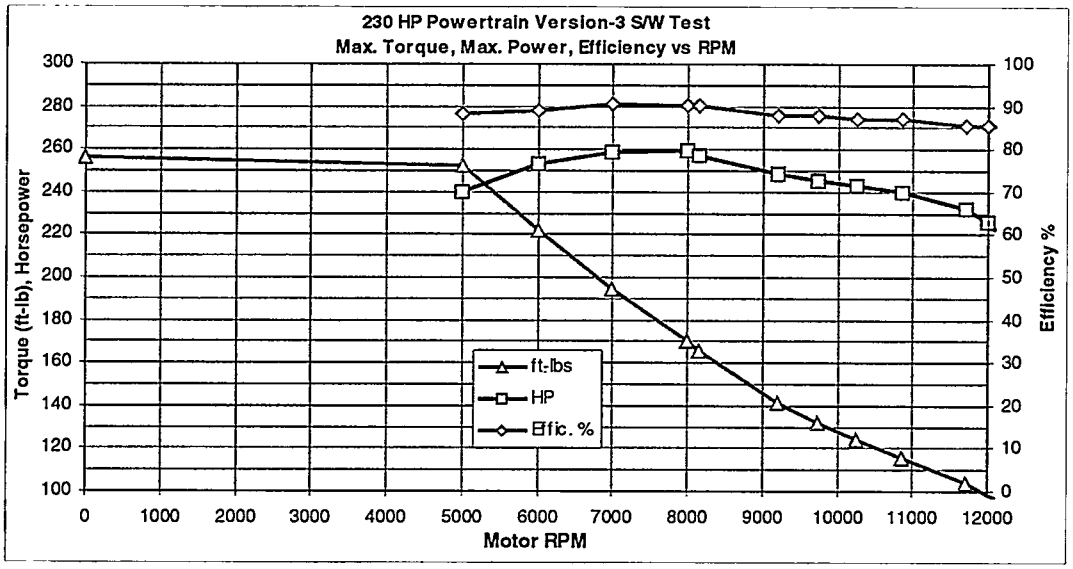

Figure 3.1-8 Version-3 Code Reaches 260 HP When Tested In 230 HP System

3.1.3 Conclusions

The VCS Version-3 code has been tested to meet the requirements for release into the production systems. It is the version of code that is in the current production system. It has substantially increased the performance capability of the systems. The 230 HP product has been measured to produce 260 HP and similarly, the 100 HP product has been measured to produce 120 HP.

The code optimization task far exceeded our expectations. With the unexpected shortening of the timeline to the level of having a single processing loop means that all of the controls are tightly coupled and thus the maximum dynamic range can be realized. This, coupled with enhanced arithmetic control, provides the 100 HP and 230 HP Powertrains the processing capability to perform well above the advertised limits.

In conclusion, the enhanced algorithms implemented in the DSP code now exceeds limit the performance of the system. For example, the improved horsepower measurement shown in this report for both the 100 HP and 230 HP products was limited by the battery's power capability. The code is now more understandable for software maintenance. Overall, the results of this software optimization task far exceeded the goals envisioned at the start of the effort.

3.2 PRODUCTION VALIDATION AND ACCEPTANCE TEST

3.2.1 Test Development Overview

The validation test program was developed through a four-step process. First, the automotive-use environment and failure mechanisms were defined. Second, tests were specified and procedures written to subject the equipment to all aspects of this environment. In the third step, the order of the tests was defined. The final step was then to compile test results. The following discussion provides an overview of the TRP activities as well as the test results for the entire design verification and production validation phases of testing.

3.2.2 Definition of the Use Environment

The initial objective in developing the test program was to establish what the product would be subjected to during the course of its useful service life and what stress mechanisms would be susceptible to this environment. Table 3.2-1 provides a list of the tests applicable to the Automotive "Use" environment, a brief definition of each component, its associated stress mode(s) and test objectives. This list was derived from a number of sources including ourselves, providing power electronics expertise, a major automotive manufacturer providing many generations of vehicle test experience, and the electronics industry which provided electronics standards and guidelines.

Table 3.2-1 Tests Specified for Use in the Automotive Environment

Category	Test Name	Operating Status	Stress Modes Accelerated	Test Objective
Performance Durability	Key Cycle	Operating	Current and Voltage Transients during power cycling	Simulate vehicle Key-ON and Key-OFF cycles by: 1) subjecting components to repeated inrush current and voltage transients 2) exercising mechanical relays.
	Aggravated Humidity	Non-Operating	Absorbed Moisture	Expose equipment to repetitive cycles of moisture to reveal moisture induced failures and operational intermittence caused by condensation at interconnections.
	Power Cycle	Operating	1) Solder Joint fatigue associated with die/wire bonds in power devices 2) Mechanical interface between power devices and coldplate.	Verify mechanical integrity of: 1) solder connections internal to power devices and 2) thermal interface material between power devices and heat sinks.
	Thermal Cycle	Operating	1) Solder joint fatigue on PWAs 2) Material compatibility 3) Material stress fracture	Verify mechanical integrity of: 1) solder joints on all PWAs and 2) propagation of stress fractures in ICs.
Environmental Durability	PWA Thermal Shock	Non-Operating	1) Solder joint integrity 2) Stress fracture	Verify mechanical integrity of: 1) solder joints on all PWAs and 2) propagation of stress fractures in ICs.
	Transportation Vibration	Non-Operating	Mechanical fatigue, wire chafing, package integrity, material fretting	Verify mechanical integrity of Powertrain in its shipping container and shipping container.

Table 3.2-1 Tests Specified for Use in the Automotive Environment

Category	Test Name	Operating Status	Stress Modes Accelerated	Test Objective
	Operational Vibration and Mech Shock	Operating	Mechanical fatigue, wire chafing, package integrity, fretting and intermittence	Verify operational integrity of product subjected to mechanical vibration and shock.
	High Pressure Spray	Non-Operating	Coating degradation, fluid penetration causing shorts or corrosion	Verify the Powertrain operational integrity after exposure to fluids from tire splashes and engine cleaning.
	Internal Fluids Compatibility	Non-Operating	Intermittent electrical performance, swelling of plastics, coating degraded	Verify the Powertrain operational integrity after exposure to fluids that could potentially exist internally.
	External Fluids	Operating and Non-Operating	Corrosion, loss of high voltage isolation, swelling of plastics, coating degradation, label adhesion/legibility	Verify the Powertrain operational integrity after exposure to potential fluids that would be in the vehicle environment.
	Sand/Dust	Non-Operating	Moving part degradation, conductive bridging, absorption of fluids/vapors	Verify the Powertrain operational integrity after exposure to foreign material such as dust or sand.
	Salt Fog	Non-Operating	Galvanic/electrolytic corrosion, potting or seal failures, surface bridging of circuits	Verify the Powertrain operational integrity after exposure to salt fog (which is a much harsher condition than road salt conditions or coastal environments).

3.2.3 Design Test Objectives and Requirements

The next step was to define the phases of test, quantify the test requirements and determine how many units would be subjected to each test. Table 3.2-2 provides a summary of this activity. The test structure and objectives were established to be commensurate with those of high volume automotive programs. The objective of the Design Verification (DV) test phase was to verify the system performance as it relates to its design. The objective of the Production Validation (PV) test phase was to validate and improve manufacturing procedures. The final phase, Continuing Conformance (CC), was performed to remove variability associated with any component or process.

Table 3.2-2 Test Definition

Test Name	Equipment Under Test	Test Definition	Units Tested/Phase					
			DV	PV1	PV2	PV3	CC1	CC2
Operational Vibration	SCU, Oil Pump, OBC	X,Y,Z axis, 1Grms ave, 2 hrs/axis, 10 - 500 hz	1	3	3	3	2	2
Operational Shock	SCU, Oil Pump, OBC	±X,Y,Z axis, four ½-sine pulses, 7G's/pulse, 17.5ms.	1	3	3	3	2	2
Transportation Vibration	Powertrain	Loose cargo environment, 1Grms ave. Y & Z axis, 2 hrs/axis, 1Grms ave, 10 - 5000 hz	0	2	2	2	2	2

Table 3.2-2 Test Definition

Test Name	Equipment Under Test	Test Definition	Units Tested/Phase					
			DV	PV1	PV2	PV3	CC1	CC2
EMI/EMC, Voltage & Load Transient	Powertrain	Internal Specification	1	1	1	1	0	0
PWA Thermal Shock	All PWAs	24 shock cycles: 19 - 0C to 60C 2 - -20C to 70C 1 - -40C to 85C	0	3	3	3	0	0
Thermal Extremes	Powertrain	-40C, 56 hp, 310VDC, 50ADC, 8000 RPM, 1 hr +59C, 56hp, 310VDC, 50ADC, 8000 RPM, 1 hr	2	2	2	2	2	2
Key Cycle Durability	Powertrain	22,400 Cycles, 7 Yr life, 90% confidence	0	2	2	2	2	2
Power Cycle Durability	Powertrain	1960 Cycles, ΔT(IGBT Junction Temp) = 128°C	0	2	2	2	2	2
Thermal Cycle Durability	Powertrain	148 cycles, Solder Joints -25°C to +85°C	0	2	2	2	2	2
High Pressure Water/Steam	Powertrain	80 - 100 psi, 46°C	0	3	3	3	0	0
Fluids Compatibility	Powertrain	**Non-operating:** Resistance to Turbo Oil in (SCU), High Pressure Steam, washer fluid, ATF, brake fluid, degreaser **Operating:** Salt Splash	0	2	2	2	0	0
Exposure to Dust	Powertrain	5 hrs, 50 micron particle, non-powered	0	1	1	1	0	0
Salt Fog	Powertrain	240 hr, 5% solution, 35C, non-operating	0	3	3	3	0	0

3.2.4 Test Execution

The flow diagram, shown in Figure 3.2-1, illustrates the order in which the major tests were performed during Production Validation test. Note that tests were executed in a series-parallel fashion to facilitate timely completion. Each block of tests were preceded and followed by a system level Acceptance test (PT Accept) to verify successful completion. The tests are performed in series and were selected based upon the stress modes.

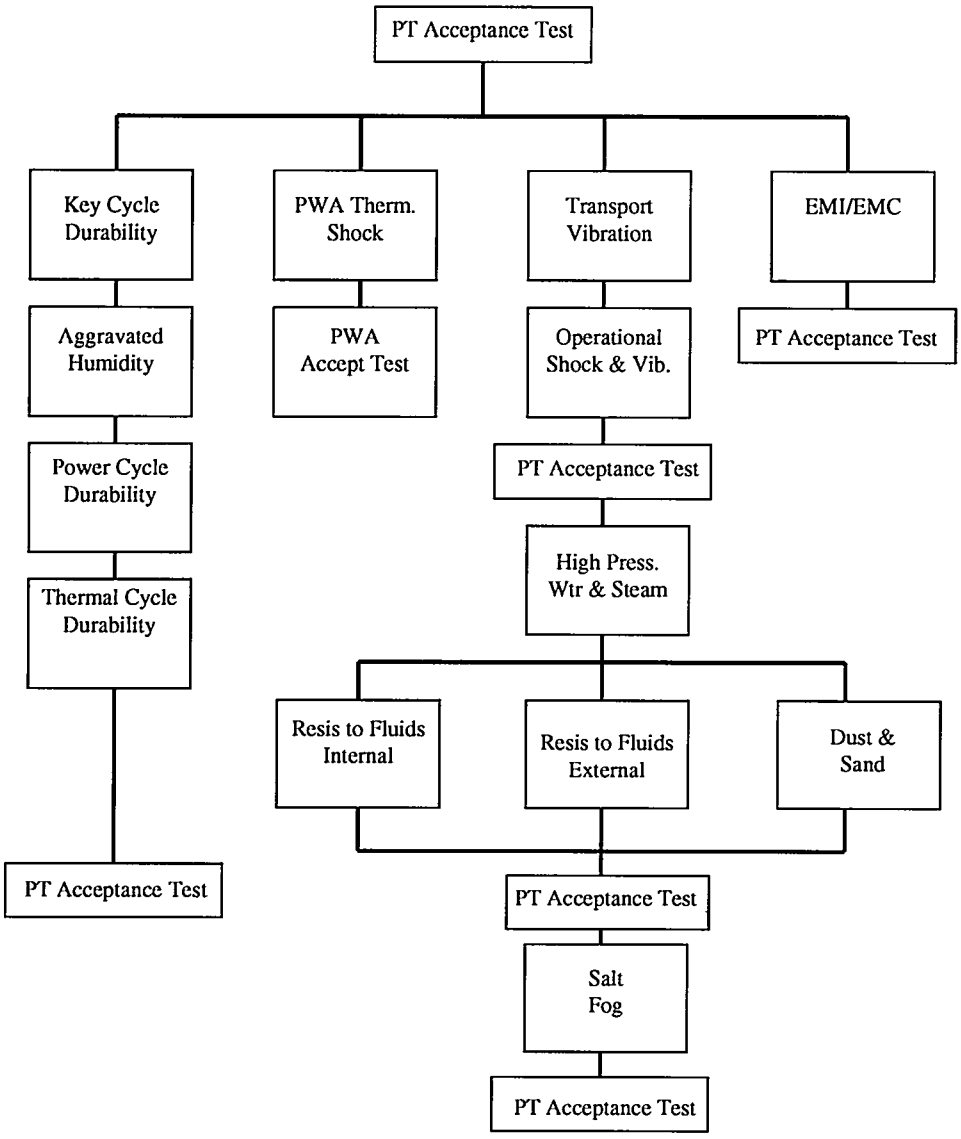

Figure 3.2-1 Test Flow Diagram

3.2.5 Test Results

The test program fundamentals, developed under the TRP Option-1 project, were utilized for all phases of test. Only the Design Verification and Phase I of the Production Validation test were executed as part of the TRP Option-1 project. The following discussion provides a summary of the results for the four iterations of tests executed as part of Design Verification and Production Validation to clearly show the benefits of multiple iterations of testing even though TRP funds were only used in the early phases of the testing.

The results of the DV and PV testing are shown in Figure 3.2-2. Although each of the tests defined above did induce failures, all of the precipitated failure types were corrected through the multiple phases of DV and PV test. Functional failures were detected as part of acceptance testing and were caused by component degradation during test. Failures induced during Thermal Cycle testing were associated with solder joint fatigue or material incompatibility. An example of this was discovered during Power Cycle testing. It was discovered that the significant difference in results was observed as a function of the ambient temperature at which

each test was performed. Testing that elevated operating temperatures above 50°C for an extended period of time revealed an incompatibility between the IGBT package and a "phase change" material being used to provide a low thermal resistance interface between the IGBT and its associated heat sink. This operating condition led to the phase change material evacuating the area between the IGBT and the heat sink and thereby causing the thermal resistance to increase with time.

Cold temperature turn-on testing uncovered issues due mainly to component parameter shift. An example of this was a value of capacitance that increased causing a voltage measurement to vary with temperature. Testing of hot temperature operation uncovered two thermal design issues. An example of such an issue was when actual levels of air flow and air temperature were measured inside the product, a component heat sink was modified to improve thermal conduction.

Humidity testing did reveal several corrosion issues; however, none were considered significant enough to affect Powertrain operation or durability. The one humidity issue, indicated in Figure 3.2-2, was due to an adhesive used to stake components for support during mechanical vibration. In this case the moisture in combination with temperature cycling caused the adhesive to relax.

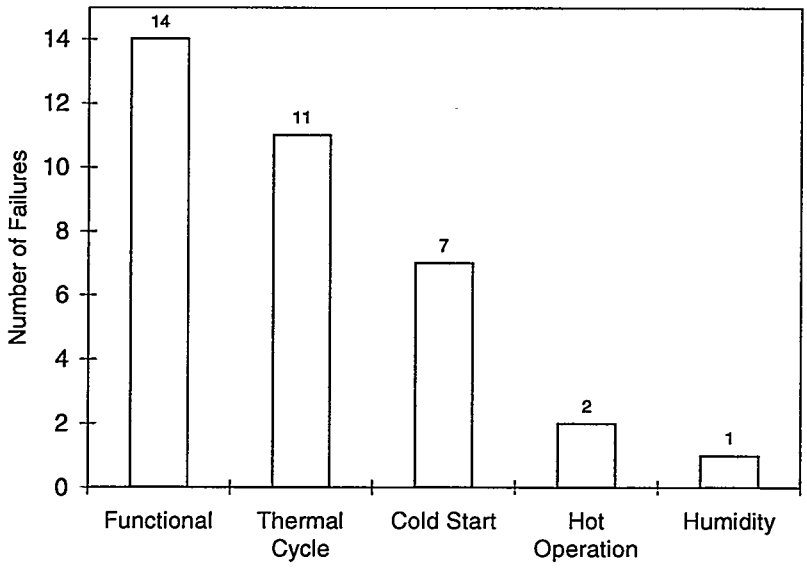

Figure 3.2-2 Number of Failures vs. Stress Mechanism

It was the goal of our product test program to enhance the product by identifing and strengthening as many stress mechanisams within the product as possible. Over the life of the test program, the number of issues arising from PV testing decreased from those experienced during DV testing as shown in Figure 3.2-3. In addition, the results of the DV and PV testing were used during the development of the Factory Acceptance Test.

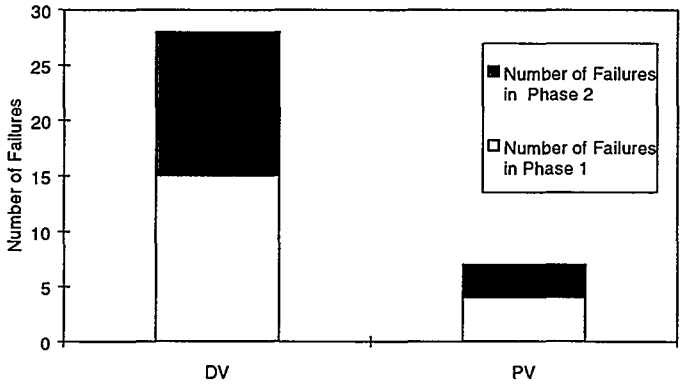

Figure 3.2-3 Product Improvement Resulting From Testing Program

It is expected that if the product is maturing the failures occurring during PV will be limited to issues of process variability. Figure 3.2-4 indicates that this did occur. As expected the process variability related issues did increase. This is due to the fact that manufacturing assembly was transitioned from engineering assembly/test personnel to the manufacturing assembly/test personnel. Examples of process related issues that were detected were improper application of pipe-joint compound and component damage during the "pick and place" board manufacturing operation. At the conclusion of the PV testing these process issues were all resolved and the improved processes put in place in the production line.

One design issue did occur during PV. It was detected during the first phase of PV and occurred during low temperature operation. In this case the equipment operated within the system performance requirement; however, a design margin in excess of the performance requirement was not achieved. The issue was resolved prior to the second cycle of PV test.

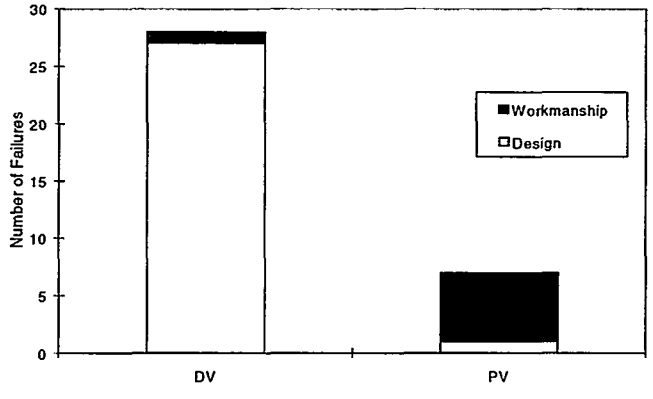

Figure 3.2-4 Design vs. Workmanship Related Issues as a Function of Test Phase

3.3 MANUFACTURING ACCEPTANCE TEST AND TEST EQUIPMENT

The task of developing the manufacturing acceptance tests was accomplished by establishing the requirements as a function of the powertrain specification, determining the lowest level of assembly at which each requirement can be tested, specifying the test equipment, and developing test procedures to verify each requirement. The following sections summarize the results of this activity.

3.3.1 Test Requirements

The primary objectives with respect to developing the manufacturing acceptance tests were 1) maximize automatic testing and 2) verify 100% of the safety requirements as part of Acceptance Test. These were considered essential to improve the accuracy and consistency of the product.

Of the 90 performance requirements 68 were amenable to automated test (see Table 3.3-1). The remaining 22 requirements addressed issues such as physical dimensions, system architecture, etc. These issues were verified manually by use of a Mount-Point gauge, inspection or a one-time qualification. All safety requirements were verified as part of the Acceptance Test procedure. Nineteen of the 20 safety requirements were amenable to automatic test. Manual intervention was required on one test to actuate an interlock on the equipment cover.

Table 3.3-1 Number of System Requirements

Requirement Type	Qty.	Test Type		% Automated Test
		Auto	Man	
System Functional Performance	90	68	22	75 %
System Safety Requirements	20	19	1	95 %

3.3.2 System and Sub-System Test Definition

The cost of detecting a failure increases as the level of assembly increases. For this reason, a hierarchy of the acceptance tests was established to perform as many tests as possible at the PWA and sub levels of assembly. Table 3.3-2 provides a list of tests and procedures created to perform the automated production acceptance test. Of the 1056 tested parameters, greater than 50% of the tests are performed at the lowest level of assembly and that 75% of the tests are performed below the final system level of assembly.

Table 3.3-2 Manufacturing Acceptance Test Summary

Item	Test Level	Test Name	# Data Points
1	System	Powertrain Functional	175
2		Powertrain Burn-In	90
Total Data Points at System Level:			**265**
3	Sub-Assembly	SCU Functional	109
4		SCU Impedance Hi-Pot	38
5		Traction Motor Functional	10
6		OBC -A	11
7		OBC -B	10
8		OBC Burn-In	6
9		EGW Pump Functional	16
10		EGW Burn-In	25
11		Current Sensor	11
Total Data Points at Sub-System Level:			**236**
12	PWA	APC/LVPS	81
13		CVC	171
14		Gate Drive	36
15		Oil Pump	77
16		Relay Drive	16
17		OBC Control	97
18		EGW	77
Total Data Points at PWA Level:			**555**

3.3.3 Test Equipment Design Overview

The primary objective in designing the test equipment infrastructure was to 1.) Make it general purpose to be easily adaptable to other products, 2.) Make it automated for reduced test time, improved accuracy and consistency, and 3.) Make it modularized to be adaptable to production volume.

Adaptability was achieved through the use of a programmable controller and programmable instrumentation. All equipment communicates via the IEEE488 bus and interfaces to a common back-plane. The controller and instrumentation was purchased as off-the-shelf commercially available equipment.

The ability to automate the test procedure greatly decreases the time required to test a system. The time required to execute all 1056 measurements, for a system, is 99 minutes, this includes

the 40 minutes for burn-in test. This provides at least a 10:1 decrease in total test time. The ability to automate test procedures also eliminates human error from the measurement data. The commercially available controller, described above, was equipped with a high-level programming language, specially developed for test applications. This facilitated quick development and debug of the required test procedures.

For the volume requirements of the 100hp and 230hp powertrain products, one complete test station was required at the product manufacturing facility and one control console was required for the PWA manufacturing facility. The modularity of the test station provides an easy and economic means of expanding the production facility's production rate. In addition, the control console can be easily reconfigured to accommodate the testing of any equipment configuration.

3.3.4 Test Equipment Design

Figure 3.3-1 through Figure 3.3-3 present the major components of the equipment required to support Production Validation and Manufacturing Acceptance test. Figure 3.3-1 illustrates the control cabinet. The controller cabinet contains a computer with monitor and mouse interface, low and high voltage power supplies, instrumentation such as VOM's, signal generators, oscilloscope, etc for automated measurement and an adapter pan. The control module can be quickly modified to test any level of assembly within a product line or test between product lines by removing and installing a new adapter pan. An adapter pan, shown in Figure 3.3-2, can easily be swapped within 60 seconds. The adapter pan provides interface between the products I/O and the I/O of the test controller. Approximately 10 adapter pans were required to support all testing of the 100hp and 230hp powertrains.

Figure 3.3-3 illustrates the high voltage power supplies developed to provide DC input power to the 100 and 230hp powertrains. While all three supplies are used for specialized testing, only the middle supply is necessary for Production Validation and Manufacturing Acceptance test.

Figure 3.3-4 and Figure 3.3-5 illustrate the first and second generation back to back fixtures. This fixture allows the output shafts of either motor to be connected together. In this configuration one motor is operated as a generator while the other as a load. The advantage with this test configuration is that the only power lost during test is that lost to heat due to the inefficiency of either system. Figure 3.3-5 shows an improved configuration. This fixture is more reliable and does not require alignment for proper operation. The cooling cart shown in the background contains the heat exchangers.

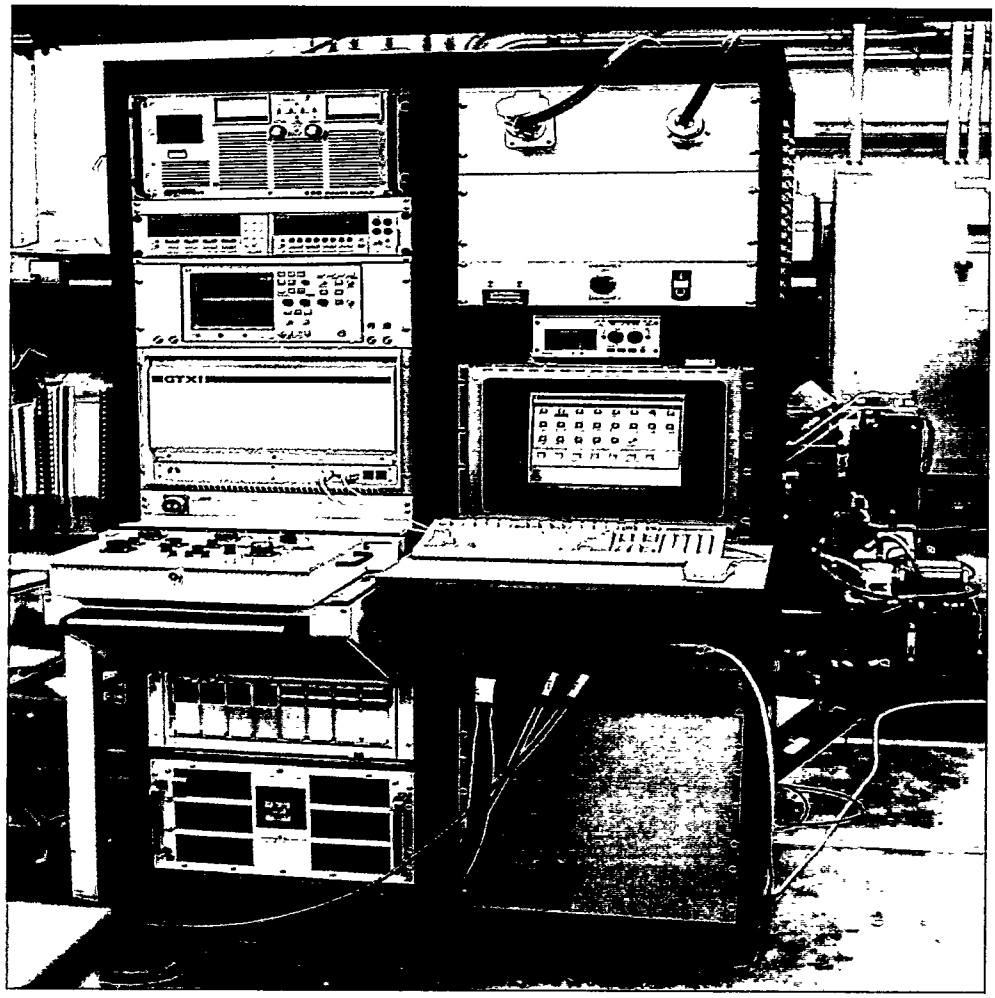

Figure 3.3-1 Automated Test Console

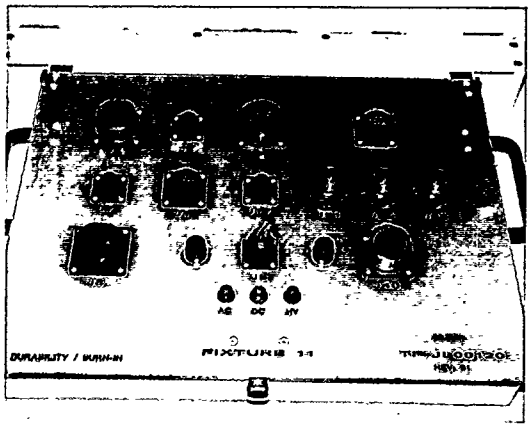

Figure 3.3-2 One of the Ten Styles of Test Console Adapter Pans

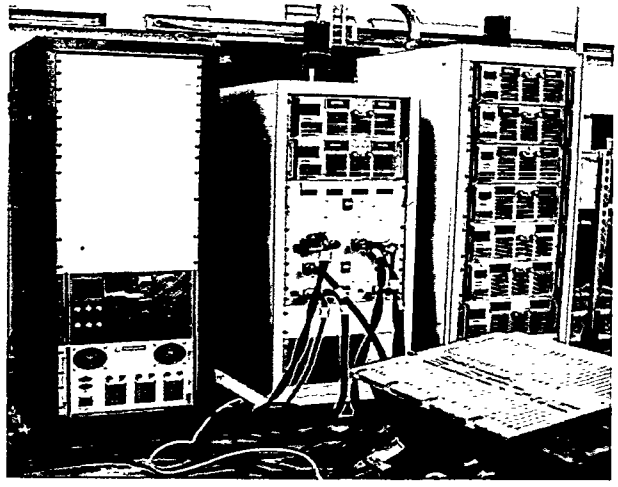

Figure 3.3-3 Test Fixture Power Supplies

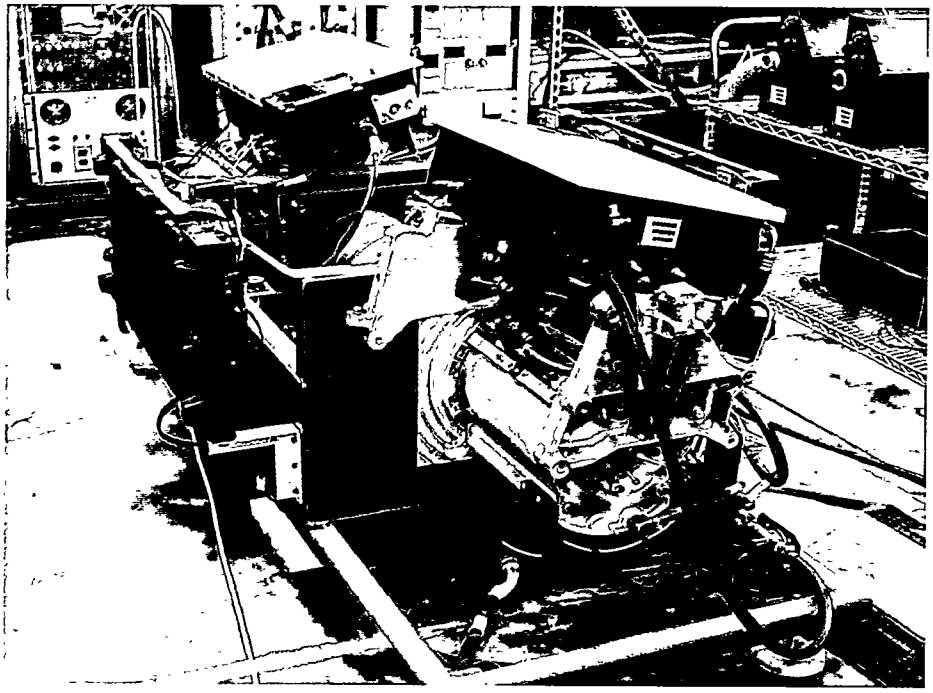

Figure 3.3-4 First Generation Back to Back Fixture

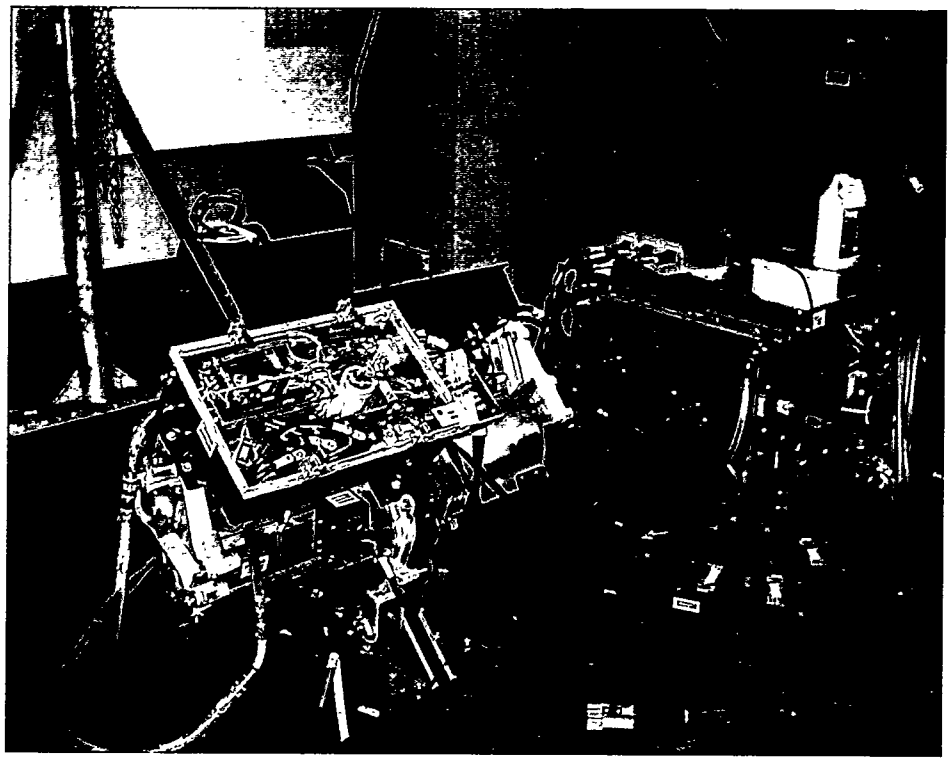

Figure 3.3-5 Second Generation Back to Back Fixture With Cooling Cart

3.4 MANUFACTURING PROCESS DEVELOPMENT

3.4.1 Manufacturing Process Objectives

The objective of this effort was to refine and enhance the manufacturing process for the electric powertrain. Included in this effort is the development of assembly flow, work instructions, and a process analysis.

3.4.2 Manufacturing Process Development Overview

The manufacturing capability for the powertrain product was developed in a three-step process. First, a build plan for the product was created. This defined the product structure, the flow of equipment in the manufacturing facility and the requirements for assembly work instructions. The next step was to analyze the product flow and the work instruction requirements to find processes that could be improved. The final step was to update the work instructions based upon the results of the analysis and feedback from preliminary assembly trials. This process provided a detailed layout for the manufacturing facility as well as concise instructions for assembly.

The product structure serves as the primary input to the manufacturing plan. With this information an assembly flow diagram is created. It is then mapped into the manufacturing facility. The details of the assembly flow diagram include 1) control stations, 2) operator and tooling requirements, 3) test and inspection station requirements, and 4) essential equipment racks and storage facilities.

Work instructions direct the assembly technician in all aspects of assembly. They provide written and graphic instructions to the assembly technicians and inform supervisory personnel of skill level requirements. The work orders specify the order in which the instructions are to be performed. The work instructions and work orders are further refined by the results of the process analysis.

The process analysis is a standard industry tool used to review the manufacturing plan against the work instructions. The objective of the analysis is to identify issues associated with product flow, instruction and training. For each issue considered, the analysis identifies the potential cause, effect, method of detection and the risk associated with not detecting an issue. The analysis provides feedback on the process implementation such as establishing quality inspection points within the assembly line.

3.4.3 Manufacturing Plan

A four-step process was used to develop the manufacturing plan for each major assembly within the product structure. The first step was to develop a process flow diagram for each major assembly. The example shown in Figure 3.4-1 is for the SCU. The Process Flow diagram identifies the subassemblies within the SCU and the order in which they were to be assembled. As the assembly continues, subassemblies were moved between staging areas. This indicates a movement from one working area or table to another. This movement is proceeded by a physical inspection or test to verify configuration control.

The manufacturing facility layout is derived from the process flow diagrams. Figure 3.4-2 illustrates a completed facility drawing for the SCU assembly area. This drawing includes work-station locations, required storage areas, and test equipment locations. The figure also includes an area designated for the expeditors. These are the manufacturing personnel responsible for documentation and moving subassemblies between staging areas.

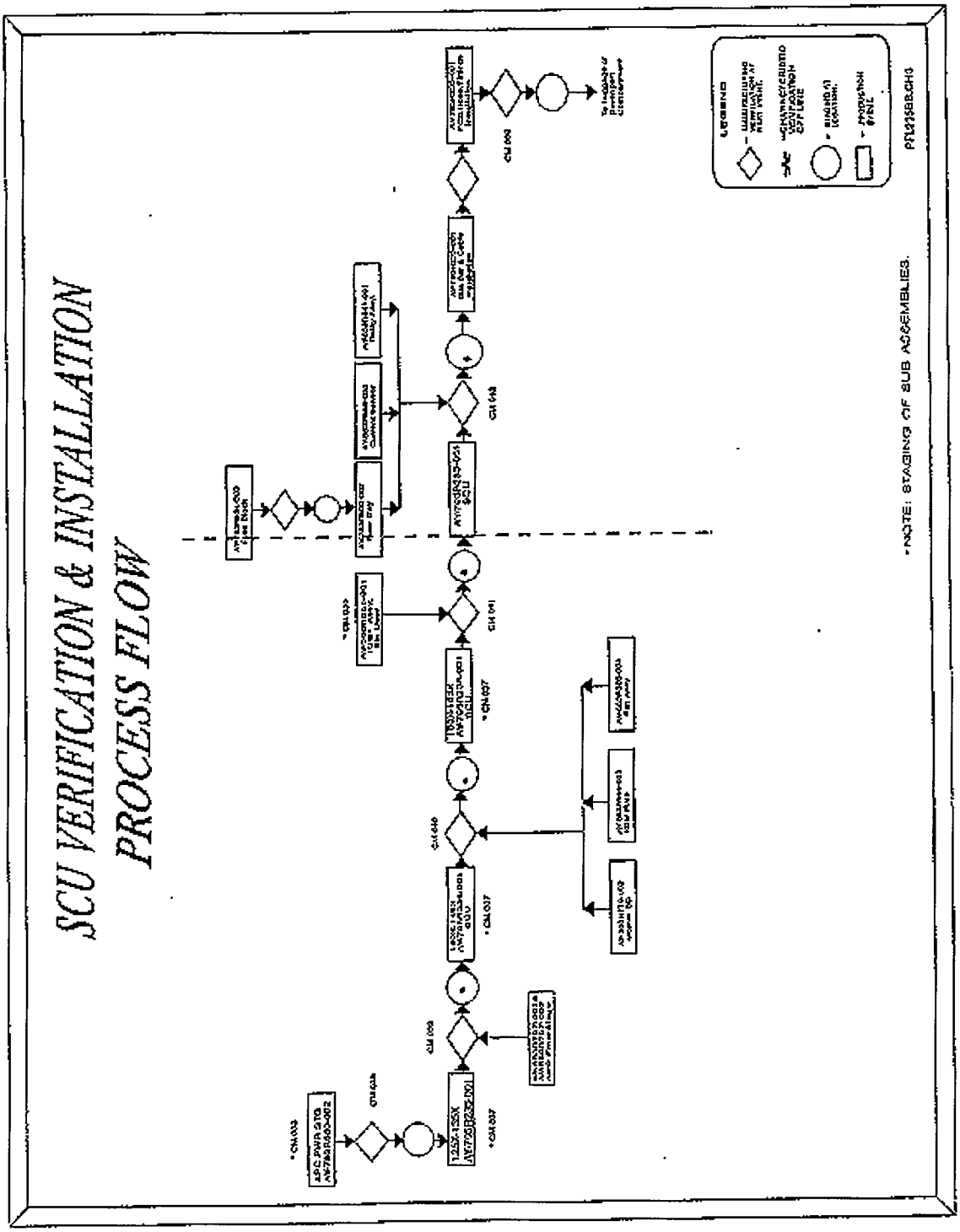

Figure 3.4-1 SCU Process Flow Diagram

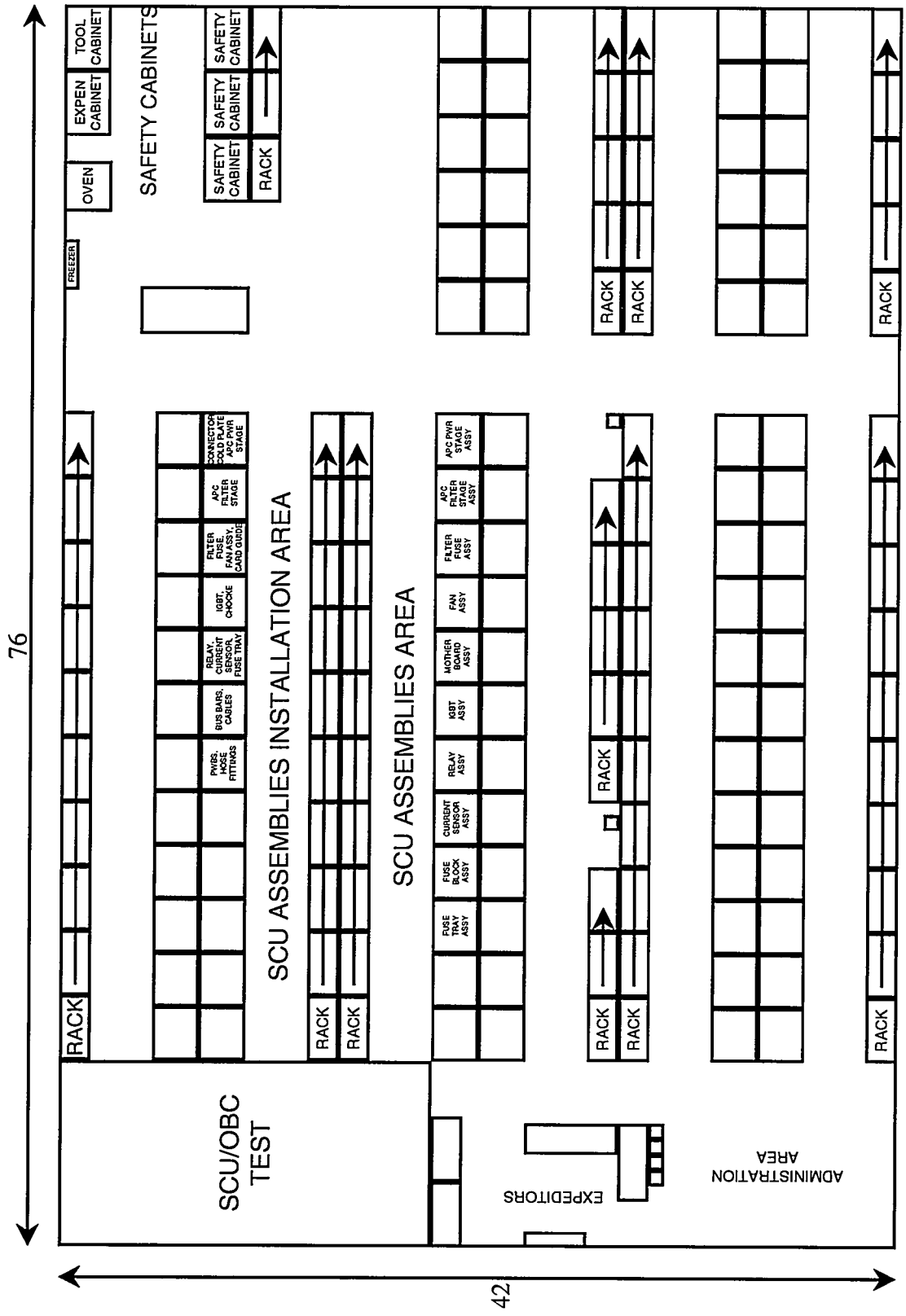

Figure 3.4-2 Floor Layout for Manufacturing Facility

Figure 3.4-3 provides another level of detail for the subassembly process flow. It identifies the number of stations required to assemble the SCU, the amount of operator time required at each station and the configuration items that are required for each subassembly.

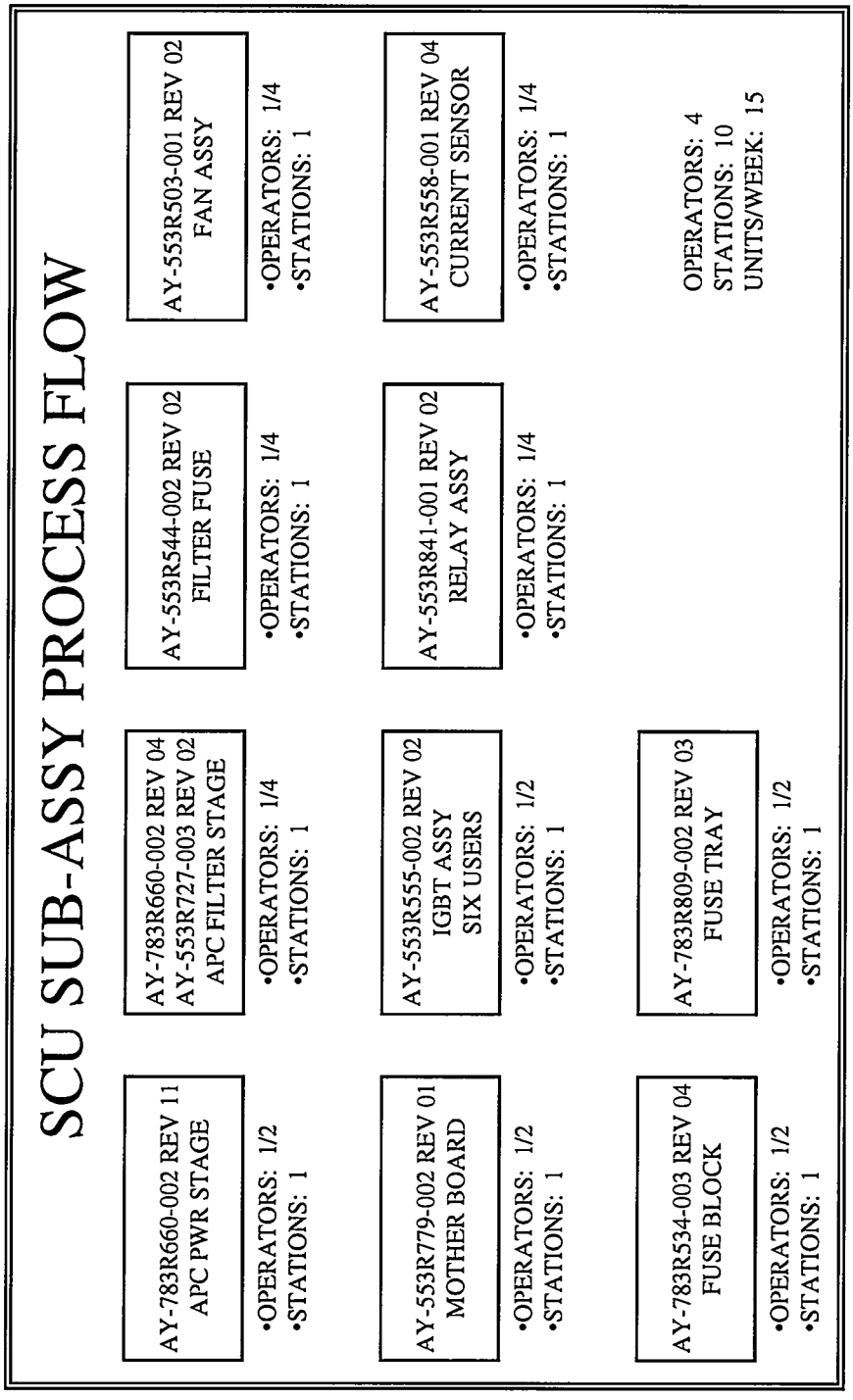

Figure 3.4-3 Sub-Assembly Process Flow Diagram

Figure 3.4-4 shows the final process flow diagram for the SCU assembly. It identifies the work-stations, the flow between stations, the number of operators required at each station, the point of verification and the tooling requirements of each station.

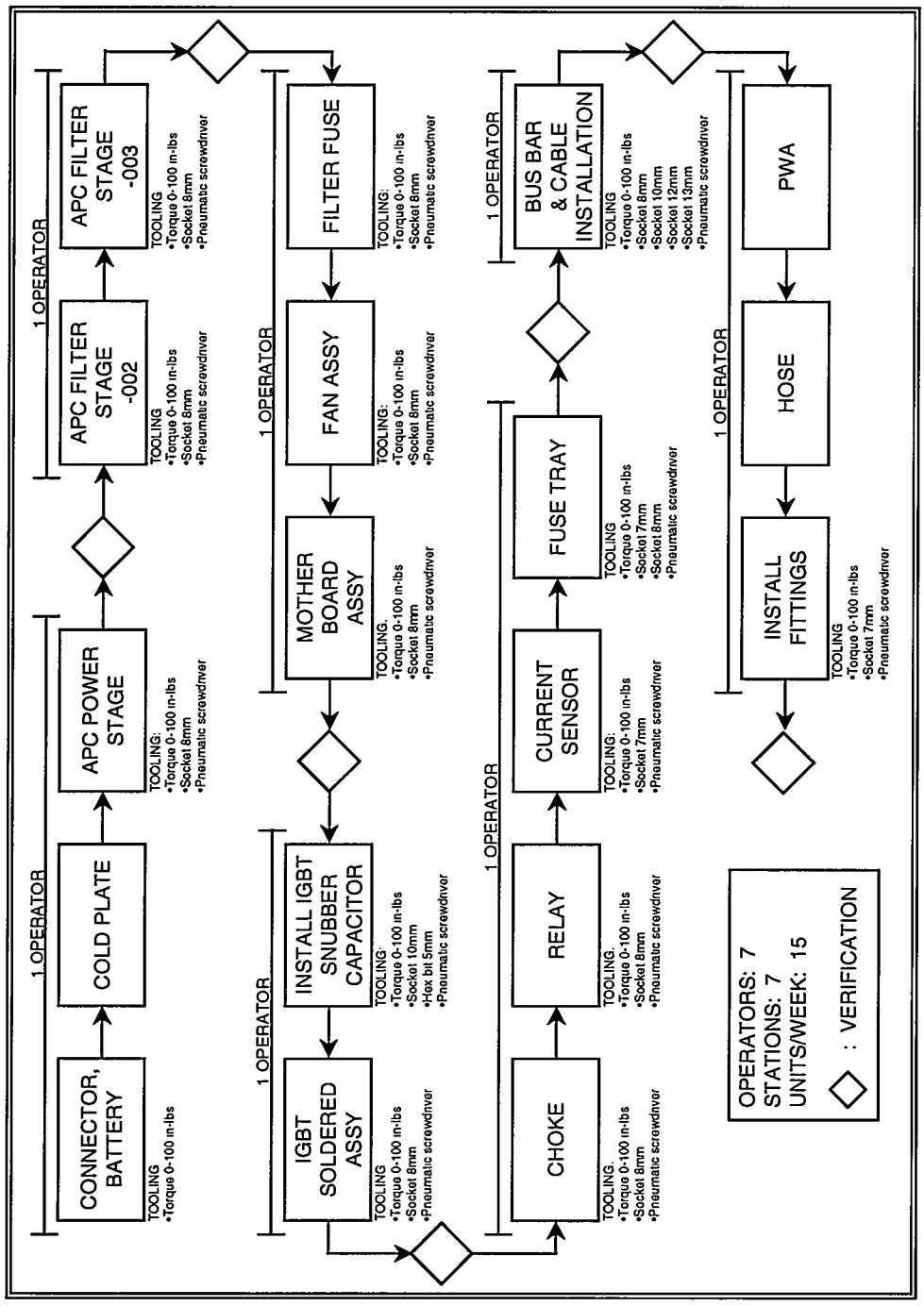

Figure 3.4-4 Sub-Assembly Installations Process Flow Diagram

3.4.4 Work Order and Work Instructions

The definition of the work orders follow from the completed process flow diagrams. They serve to document the order in which the work instructions are to be executed. The work instructions provide detailed documentation and graphics to assemble an item. While creating the work instructions a complete list of manufacturing tools is determined. This list is then used to update the process flow diagrams. To begin an assembly task the assembler will have a "kit" of parts, a work order and a work instruction. In addition, the graphic aid(s) associated with the work instruction are displayed at the work station for easy viewing by the assembler.

Figure 3.4-5 and Figure 3.4-6 provide a sample work instruction and graphic aid. Step 4.1.7.1, of Figure 3.4-5, provides instruction for aligning a thermal pad on the EGW Pump Electronic Assembly. It references the graphic shown in Figure 3.4-6 for illustration and provides a caution about damage to the thermal pad. Step 4.1.7.2 references items from the parts list. Work instructions are performed against a "kit" (container) of parts. The parts within this kit are labeled with their respective item numbers from the assembly parts list. Step 4.1.7.3 provides instruction for tightening a fastener. The instruction calls out the tools required for this procedure and the fastener torque where applicable.

EGW CONTROL-01
REV. A
Page 8

4.1.7 FINAL ALIGNMENT AND MOUNTING OF THE INSULATING PAD TO THE CONTROL ASSEMBLY HEATSINK

4.1.7.1 Make a final alignment of the insulating pad between the control assembly heatsink and the U1 component on the Pump Control Interface PWA. Align the insulating pad such that the perpendicular edges of the pad are parallel with the perpendicular edges of the U1 component on the PWA. See Figure 4.

Caution: If adjustments must be made to the insulating pad, make sure that you first lift the assembly slightly before moving the insulating pad to avoid damaging it.

4.1.7.2 Install 1 each of items #15, #17, #18 and #19 into the hole used to mount the U1 component of the Pump Control Interface PWA to the heatsink. See Figure 4.

Note: Install the screw such that its head rests against the surface of the control assembly heatsink and the flat washer, lock washer and nut rest against the U1 component on the Pump Control Interface PWA. See Figure 4.

4.1.7.3 Using the .018" Flat screwdriver, tighten items #15 and #19 until they are snug. Do not over-tighten this hardware because the threads on the plastic screw will strip very easily.

4.1.7.4 Using an ohm meter check for proper isolation between the U1 component and the control assembly heatsink. See Figure # 4 for ohm meter probe locations..

Figure 3.4-5 Work Instruction for the EGW Pump Control Assembly

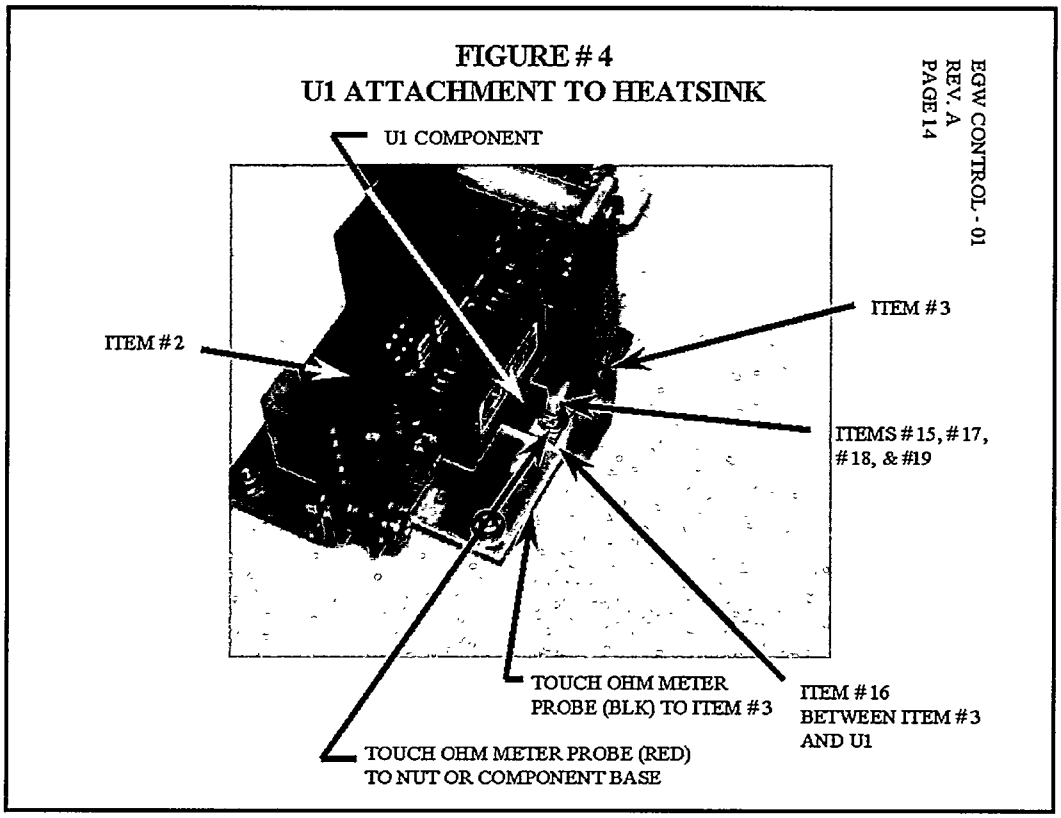

Figure 3.4-6 Graphic Aid for the EGW Pump Control Assembly

3.4.5 Process Analysis

The final step in completing the manufacturing plan is to perform the process failure mode & effects analysis (PFMEA). This uses the process flow diagram and preliminary work instructions as input to analyze the effects of improper sequencing of process flow and improper execution of steps within the work instructions. Table 3.4-1 provides a sample worksheet for the PFMEA of the motor assembly work instruction. In this example, each step of the work instruction is listed, a reasonable method of failure is proposed, the effect and failure mechanism(s) are identified and a method of failure prevention is given. Several risk values are also estimated during the analysis of each issue. The first entry in Table 3.4-1 is step 4.5.1 from the work instructions for the traction motor assembly. In performing this step, contamination is considered to be a source of failure. The most likely deleterious effects of contamination are a clogged spray ring or contaminated cooling oil. These effects have been assigned a risk factor of 7 indicating that they will not damage equipment but will be detected by the customer. The most likely source of contamination is from the work station area. The likely hood of contamination entering from the work station environment is assigned 2 out-of-10. The next column of the PFMEA worksheet indicates existing corrective action. In this case Operator training and an inspection note are present in the work instruction. The final column of the worksheet (28) represents the product of all the risk factors. In our analysis, risk products above 100 required the addition of a separate quality inspection step or a physical test to verify compliance.

Table 3.4-1 Process Failure & Effects Analysis

MOTOR ASSEMBLY								
Process Function / Requirement	Potential Failure Mode	Potential Effect(s) of Failure	SERV	Potential Cause(s) / Mechanism(s) of Failure	OCCUR	Current Process Controls	DET	RPN
4.5.1 Place stator / housing assembly ITEM #001 on clean work surface	Contamination	Clogged spray ring contaminated cooling oil	7	Operator induced contamination or dirty fixture	2	Operator training, assembly graphic and assembly inspection checklist	2	28
	Damaged Assembly	Shortened life or rework required	7	Operator mismatches lift fixture	3	Checked by operator at assembly level	2	42
4.5.2 Position motor with drive end up	Wrong end is up	Out of sequence operator actions to correct	4	Operator does not position fixture	2	Operator training, assembly graphic and assembly inspection checklist	2	16
4.5.3.1 Clean mating surfaces of endbell/motor housing	Mating surfaces not abrading with Scotch Brite	Poor sealant adhesion, possible oil leak	7	Operator failure to follow procedure	2	Operator training, assembly graphic and assembly inspection checklist	2	28
Insert oil passage tube	Oil passage tube ITEM #015 omitted	Sealant could get into the oil passage and contaminate motor spray ring	7	Operator omitted part	2	Operator training, assembly graphic and assembly inspection checklist	2	28
Clean and prime mating surfaces	Failure to de-grease both mating surfaces	Oil passage could leak cooling oil	7	Operator failure to follow procedure	2	Operator training, assembly graphic and assembly inspection checklist	2	28
	Failure to apply even coat of primer ITEM #027 to both mating surfaces	Oil passage could leak cooling oil	7	Operator failure to follow procedure	2	Operator training, assembly graphic and assembly inspection checklist	2	28
	Primer not allow to fully dry	Oil passage could leak cooling oil	6	Operator failure to follow procedure	2	Operator training, assembly graphic and assembly inspection checklist	2	24
4.5.3.2 Mix two part polyamide sealant ITEM #024	Two part mix not prepared properly	Sealant/adhesive sets too fast	7	Operator procedure failure	2	Operator training, assembly graphic and assembly inspection checklist	2	28
	Two part mix not prepared properly	Sealant/adhesive does not set	7	Operator procedure failure	2	Operator training, assembly graphic and assembly inspection checklist	2	28
4.5.3.3 Apply continuous 1/8" bead of polyamide sealant to both mating surfaces	Sealant bead is not continuous	Loss of cooling oil, limited torque, power failure	7	Operator does not apply continuous sealant bead	2	Operator training, assembly graphic and assembly inspection checklist	2	28

3.4.6 Manufacturing Capability Improvement

The detailed manufacturing documentation, developed with the assistance of the TRP project, was essential during the course of product development. The documentation provided a means of incorporating corrective action for process improvements generated through the PFMEA, product test and the product build cycles. Table 3.4-2 provides examples of issues that resulted in capability improvements.

Table 3.4-2 Examples of Manufacturing Capability Improvements

Issue	Source	Corrective Action
Consistency of epoxy bonding at traction motor endbells	Product test	Add adhesion promoter material to assembly work instruction
Concentricity of traction motor housing	Manufacturing assembly	Change expansion mandrel design
Slow bearing installation procedure	Manufacturing assembly	Add tool to install bearings simultaneously
Proper mixing of sealant materials	PFMEA	Add automatic mixing station
Improper motor phase lead length	PFMEA	Add measuring tool to replace tape measure.

3.4.7 Conclusion

The process flow diagrams, work orders and work instructions provided manufacturing capabilities to build Powertrains in high volume, with minimal test time and with consistent high quality in parts and workmanship. The detailed documentation and graphic aids provide a repeatable assembly process that can be easily updated to accomplish corrective action for issues associated with manufacturing variability.

4. EXPANDED POWERTRAIN APPLICATION

Part of the effort to reduce electric vehicle powertrian cost has been to find alternate applications for the powertrain components so that production volumes can be increased. Energy systems and hybrid-electric vehicles have been identified as applications that require technology and components similar to pure-electric vehicles. Both areas also have the potential for high-volume production. In addition, there have been a number of support systems that have proven to be needed for the pure electric vehicle that have been studied and/or tested to support acceptance of electric vehicles in fleet use. This section describes the efforts undertaken to expand the application base of the powertrain or its sub-assemblies.

4.1 INDUSTRIAL TURBO-GENERATOR SOFTWARE DEVELOPMENT AND TEST

The effort undertaken in this task was to apply the power electronics and controls portion of the electric vehicle powertrain for converting the output of a small (50 kW) turbine-generator to a 480v, three-phase power source compatible with the electric utility grid. The TRP/NGC funding was used to modify the motor controller software and test its new functionality in both the laboratory and in field evaluation at electric utilities.

4.1.1 Goals and Objectives

The Industrial Turbo Generator (ITG) was selected as a target application in which the power electronics required to interface the generator with the utility power grid is similar to the electric vehicle power inverter. This application leveraged technology, hardware, and experience from several previous programs: the EV powertrain development provided the basic power electronics hardware and software, the 135KW Battery Charger provided experience and technology for the utility interface, and the DOE funded Automotive Turbine Generator effort provided the turbine starter electronics. These technologies were integrated into the Alpha ITG unit shown in Figure 4.1-1and were successfully demonstrated at electric utility sites.

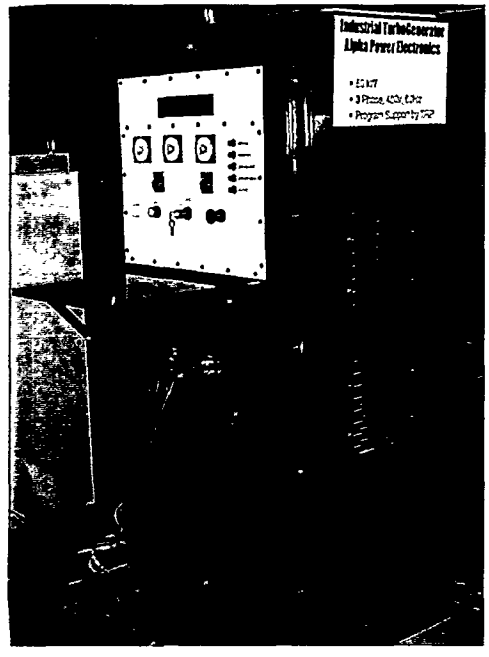

Figure 4.1-1 Alpha ITG

4.1.2 Summary of Results

The ITG's functional block diagram, see Figure 4.1-2, shows the main inverter which is the same inverter used in the electric powertrain. The ITG can be operated in either of two modes. In the "grid connected" mode of operation, the ITG acts as a current source driving energy into a utility's electric grid. In the "off-grid" mode of operation, the ITG acts as a voltage source providing the necessary current to regulate its output voltage at 480 volts.

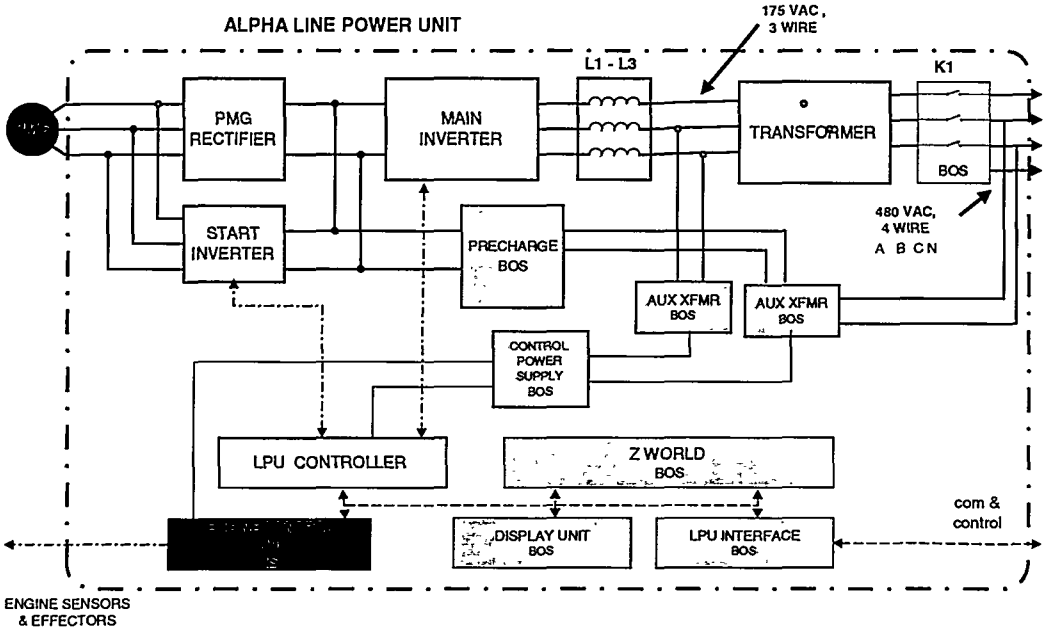

Figure 4.1-2 ITG Functional Block Diagram

The changes necessary to take the existing powertrain software and have it provide control of ITG power electronics included modifying the micro-controller software, the DSP vector control Software, and the engineering test monitor software. In addition, new software had to be developed to provide control and monitoring of ITG system. This software was tested with the power electronics in the engineering lab, integrated with the PM turbine generator and tested in the field at utility sites.

During the ITG development and evaluation efforts, the software was enhanced to provide additional capabilities of operation. These enhancements included 50Hz operation, transformer-less utility interface, off-grid operation, black start, and parallel operation of multiple units. These capabilities were added to expand marketability and reduce cost.

4.1.3 Results

The ITG control structure that was developed is shown in Figure 4.1-3. There are six software items included within the ITG control structure, the ITG host software, communications software, ECU software, micro-controller (uC) software, DSP software, and monitor software. The three software elements shown in red were modifications of software supplied from the standard powertrain product, the two elements shown in green were newly developed in support of the ITG effort.

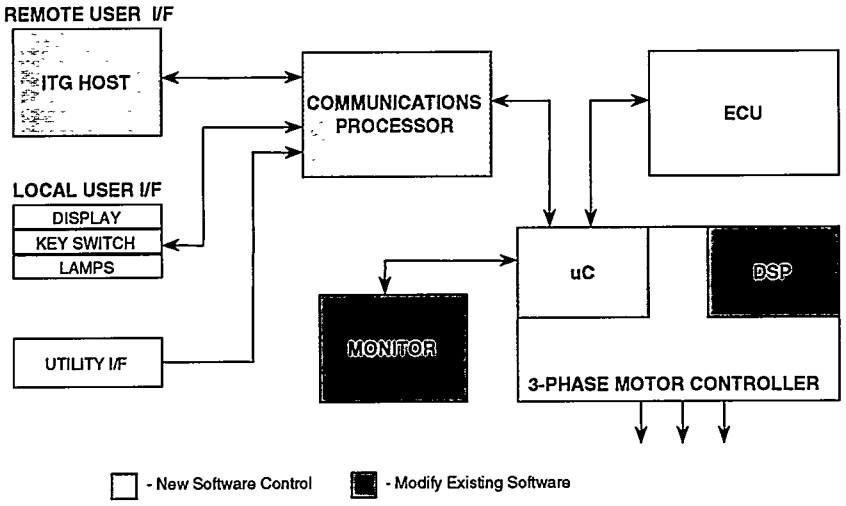

Figure 4.1-3 ITG Control Block Diagram

4.1.3.1 Micro-controller Software

The micro-controller that provided the interfaces and control of the EV motor controller was modified to provide similar control for the ITG. The new Mode Control Software was coded in the "C" programming language and uses a real-time control loop to execute and control the various modes of operation for the ITG. It provides the drivers necessary to communicate to both the Engine Control Unit (ECU) and the Communications Processor. Also, it contains the necessary code to provide continuous diagnostic checks for fail-safe operation. It uses both analog and digital inputs and outputs to provide a complete control interface. The communication interfaces also provide a path for reporting real-time operation parameters for data logging and system development. This software is easily adaptable to other Turbine Generator applications.

The Mode Control Software was required to provide the mode control for the following modes of operation: Initialization, Neutral, Pre-Charge, Turbine Start, Power On-line, Power Off-line, and Shutdown. Each of these modes is described below.

Initialization mode
The Initialization mode occurs after reset or power-on. It initializes global variables, initializes serial communication ports, executes Built-In-Test, and initializes the real-time interrupts and input capture interrupts.

Neutral mode
The Neutral mode monitors commands from Communications Processor and ECU to determine the next mode of operation. Checks critical system parameters.

Pre-Charge mode
The Pre-Charge mode enables the pre-charge circuitry to charge the high voltage DC link. It checks on the rate of charging to determine correct hardware function. It also performs a diagnostic check of the IGBT bridge to identify open or short types of failures. Upon completion of charging, it closes the main contactor and disables the pre-charge circuitry.

Turbine Start mode
The Turbine Start mode resets the starter IGBT and performs basic diagnostic checks and verifies correct DC link voltage. It sets the speed value to control the maximum speed that the

starter will spin the turbine and enables the starter circuitry. It monitors the speed information received from the ECU, monitors fault signals from starter circuitry, and monitors the DC current draw to determine successful start.

Power On-line mode

The Power On-line mode accepts a power command from the ECU and enables the 3-phase inverter in current mode. It performs various system checks to maintain safe operation such as DC Link voltage and cold plate temperatures.

Power Off-line mode

The Power Off-line mode is entered when loss of the utility power is detected or when commanded by the communications processor. It opens the main contactor to remove the ITG from the grid, switches the inverter into voltage mode, and sets the power level to the level necessary to power the local loads of the ITG. It performs various system checks to maintain standby operation and checks for utility authorization to return to Power On-line mode.

Shutdown mode

The Shutdown mode disables the 3-phase inverter and opens the main contactor. It waits for 5 minutes to allow for a cool-down period then re-initializes global variables and resets fault codes.

The uC processor had to communicate with two new processors (ECU and Communications Processor) requiring communication links to be added. The ECU controls the fossil-fueled turbine generator and communicates to the LPU via an RS-422 Interface. The Communications Processor handles the interface to the operator via front panel controls or a remote communication interface (ITG Host). In addition, it communicates to the LPU via an RS-422 Interface. The two new communication protocols are shown in Table 4.1-1. The Turbine Starter also required an additional control interface from the LPU. This was implemented using discrete digital I/O and an analog sense of the DC current.

Table 4.1-1 ITG Communication protocol

ECU to LPU Message Content:		LPU to ECU Message Content:	
Byte	Byte Description	Byte	Byte Description
1	ECU Status Byte	1	LPU Status Byte
2	Maximum Power Limit	2	Power Level Command
3	Undefined	3	Actual Power
4	Speed Command	4	Actual DC Voltage
5	Data Identifier	5	Undefined
6	Data	6	Check Sum
7	Data		
8	Check Sum		
Comm to LPU Message Content:		**LPU to Comm Message Content**	
Byte	Byte Description	Byte	Byte Description
1	Mode Command	1	Mode Status
2	Power Level Command	2	LPU Data ID
3	Status 1	3	Data MSB
4	Status 2	4	Data LSB
5	Check Sum	5	ECU Data ID
		6	Data MSB
		7	Data LSB
		8	Check Sum

4.1.3.2 DSP Vector Control Software

The DSP provides the actual 3-phase control of the IGBT's driving an AC induction motor in a motor controller application. In this case, the IGBT's are driving the utility grid at a fixed frequency of 60 Hz. The basic vector control algorithms remain the same but there are a few differences as outlined below.

The code was modified from using a resolver feedback for motor position to using a utility grid frequency signal feedback. If the ITG is to be able to connect to a utility grid and drive power onto the grid, it must be able to sense and be synchronized to the utility voltage. Also, if the ITG is operating in a stand-alone mode or the grid is temporarily disconnected then its output power frequency must be self-regulating. The line synchronization code provides the following features for the ITG:

- Synchronized output power to the utility grid
- Validation of the grid frequency
- Power factor control
- Self regulated output frequency during stand-alone mode
- Smooth transition from stand-alone to grid connected mode

Fault protection code was developed to monitor the AC voltage level of the utility grid. The ITG will go off-line if either an over-voltage or under-voltage condition is sensed. In "On-Grid" mode of operation, the ITG unit is operating as a current source. In this mode, the DSP uses current feedback to regulate its output power. In the case of a fault or loss of utility authorization, the ITG unit will transition to off-line mode and operate as a voltage source. In this mode, the DSP code senses DC link voltage and uses a feed-forward control loop to maintain the proper output voltage. As a voltage source, the ITG provides the power needed to run the local loads of the system.

4.1.3.3 Monitor Software

The PC based engineering monitor provides real-time monitoring of the modes and parameters associated with the operation of the LPU. It communicates with the LPU via a standard RS-232 interface. It also provides a method for re-programming the LPU code and modifying system parameters. This software was updated to include all the new values and formatting for the ITG system.

4.1.3.4 Communications Processor Software

The communications processor, shown in Figure 4.1-4, interfaces with the front panel for local control and displays of the ITG's output and with the grid operators via a telephone line. The control-program performs the following basic functions: a) maintains a real time clock, which provides the capability to turn the unit on or off at some user selected (via the ITG Remote Host program) date and time, b) processes all front panel and other system status inputs, provides this information to the LPU processor and the Remote Host, and uses it for internal processing c) processes communications with the Remote Host, d) processes communications with the LPU processor, e) controls the outputs which drive the front panel indicating lamps, and f) processes the information for, and drives the front panel alphanumeric display.

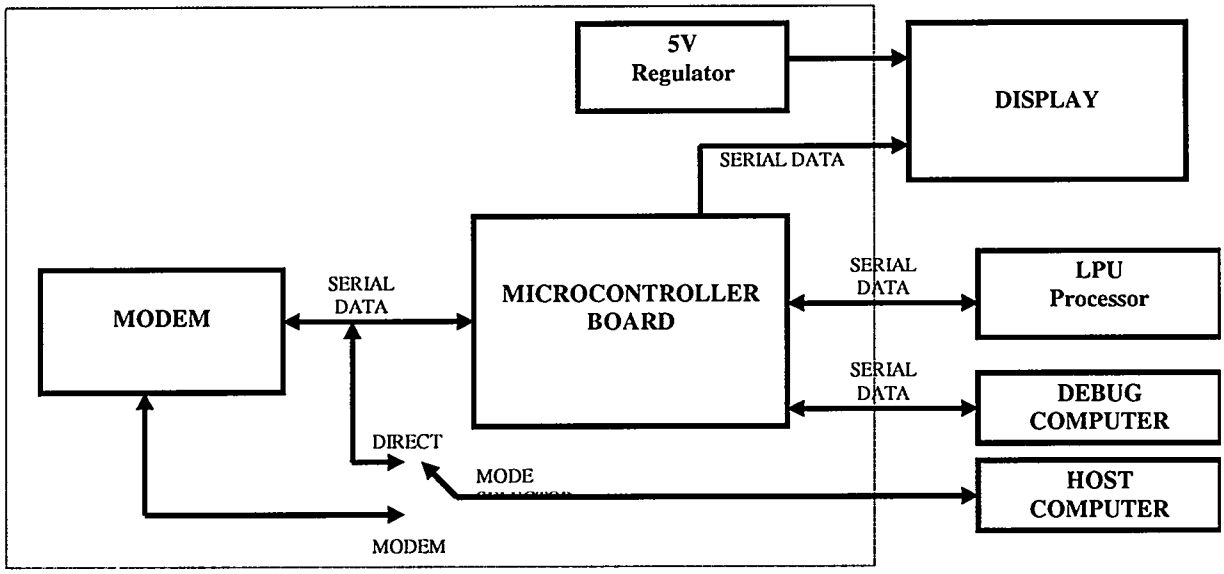

Figure 4.1-4 - Communications Processor Block Diagram

The control program runs on the micro-controller board that is part of the Communications Processor of the ITG product. The micro-controller board presently used is a "Little Giant" manufactured by Z-world Engineering, of Davis, California, and the processor on the board is a Z180 processor by Zilog. The software is written in "C", and compiled using the "Dynamic C" proprietary compiler supplied with the Z-world micro-controller board. The software is portable to any processor that has a "C" compiler available. The compiled program is programmed into an Ultra Violet Erasable Programmable Read Only Memory (EPROM) which is installed on the micro-controller board.

Real Time Clock Processing

The micro-controller board contains a hardware real time clock. This software provides a function to read from and write to this real time clock in order to maintain a local variable which contains the current system data and time. The software also maintains three variables that contain the date and time for the unit to turn on (if in remote mode), the date and time for the unit to turn off, and the date and time for the unit to report status back to the Remote Host.

Input Processing

The software reads the following digital inputs: manual start indication, remote start indication, open contactor indication, emergency stop indication, utility authorization indication, and a loss of phase indication. This information is processed and passed along to the LPU processor and the Remote Host processor. The information is also used to determine the proper command to give to the LPU processor with regard to turning on or off the unit.

Host Processing

The software communicates with the Remote Host program. This communication takes place over an RS232 data link, either through direct connection or through a modem. In the case of the modem connection, the software controls the operation of the modem - including initialization, dialing, hang-up, etc. The data transmitted over this link consists of a 195 byte message from the Host to the ITG, and a 342 byte message from the ITG to the Host. These messages contain all of the information required to control the ITG product (including setting times, power levels, phone numbers, front panel display parameters, etc.), and all of the status information from the ITG to be displayed at the Remote Host (including power, voltage, current,

fault status, etc.). The user selected phone number and power level are maintained in battery backed RAM on the Communications Processor until they are changed again by the user.

LPU Processing

The software communicates with the LPU processor. This communication takes place over an RS422 data link through a direct connection. The data transmitted over this link consists of a 5 byte message from the Communications Processor to the LPU Processor, and an 8 byte message from the LPU Processor to the Communications Processor. The information that is exchanged over this interface is front panel, system status, and mode commands from the Communications Processor to the LPU Processor, and LPU status information to the Communications Processor. The Communications Processor takes this information and formats it into messages to the Remote Host, and uses it for the front panel display processing.

Lamp Control Processing

This software controls the 5 lamps on the front panel shown in Figure 4.1-5. These lamps indicate System OK, Emergency Stop Activated, Contactor Open, Contactor Closed, and Air Filter Blocked. By using the information gathered in the Input Processing, and the LPU Processing, the Communications Processor determines the proper state for these lamps, and drives them to that state.

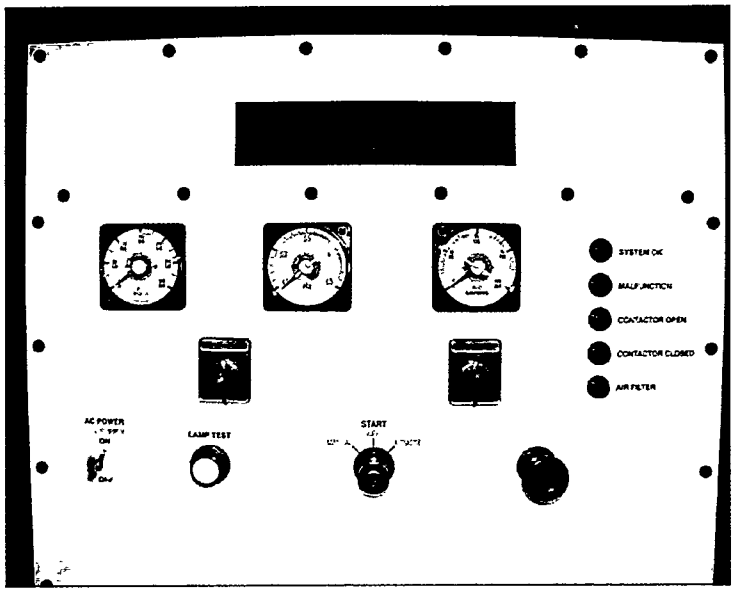

Figure 4.1-5 - ITG Front Control Panel

Display Processing

This software controls the front panel display of the unit. The display is a 2 line by 40 character alphanumeric display. Communication to the display is via an RS422 connection. The software scrolls through a list of user selected system parameters at the user selected interval, and displays the name of the parameter, the current data for the parameter, and the units of the parameter on the alphanumeric display. The user can configure this display to show any or all of the available system parameters by means of the Remote Host program. The selected configuration is maintained in battery-backed RAM on the Communications Processor until it is changed again by the user.

4.1.3.5 ITG Host Software

This software program runs on windows-based personal computers. The program runs under the Microsoft Windows operating system, and is written in the Visual Basic language, using the Microsoft Visual Basic compiler. The program will run on Windows versions 3.1 and above.

The program uses a graphical user interface, and is used to remotely control, via direct RS232 serial connection or via telephone line using a modem, the ITG equipment. The user can connect to any one of a number of ITG units by means of a menu selection. The user can then view current system data on the selected ITG (e.g., power, voltage, current, fault status), and can control the unit (e.g., turn on, turn off, set power level). The program itself is password protected so that unauthorized users cannot run the program. The control functions are also password protected, so that viewing privileges can be distributed to multiple users without distributing control authority. The basic functions of the program are listed below.

Figure 4.1-6 shows the ITG Host Software's Main Menu. The main form (screen or page) contains a drop down menu across the top of the form with the following selections: File, Options, Data Logs, Com Ports, Phone, View, and Help. The main form also contains a section for the user to make selections with regard to: ITG Unit ID, Mode Command, Power Command, Current Time, Time to Turn On, Time to Turn Off, Time to Report Data, and Phone Number to Report to.

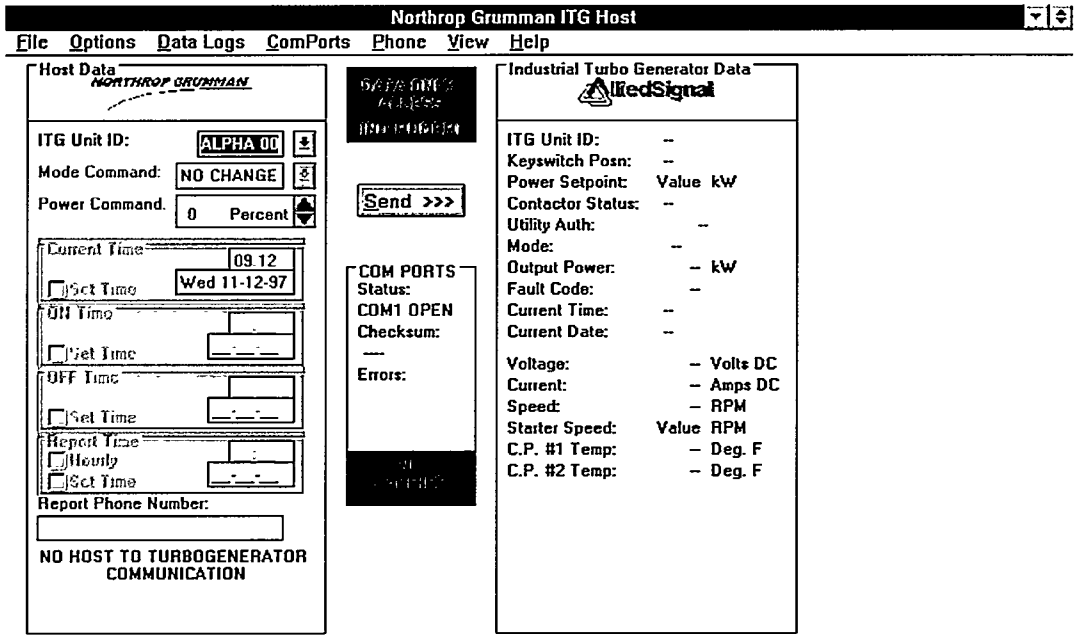

Figure 4.1-6 - ITG Remote-Host Main Menu

The main form includes a section where current ITG Data is displayed. This data includes ITG Unit ID, Key Switch Position, Power Set-point, Contactor Status, Utility Authorization Status,

Mode, Output Power, Fault Code, Current Time, Current Date, Voltage, Current, Speed, Starter Speed, Coldplate 1 Temperature, Coldplate 2 Temperature.

The main form also includes some general status information: Data Only or Control Privileges, Modem or Direct Connection, Com Port ID, Presence of Carrier Indication, and ITG Status.

The "File" selection in the main menu allows the user to exit the program.

The "Options" selection in the main menu allows the user to perform the following actions: Configure the ITG Display, select Full Control or Data Only Access, select Direct Connection or Modem Connection, and select Sound or No Sound. If "Configure the ITG Display" is selected, the user is presented with another form which he can fill out in order to control the data that is displayed on the front panel of the ITG and the duration that the data is displayed before displaying the next parameter. Configuration of the display output is performed by selecting parameters from a predefined list and inserting them into a second list in the order desired. This second list is then transmitted to the ITG when the list is complete. All user actions are graphical in nature - that is, they can be performed using a mouse to drag and drop.

The "Data Logs" selection in the main menu allows the user to Start Recording, Stop Recording, or Retrieve the ITG Event Log. If the user selects Start Recording, all data transmitted between the ITG Host and the ITG will be recorded in a comma-delimited file on the hard drive of the computer which is running the ITG Host program, until Stop Recording is selected. This file is suitable for direct import into an Excel spreadsheet. The ITG Event Log is a 100-second buffer of all communication between the ITG Communications Processor and the LPU control processor when the power level is non-zero. The "Retrieve" option transmits this buffer from the ITG to the ITG Host, storing the data in a comma delimited file. The 100-second buffer is useful for analysis after a fault or failure.

The "Com Ports" selection in the main menu allows the user to select between Com1, Com2, Com3 or Com4 on the personal computer.

The "Phone" selection allows the user to Dial the selected unit, to Hang-up, or to Setup Phone Numbers for all of the units. The Setup selection presents the user with a separate form to fill out, allowing the user to change any of the stored phone numbers. The phone numbers are stored in a file on the hard drive of the personal computer for access anytime the program is run.

The "View" selection of the main menu allows the user to select the type of ITG status data that is displayed on the personal computer screen. The choices are: Normal, Software Versions, Scheduled Events, LPU Status, Faults, ECU Data, ECU Faults, ECU Shutdowns. Each selection pops up a different window on the display showing the current values for the selected data.

The "Help" selection on the main menu allows the user to view general information about the ITG Host program, such as copyright information, version number, programmer's name and address, etc.

4.1.3.6 ITG Integration and Test

NGC was responsible for the design, assembly and test of the power electronics portion of the ITG unit. As described above, the inverter bridge and control electronics were hardware previously developed under the electric vehicle program. This hardware was modified for the ITG and additional hardware and control electronics were designed as needed. All the electronics were mounted in a cabinet that included a front control panel – this was provided by an outside vendor and specified by NGC and Allied Signal.

Except for the ITG Host computer, all the electronics were installed inside the cabinet as shown in Figure 4.1-7. This included the Line Power Unit (LPU), control hardware, cooling system, and balance of system (BOS) components. The BOS consisted of contactors, relays, transformers, power supplies, fuses, and any other components required to interface to the utility grid. This also included the necessary power supplies required by the turbine electronics.

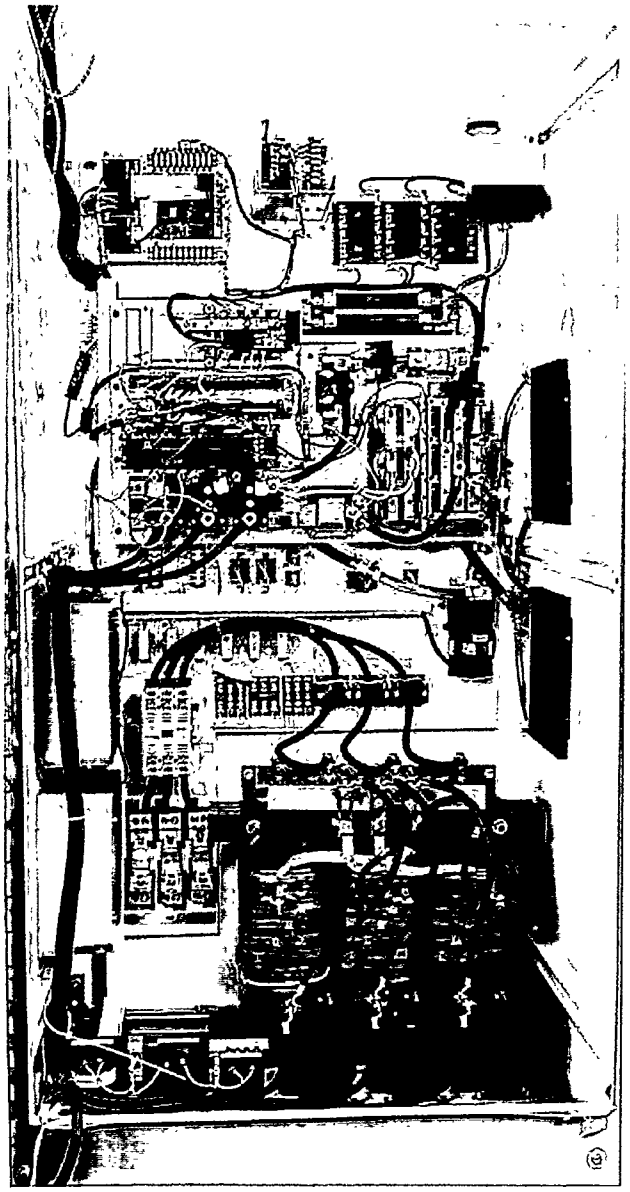

Figure 4.1-7 Interior of ITG Cabinet

Testing of the units at NGC was done without a turbine driven power source. The basic setup for testing was to use batteries and power supplies to simulate the turbine power source. The output was connected directly to a 3-phase 480 VAC grid. These units were designed for grid connection only not stand-alone as described below. The units have two basic modes of

operation, which were tested and verified. The normal mode of operation was grid connected current source. In this mode, we tested the output power level from 0 kW to full power, 50 kW. The second mode tested was voltage-mode when the grid was disconnected from the unit or utility authorization denied. We also verified correct transition between the 2 modes of operation.

The integration with the turbine generator involved developing and testing the control interface between the LPU and Engine Control Unit (ECU). Also, extensive testing was done with the LPU controlled starter that is used to start and motor the turbine. After the system testing and integration was complete, ITG units were installed at a utility company test site. Figure 4.1-8 shows the first ITG unit installed at an electric utility site All of the field installations and testing were done in the United States with the exception of one unit sent to France (see 50Hz operation below). At the customer sites, further testing work was done. Since these installations were outside and in varying climates, most of the challenge in the testing was to solve specific environment related issues. The ITG units were operating at the following customer sites:

- UniCom – Chicago, IL
- ENERGIST – Newark, NJ
- SONAT – Tampa, FL
- New Energy Venture – Tucson, AZ
- EDT - France

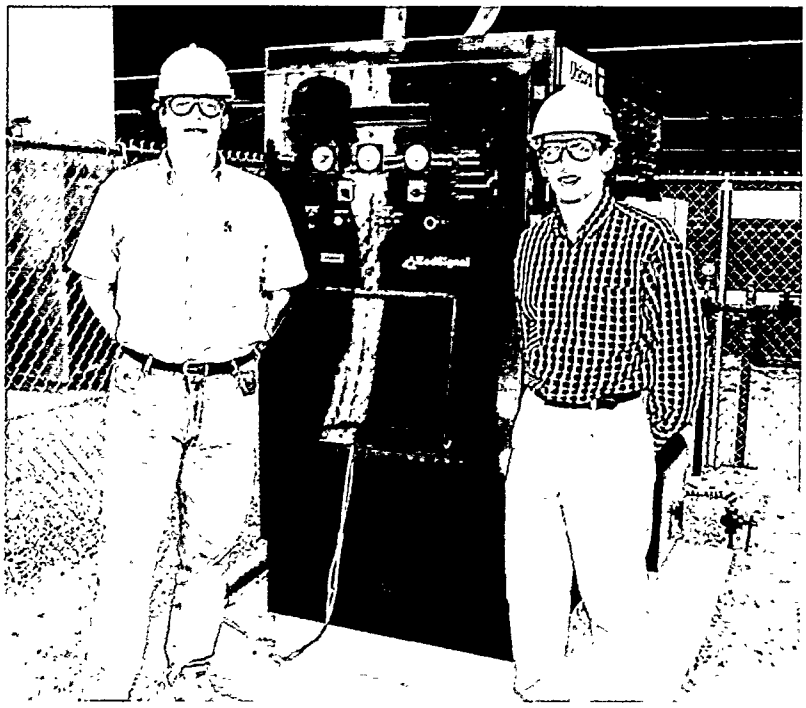

Figure 4.1-8 - NGC Engineers and ITG unit at UniCom

4.1.3.7 Enhancement to ITG Software & Algorithms

50Hz Operation

The ITG system required both hardware and software modifications to support a 50Hz grid connection. This requirement came about as a result of needing to have a unit operational for

testing and analysis at a French utility company, Electricite de France in Moret sur Loing, France. The goal was to operate the ITG connected to a 50Hz, 3-Phase, 415 VAC power grid. It was also required that the unit provide a means to vary the output power factor, which was normally set to a power factor of 1.

The following changes to the ITG unit were required:

- New Output Transformer for a 50Hz, 415 VAC grid.
- New 50Hz Cooling Fan and Pump
- Additional output Filter to reduce the EMI
- Improved Loss of Phase sense circuit
- Line synchronization code modified for 50Hz
- VAC over/under fault sense levels updated
- Power Factor Control – set via the Monitor

The modifications to the electronics were completed and the ITG was installed by Electricite de France in Moret sur Loing. The unit was subjected to rigorous testing by the French utility. The ITG was able to pass the testing of its 50Hz mode.

Transformer-less Utility Interface

As a cost reduction effort, the ITG design was modified to enable a direct connection to a utility grid without the need for a step-up voltage transformer. The original design used a transformer that allowed the 175 VAC IGBT (Inverter Bridge) output to drive a 480 VAC grid. The modified design can drive a 208 VAC grid. By eliminating this step-up voltage transformer, the system installation cost is reduced by more than $2500. The unit could still interface to the higher voltage grid but would now require a customer supplied transformer.

These changes also prompted the need to improve the harmonic distortion to meet IEEE-519. The distortion was improved by two modifications. First, filter capacitors were added to the output of the inductors to form an L-C filter. Second, an additional current sensor was added so the DSP could now sense the current of all three phases. This enabled the use of a modified vector transform equation to use feedback from three phases in place of the two- phase feedback used in the basic inverter.

Stand-Alone Operation

Stand-alone operation is required for power generation at installations where there is no grid present. Also, this mode of operation is needed when the unit is used as an emergency power source in the event that the utility grid is disabled. This feature alters the basic operation of the power electronics and control software. The ITG changes from being a current source with balanced loads to operating as a voltage source with varying and possibly unbalanced loads. Also, the unit must provide control to transition between these two modes of operation.

This mode was developed for 208 VAC transformer-less operation. The same output L-C filter configuration was used as described above. The inductance and capacitance was varied to optimize the harmonic distortion for both modes of operation. In voltage mode, the addition of a fourth wire for neutral was added. To provide necessary control feedback, voltage and current sensors were added to the capacitors for each phase of the output filter.

The "voltage-mode" described for the original ITG design only provided power to maintain the local loads of just the unit. It had a limited power range and assumed balanced loading. This was implemented using a simple feed-forward control algorithm based on DC link voltage. The new "voltage-mode" needed to provide independent control of each phase over the full power range. This required new phase dependent vector transformations that closed the loop on the

capacitor voltage and current sense. Each phase would now maintain the correct voltage over the full power range and under all loading conditions.

Black Start

The "Black Start" feature allows the ITG unit to start when there is no grid. Normally, the utility grid provides the power to turn-on the system, pre-charge the DC link, and start the turbine. Once the system is up and running, it provides its own power in the event of a utility outage. This feature is mainly needed to operate in a stand-alone environment.

An analysis was done to explore the system requirement to provide this feature. The specifications required by the initial design were:

- 24V battery power source
- Turbine starter requires 300 VDC
- Provide power for 5 possible start attempts
- Provide power for power supplies, lamps, fans, etc.
- Allow 6-8 hours to recharge battery

The approach was to use simulation software to model the system needed to provide all the features outlined above. The design was a 24VDC to 300VDC boost chopper. While the design proved to be sufficient, the components required were quite expensive. Two conclusions were made. One, if a boost chopper design was used, the battery voltage should be increased to 36V to reduce the current requirements of the power electronics. Second, the components required for the boost chopper were more expensive than the cost of just batteries and a small charger. The analysis was completed but the design was not implemented in any of the ITG units.

Multiple Units

This design is a system whereby multiple ITG units can be connected together on the same power grid in order to increase the power generation capability. A means to control the power and power factor of each unit using a high-speed serial data bus and a master control computer is described. This method minimizes the interconnecting wiring required.

Small, Micro-turbine generating equipment is limited in power capability today to a range of approximately 100 kW per unit. In order to provide more than 100 kW at a particular site using this type of equipment, it is necessary to connect multiple units in parallel. In order to do this, the units must be carefully controlled by a system master controller in order to optimize turbine generator operation. A method to control a cluster of ITGs is described in the following paragraphs.

Multiple units are connected by means of an optically isolated, 4 wire serial bus, using an RS485 format or equivalent. Twisted pair wire is used between units. A total of 64 units can be directly connected together on a single bus using this method (under RS485 rules). Multiple buses connected to the same master controller can support larger numbers of units. The maximum length for each 64 unit bus (under RS485 rules) is 4000 feet. The bus is dedicated specifically to the control of power level and power factor for each unit. See Figure 4.1-9 for a block diagram of this concept. With the maximum 64 units attached to the bus, the maximum update rate will be once per second per unit at a baud rate of 19.2 K baud, assuming a 10 byte message and a 10 byte reply for each unit, and round-robin polling. With fewer units connected to the bus, the update rate can be proportionately faster. Each unit on a bus will be assigned an address (or ID), and will only reply to messages that contain the assigned ID. The command from the master controller will include the following: the destination ID, the source ID, a

message counter, the power command, the power factor command, and message integrity bytes. The reply from the addressed unit will include the following: the destination ID, the source ID, a message counter, the current power level, the current power factor, and message integrity bytes.

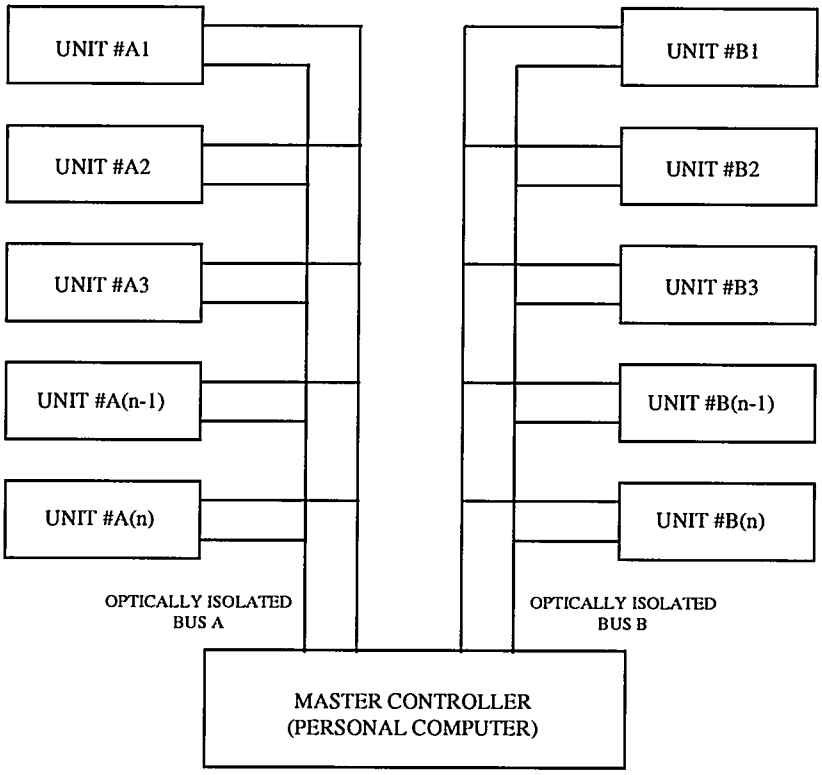

Figure 4.1-9 - Multiple Unit Control Block Diagram

This scheme provides power and power factor control of multiple small generators connected to a master controller by means of a high-speed dedicated serial bus. The number of units connected, the baud rates, the signal voltage levels, and message lengths are specific examples for the envisioned implementation. This design allows the reconfiguration of the entire set of units to meet the needs of specific applications. By providing a means to command the power that each unit is to deliver, this scheme allows the entire network of units to compensate for one or several "weak" units, or to compensate for a unit that the master controller has determined is not functioning properly and has taken off-line. This will provide for graceful degradation of the network of units, extending the operating time between required maintenance events.

4.1.4 Conclusions

The ITG program was quite successful in leveraging technology from previous programs. This was especially true for the core power conversion section taken from the electric vehicle program. By expanding the use of this technology, both programs will benefit from cost savings and technological developments in the future. Market research indicates that the ITG will have higher volumes than electric vehicles for the next ten to twenty years.

The software development was a substantial portion of the ITG operation and control. Because of this, the design lends it self to easy adaptation to future design requirements such as power levels, operational modes, or utility interfaces. This design also is a stepping stone to the development of state-of-the-art military gen sets. Since the design is already compact, multi-fuel capable and quiet, it could easily be made more rugged and transportable to meet military applications.

Due to the software and hardware enhancements and design simulations, the basic ITG can be transformed into a versatile power generation product with a wide range of applications across global markets. The Alpha units have been proven in both the lab and at customer sites. The stage is set to produce the ITG design to meet the needs for a growing distributed power generation market. The concept of what a high volume production unit may look like is shown in Figure 4.1-10.

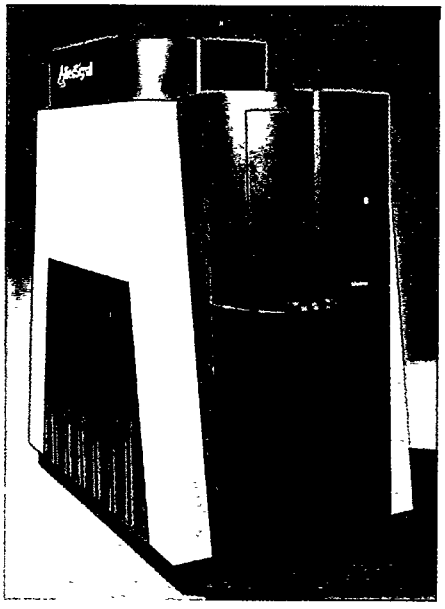

Figure 4.1-10 – Artist Concept of Production ITG

4.2 HYBRID-ELECTRIC POWERTRAIN

The pure-electric bus has been proven to have the range to meet the daily needs of over 40% of the school bus routes in the United States. Another viable market for the powertrain is the transit bus market. Unlike school bus systems, transit bus systems are revenue producing and continually strive to increase ridership through advertising, passenger comfort, and reliable service. The transit buses have a higher purchase price, have higher daily usage, and have a longer service life than school buses. Pure-electric buses would only cover a small portion of the transit bus market due to their limited range but, if the electric powertrain was adapted into a hybrid-electric configuration, it could meet the needs of virtually all transit systems.

4.2.1 Goals and Objectives

The goal of the hybrid-electric project was to study and evaluate hybrid-electric controls and vehicle operation utilizing a prototype hybrid-electric vehicle both in the lab and in actual revenue service. The objective was to improve upon the vehicle range and reduce any special considerations required of electric buses when operators planned their transit system routing.

4.2.2 Results

The electric bus powertrain (motor and motor-controller) were integrated with an APU. The energy/power management software was modified to account for the APU and the new battery pack configuration. The hybrid-electric bus tested was a transit bus of 33 feet, 33,000 lb. GVWR, air conditioned, and diesel heated. This bus was ultimately tested in revenue service by a transit agency which also had several pure electric buses as part of its alternate fuel fleet. In planning for the hybrid operations, the 230 hp powertrain had to be modified in software and hardware to handle half of the on board battery complement that it was accustomed to operate with in the total electric mode. Figure 4.2-1 shows the resulting layout of the hybrid electric powertrain.

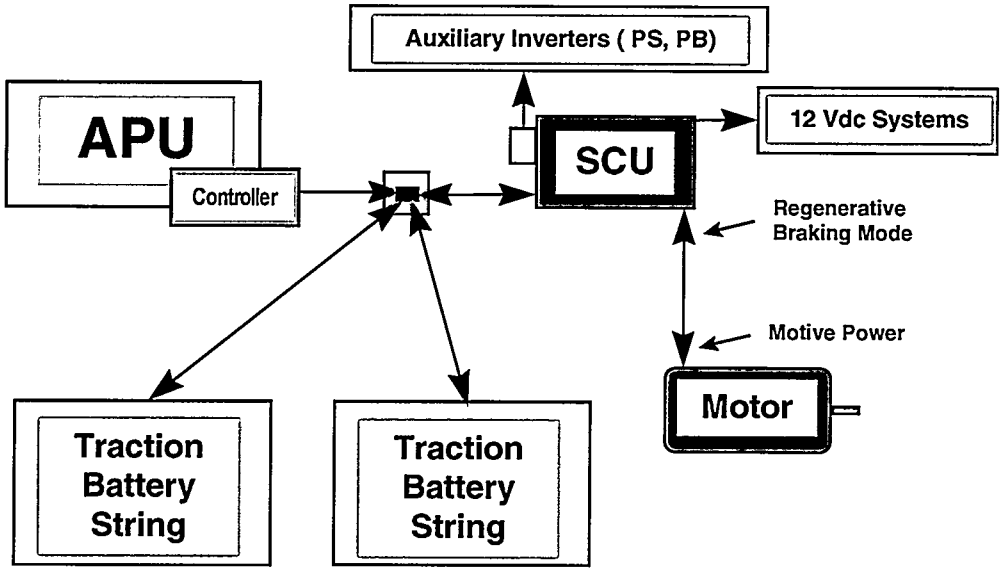

Figure 4.2-1 Hybrid-Electric Bus Block Diagram

Prior to the building of the hybrid-electric bus, data was collected from various other test programs. One such evaluation was a test in which an electric transit bus towed a trailer with a 50kW generator to simulate hybrid transportation (see Figure 4.2-2). An endurance test using this vehicle set-up was a trip of approximately 775 miles, from Baltimore, MD to southern Georgia. Fuel consumption, state of charge changes and other data were collected during the trip. This data, along with information from transit agencies, was used to determine the appropriate size of the on-vehicle generators in the prototype hybrid-electric bus.

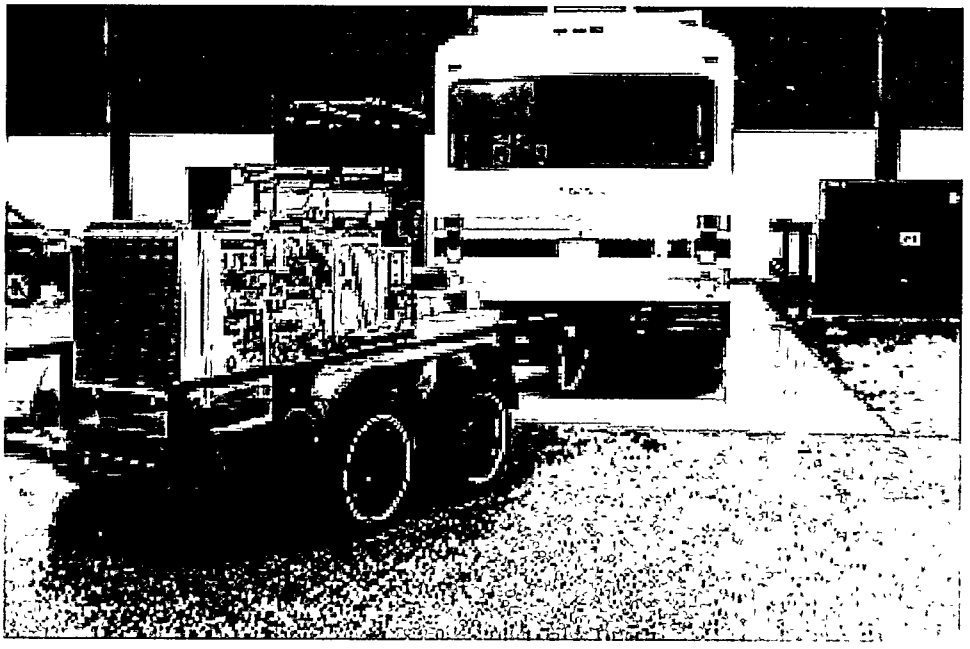

Figure 4.2-2 Hybrid-Electric System Evaluation Set-Up

A 35kW generator was selected for its efficient operation and its applicability to the average routes of the transit agency where the initial hybrid-electric bus was to be evaluated. Figure 4.2-3 is a photograph of the hybrid bus with the Isuzu generator installed.

4.2.3 Hybrid-Electric Bus Generator

Testing of the first hybrid-electric bus operating on the transit system's standard routes indicated that the engine was correctly sized for the application. The average power appeared to be around 25 kW. No air conditioning load was used during these test runs which would add another 7 kW load to the required APU output power.

The initial fuel mileage was about 8 mpg. This fuel mileage provided for a range of almost 320 miles using the forty gallon fuel tank. Isuzu was later contacted for an optimization program to see if the "sweet spot" of the engine could be adjusted for the optimum operating point. The first attempt was to reduce the engine set point speed to get Black Smoke at about 32 kW. Isuzu provided data and instructions for further tuning the engine and an increase of several percent in efficiency was achieved. By optimizing the APU controls, a fuel mileage of 11 mpg was achieved. The mileage achieved by standard diesel powered buses running the same route was in the range of 5 mpg to 8 mpg.

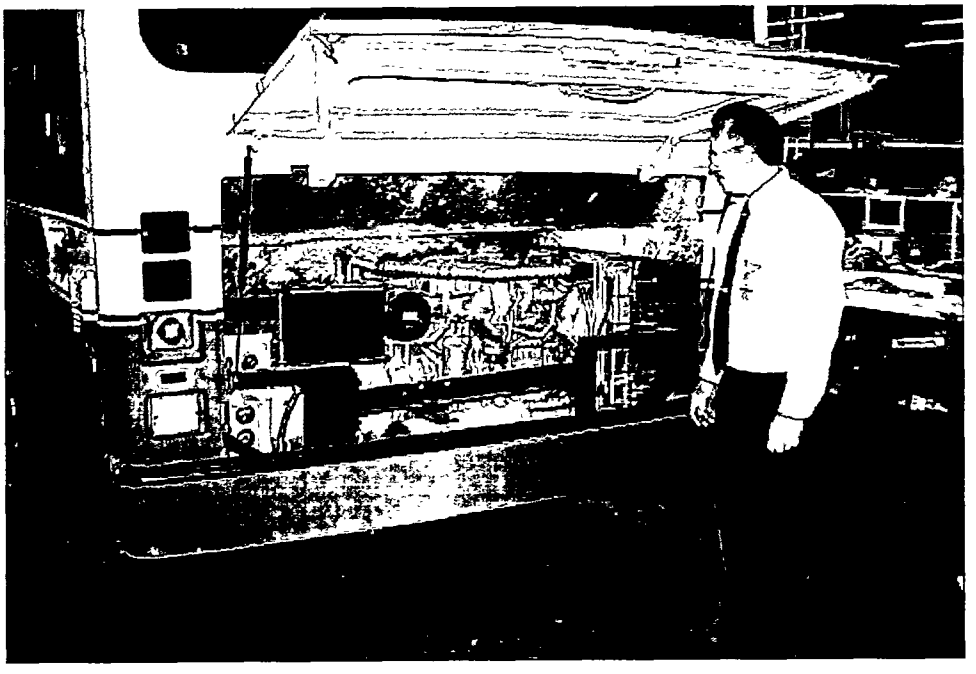

Figure 4.2-3 Hybrid-Electric Transit Bus with APU

Cooling of the APU was a concern as its temperature increased about 20°C during high speed running. Additionally, the batteries were monitored for heating effects during charge and discharge. Temperature variations were noticed. The batteries were instrumented to monitor heating during charge and discharge with a BMS. It was found that generator output must be controlled to minimize temperature variations in the batteries. Without monitoring battery temperature and compensating for the batteries temperature, the battery cycle life would be degraded.

During test of the initial hybrid-electric bus, energy usage for a nine mile driving course was collected. The collected test data is shown in Figure 4.2-4. The graph shows relative speed compared to position during the test loop.

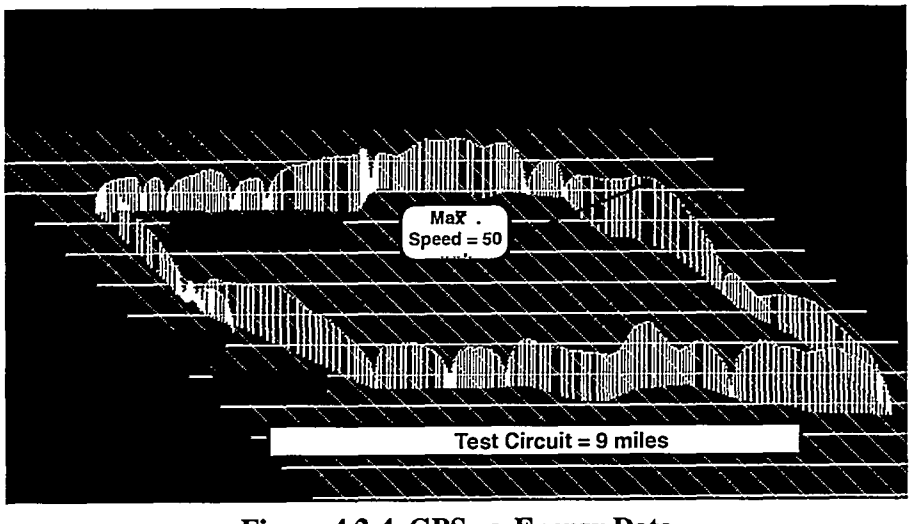

Figure 4.2-4 GPS vs. Energy Data

4.2.4 Conclusion

A simple control application of constant speed allows the hybrid power plant to run efficiently with low emissions. Proper sizing of the APU is critical in determining whether the vehicle will be charge depleting or charge sustaining. Valuable information on battery reactions during hybrid applications indicated that an exacting voltage control method should be used at the output of the APU. The temperature of the batteries would tend to rise above recommended levels if the APU was allowed to carry the state of charge past 80%. Two control theories on the APU were spawned from this data. One method was to control the voltage setting on the APU so that the batteries could not attain a charge greater that 80%. The other method was to turn on and off the APU in an attempt to maintain the state of charge between 30 and 70%.

Additional areas requiring strict management of the energy/power within the hybrid-electric system were during voltage swings due to high current accelerations & regenerative braking, equalizing schedules for batteries, and individual battery monitoring.

The hybrid-electric drive system met the goals of the project. The hybrid-electric buses provided additional range and simplified vehicle planning and battery state-of-charge maintenance. The hybrid-electric also decreased fuel consumption by as much as 50%. The success of the initial hybrid bus in the transit system's fleet has led to the decision to acquire additional hybrid-electric buses for use in their fleet. These additional hybrid-electric buses incorporate the improvements determined during the testing of this first hybrid-electric bus.

4.3 ELECTRIC VEHICLE AUXILARY SUBSYSTEMS

With the introduction of electric powertrains, an area that seemed to be lacking with most heavy vehicle OEMs and vehicle operators was the ability to integrate and support other vehicle systems, beyond the powertrain, that are found on electric vehicles. High voltage systems, charging systems, battery systems, and electronic systems integration were a few of the areas that appeared to need support in order to bring electric transportation to market.

4.3.1 Goals and Objectives

Northrop Grumman's objective for the EV sub-systems efforts performed, was to provide the engineering guidance for electric and hybrid-electric bus transportation systems. The goal of the effort was to have all of the system's major components perform and support one another seamlessly. The intent was to improve on the transit operator's objectives for electric transportation and to address the clean air objectives across the United States and international communities. The vehicle system's various major components for electric and hybrid-electric transportation were tested at transit agencies by introducing electrically powered buses to actual revenue service. This testing was to validate the technologies from a systems operation level. Figure 4.3-1 shows an electric bus with the Northrop Grumman 230 HP powertrain.

Figure 4.3-1 Electric Transit Bus with 230 HP Powertrain

4.3.2 Results

System enhancements were made throughout the electric transportation system's major components. The sub-systems analysis as well as laboratory and field testing addressed system level issues such as environmental conditions, the bus cooling system, the battery management system, the battery energy storage system and both fast and slow charging. Summarized below are the major improvements that contributed significantly towards achieving the goals envisioned for the electric transportation system.

Environmental Conditions

Electric and hybrid-electric buses were fielded into revenue service at various transit agencies across the United States. These locations provided a harsh environment of temperature

extremes and weather conditions. Several occurrences of under-body water penetration required changes in sub-system installation locations and materials. Pressurizing of the electronics compartments and selecting waterproof connectors were some of the enhancements accomplished. Newly developed high voltage connectors and cabling were also tested.

Another example of an environmental issue was uncovered when the powertrain electronics detected chassis isolation faults. It was determined that the chassis fault detection was valid and that the fault was being caused by moisture in the battery compartments and junction boxes. With the detection of such a fault, the operator would take the bus out of service for repair. Environmental improvements to the chassis and battery packs greatly reduced the number of chassis faults. In addition, upgrades to improve the operator's high voltage display unit virtually eliminated the conditions that generated the chassis faults.

Cooling System

The Cooling system was put to the test at high temperatures during the summer and low temperatures during the winter. Summertime saw temperatures in the 100's sometimes exceeding 130°F coming off the pavement. This lead to enhancements for improved cooling for power electronics and associated accessories. Temperatures would reach lows of -30°F during several weeks in the winter. Due to the cold extremes the cooling system was enhanced with bypass valves for pressure relief and the electric heater was replaced with a diesel heater to meet passenger comfort needs. Cooling system and battery issues were addressed on a case by case basis and then improvements implemented. One such improvement was to keep the vehicles in ambient 40°F locations overnight and/or while charging. This prevented the cold soaking of the lead acid batteries and enhanced the driving range during cold weather. Figure 4.3-2 shows the cooling system as it is typically installed in an electric bus.

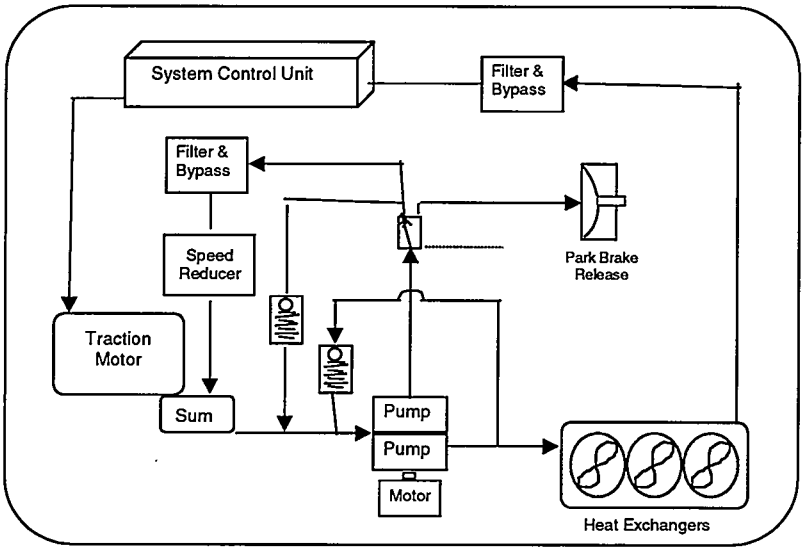

Figure 4.3-2 Electric Bus Liquid Cooling System

Battery Management

The extreme temperatures also appeared to contribute towards an increased battery failure rate. This led to the installation of a battery management systems (BMS) for all battery packs on the buses. The BMS extended the life of batteries by identifying weak cells early, monitoring the weak cells to validate if they are revived during pack equalization, and notifying operators to

replace the cell before it leads to damaging other batteries in the pack. The ability to detect high temperatures in packs during charge and discharge also increased the life of the cells. Progressive battery testing has led to changes in battery manufacturers as well as changes in charging algorithms. Figure 4.3-3 shows the four battery pack installed in the electric bus chassis.

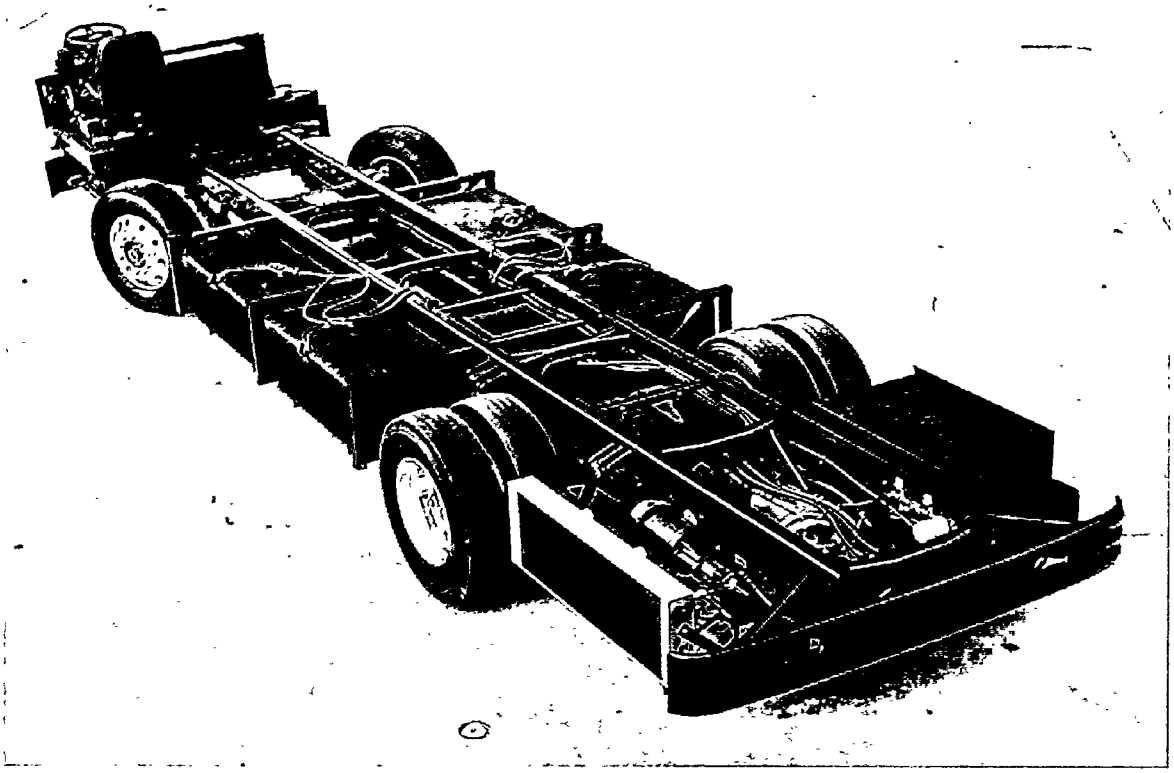

Figure 4.3-3 Electric Bus Chassis Showing Installed Drive

Battery Energy Storage System

At one of the transit facilities, enhancements to a Battery Energy Storage System (BESS), greatly improved the ability to maintain multiple electric vehicles with varying battery configurations. As improvements were made to the vehicles, the BESS was also adapted in configuration. Also charging could be accomplished from the utility grid or the storage batteries. The ability to take advantage of charging the storage system at night during cheap utility electric rates and using the stored energy during the day saves the transit agency dollars and provided an additional level of independence from the effects of power outages. The charging facility is depicted in Figure 4.3-4 and Figure 4.3-5.

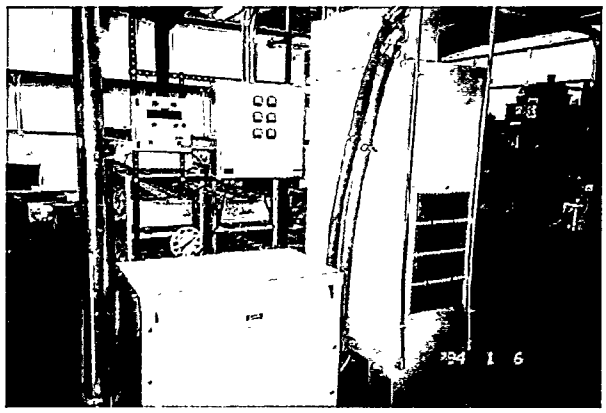

Figure 4.3-4 BESS Energy Conversion Electronics

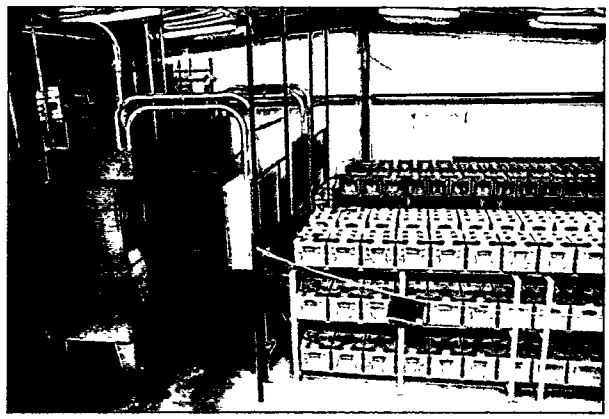

Figure 4.3-5 BESS Battery Storage Rack

Charging Station

During the test period the charging stations continued to be optimized and enhanced to accommodate the differences in battery types/manufacturers and vehicle configurations. The charging station facility provided fast charging (135 kW) and slow charging of buses, equalization of battery packs, and communication with the battery management system. All enhancements were accomplished maintaining simple operator interfaces. The charging station is shown in Figure 4.3-6.

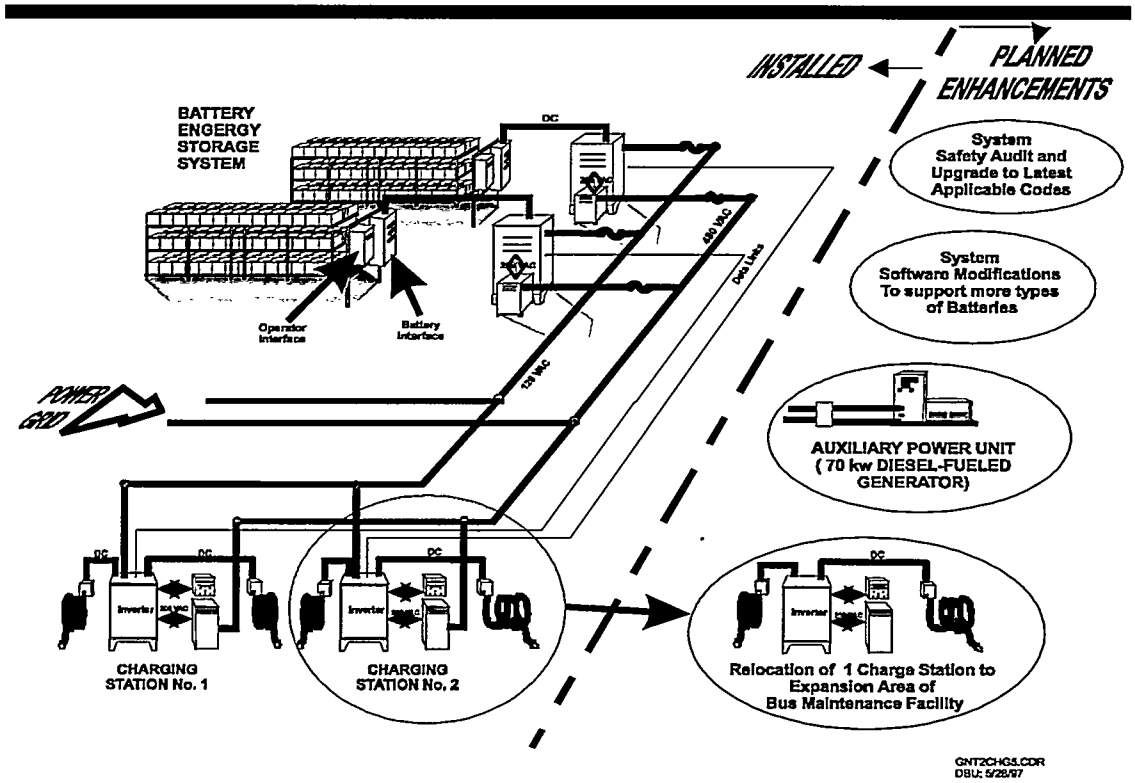

Figure 4.3-6 Charging Stations Integrated with BESS

4.3.3 Conclusions

The practical application of the technologies in real life revenue service of the electric transportation system, provided invaluable data leading to system improvements. It provided a basis for recommending improvements and product enhancements from an economical and user-friendly point of view. The results of the testing have been a positive and have been an integral step (in addition to the controlled "bench" or lab test environment) in bringing a new transportation technology to market.

In summary, the use of several test sites provided valuable lessons on system performance during vehicle use in operational transit environments. Battery management techniques have led to system changes to safeguard the batteries at temperature extremes. The charging infrastructure improvements have increased the cycle life of batteries and lowered the operating costs of the transit agency. The BESS charging facility will be capable of handling a variety of batteries from different manufacturers as advances to battery technology become available and are introduced. System cooling enhancements have extended the environmental operability of the systems, addressing the needs of a broader customer base.

Batteries continue to appear as the sub-system having negative impact on the system developers and transit operators. Limited range has been addressed by hybrid-electric powertrains. However most of the vehicle cost and maintenance issues are directly attributable to the poor performance of batteries when applied to electric vehicles. Batteries need to be more reliable, longer cycle life, and considerably less expensive than they are presently.